In compliance with the Canadian Privacy Legislation some supporting forms may have been removed from this dissertation.

While these forms may be included in the document page count, their removal does not represent any loss of content from the dissertation.

# Efficient all-digital symbol-timing recovery techniques for burst-mode demodulators

### Nguyen Doan Vo

Department of Electrical and Computer Engineering

McGill University

Montreal, Canada

January 2003

A thesis submitted to the department of Electrical and Computer Engineering and the committee on Graduate Studies in partial fulfillment of the requirements for the degree of Master in Engineering



National Library of Canada

Acquisitions and Bibliographic Services

395 Wellington Street Ottawa ON K1A 0N4 Canada Bibliothèque nationale du Canada

Acquisisitons et services bibliographiques

395, rue Wellington Ottawa ON K1A 0N4 Canada

> Your file Votre référence ISBN: 0-612-88395-7 Our file Notre référence ISBN: 0-612-88395-7

The author has granted a nonexclusive licence allowing the National Library of Canada to reproduce, loan, distribute or sell copies of this thesis in microform, paper or electronic formats.

The author retains ownership of the copyright in this thesis. Neither the thesis nor substantial extracts from it may be printed or otherwise reproduced without the author's permission.

L'auteur a accordé une licence non exclusive permettant à la Bibliothèque nationale du Canada de reproduire, prêter, distribuer ou vendre des copies de cette thèse sous la forme de microfiche/film, de reproduction sur papier ou sur format électronique.

L'auteur conserve la propriété du droit d'auteur qui protège cette thèse. Ni la thèse ni des extraits substantiels de celle-ci ne doivent être imprimés ou aturement reproduits sans son autorisation.



### **Abstract**

The major objective of this thesis is to investigate efficient all-digital symbol-timing recovery for burst modems. The study consists of new symbol-timing estimation algorithm and new optimal interpolation filters. The proposed feed-forward STR algorithms are optimal in the sense of maximum-likelihood estimation. Estimations are very accurate and converge rapidly within a preamble length as short as 4 symbols, suitable to burst-mode modems. In addition, they can operate at a sampling rate as low as twice the symbol rate. The proposed synthesis method of the optimal interpolation filters is optimal in the sense of minimum mean-square error jointly in time, and frequency domain, and symbol-timing estimation error.

Mathematical derivations, analysis, simulations, and implemented structures of the new algorithms are presented. Oversampling techniques combined with interpolation are studied to achieve better accuracy with a cost in increasing implementation complexity and lowering operational clock rate.

## **Avant-propos**

L'objectif principal de cette thèse est l'étude de systèmes entièrement numériques de récupération du temps de symbole (RTS) pour des modems transmettant par salves. L'étude consiste à développer de nouveaux algorithmes d'estimation du temps de symbole et de nouveaux filtres optimaux d'interpolation. Les algorithmes RTS à action directe proposés sont optimaux au sens de l'estimation par le critère du maximum de vraisemblance. Les estimations sont très précises et convergent rapidement à l'intérieur d'une longueur de préfixe aussi courte que 4 symboles, convenant à des modems transmettant par salves. De plus, ils peuvent opérer à un taux d'échantillonnage aussi bas que deux fois le taux de symbole. La méthode de synthèse proposée pour les filtres optimaux d'interpolation est optimale au sens du minimum de la moyenne de l'erreur quadratique conjointement en temps, fréquence et erreur d'estimation du temps de symbole.

Les développements mathématiques, l'analyse, les simulations et les structures réalisées des nouveaux algorithmes sont présentés. Des techniques de sur-échantillonnages combinées à des techniques d'interpolation sont étudiées afin d'obtenir une meilleure précision au prix d'une complexité de réalisation accrue et d'une baisse du taux d'horloge opérationnel.

## **Acknowledgements**

My studies were supported by Fonds pour la formation de Chercheurs et de l'Aide à la Recherches (FCAR) and through the grants awarded to my supervisor, Professor Tho Le-Ngoc. I thank them for their financial support.

I would like to express my deepest gratitude to my thesis advisor, Professor Tho Le-Ngoc, for his valuable support and guidance. Professor Le-Ngoc provided me with the excellent research resources, highly intellectual assistance, and generous support during my work time at McGill university. His friendship and advice were instrumental in the completion of this work.

I would like to thank Prof. Paul Fortier (Université Laval) who helped to translate the abstract into French.

My thanks to my father and mother are beyond words. I am thankful to all members of my great family, especially my uncle Bach and his family, and all my friends for their constant support and encouragement. Without them, I would have a hard time to start my study. Finally, my warmest thanks go to my wife who has always encouraged me and been with me. Without her love and support, my work would have been much more difficult. It is to all of them I dedicate this thesis.

# **Contents**

Abstra	ct	i
Avant-j	propos	ii
Acknov	vledgements	. iii
Conten	ts	. iv
List of	Figures	. vi
	Tables	
	Symbols	
	r 1. Introduction	
1.1	Burst-Mode Communication	
1.2	Timing Synchronization for All-Digital Receiver	
1.3	Motivation for Research	
1.4	Outline of the Thesis	. 8
1.5	Contributions of the Thesis	. 9
Chapte	r 2. Interpolation Filters	10
2.1	Signal Reconstruction, Interpolation and Resampling	
2.2	Polynomial-based Interpolation Filters	
2.3	Symmetric Polynomial-based Interpolators	16
2.4	Arrangement of Interpolation and Detection Filters and Complexity Issues	19
2.	4.1 non-symmetric g(t):	21
2.	4.2 symmetric g(t):	22
2.5	Frequency Response of Polynomial-based Interpolation Filters	23
2.6	Conclusion	25
Chapte	er 3. Digital STR Employing Interpolation Filters	<b>26</b>
3.1	General Structures	26
3.2	Representation of Received Baseband Signals	29
3.3	Maximum-Likelihood Estimation Technique	31
3.4	Derivation of the Proposed Algorithm	34
3.5	MSE in symbol-timing estimation of some second-order interpolators	
3.6	Estimation of Symbol Frequency	
3.7	Conclusion	
	er 4. Optimal Interpolation Filters for Digital STR	
4.1	Proposed Cost Function	
4.2	Algorithm Derivation	
43	Design Examples	50

4.4	Con	clusion	58
Chapter	r 5.	Performance of Proposed STR Employing Interpolators	59
5.1	Bias	s and Variance of Symbol Timing Estimator	59
5.	1.1	Bias in timing estimation	59
5.	1.2	Variance of the timing estimation error	60
5.	1.3	Minimum mean square error (MMSE)	63
5.	1.4	Bounds for Gaussian Noise Contributed Error	65
5.2	Alte	ernative Interpretation and Acquisition Time	66
5.3	BEI	R Degradation	69
5.4	Sim	ulation Results	74
5.5	Con	clusion	78
Chapter	r 6.	STR Techniques in Systems using Oversampling	<b>79</b>
6.1	PA	M Systems using Oversampling	79
6.	1.1	Maximum-Likelihood Algorithm for Timing Estimate	79
6.	1.2	Variance of Error due to Algorithm Precision	81
6.	1.3	AWGN Contribution.	84
6.	1.4	Case-Study: Optimal Lagrange Parabolic Interpolators	86
6.2	QA.	M Systems using Oversampling	89
6.3	2.1	Algorithm Derivation	89
6	2.2	Variance of Error due to Algorithm Precision	90
6.3	2.3	AWGN Contribution	91
6.2	2.4	Simulation Results	92
6.3	Con	clusion	97
Chapter	r 7.	Conclusion	99
7.1	Sun	nmary of Results	99
7.2	Top	ics for Further Research	100
Bibliog	Bibliography101		
Appendix A.Some Known Interpolation Filters 108			
Append	lix B	.Unbiased Timing Error Estimation 1	110
B.1	•		
B.2	<u> </u>		
B.3			
Append		Impulse Response of the Raised-Cosine Filter and Its Derivatives	

# **List of Figures**

1.1	Time Division Multiple Access (TDMA) Bursts	2
1.2	Symbol Timing Recovery method	6
1.3	Classification of Estimation Techniques	7
2.1	Sample timing relations	. 11
2.2	Impulse Response of the sinc() Interpolator	. 14
2.3	FIR filter at the l-th branch	. 16
2.4	Original Functional Diagram of the Farrow Structure	. 16
2.5	Modified, Low-Complex Farrow Structure for L=2	. 19
2.6	Three different arrangements of interpolation filters	. 20
3.1	Simplified block diagram of an all-digital receiver	. 28
3.2	Components of the symbol-timing recovery block	. 28
3.3	A simple parameter updater	. 28
3.4	A simple control state diagram	. 29
3.5	Typical PAM-2 burst	. 30
3.6	Cosine wave at sampling points	. 37
3.7	MSE of timing function versus γ.	. 41
3.8	Symbol Timing Error versus μ	. 41
3.9	Samples at different estimate time	. 43
4.1	MSE (ISI) at the decision points when Tsym/Ts is equal to a) 2, b) 4, c) 8	. 54
4.2	Frequency responses of four interpolators (Ts/Tsym=2)	. 55
4.3	Frequency responses of four interpolators (Ts/Tsym=4)	. 56
4.4	Frequency responses of four interpolators (Ts/Tsym=8)	. 57
5.1	Sine wave reconstruction using different interpolation filters	. 67
5.2	BER Degradation for Parabolic Interpolation Filter: (a) 2-PAM (b) 4-PAM	. 72
5.3	BER Degradation for Vesma's Interpolator-Type II: (a) 2-PAM (b) 4-PAM	. 73
5.4	Convergence behavior at different window size N for the parabolic filter	. 75
5.5	Convergence behavior at different window size N for Vesma filter Type II	. 76
5.6	Symbol Timing Error Variance for Parabolic Interpolation Filter	. 77
5.7	Symbol Timing Error Variance for Vesma Interpolation Filter II	. 77

6.1	Cosine wave at general sampling rate (for $\mu = 0.3$ )	. 80
6.2	MSE of Estimated Timing versus Sampling Rate λ	84
6.3	Symbol Timing Error Variance (λ=2)	87
6.4	Symbol Timing Error Variance (λ=4)	88
6.5	Symbol Timing Error Variance (λ=8)	88
6.6	MSE of STR versus preamble length N (without noise)	93
6.7	MSE of ISI versus preamble length N (without noise)	93
6.8	MSE of Estimated Timing versus Eb/No for sampling rate $\lambda = 2$	94
6.9	MSE of Estimated Symbol Timing versus Eb/No for sampling rate $\lambda = 4$	95
6.10	MSE of Estimated Symbol Timing versus Eb/No for sampling rate $\lambda = 8$	95
6.11	MSE of Estimated Symbol Timing versus preamble length N	96
6.12	MSE of ISI vs. Eb/No for sampling rate $\lambda = 2$	96
6.13	MSE of ISI error vs. Eb/No for sampling rate $\lambda = 4$	97
6.14	MSE of ISI error vs. Eb/No for sample rate $\lambda = 8$	97

# **List of Tables**

3.1	Assumptions for the proposed STR	30
3.2	MSE of timing estimation	39
4.1	Design parameters	51
4.2	Simulation Assumptions	51
4.3	Filter Coefficients for the Optimal Interpolators Type I	51
4.4	Filter Coefficients for the Optimal Interpolators Type II	52
4.5	MSE of STR and ISI, and Maximum Image Attenuation (Tsym/Ts = 2)	52
4.6	MSE of STR and ISI, and Maximum Image Attenuation (Tsym/Ts = 4)	53
4.7	MSE of STR and ISI, and Maximum Image Attenuation (Tsym/Ts = 8)	53
5.1	Simulations' Parameters	74
6.1	Optimal $\alpha$ for different sampling rate $\lambda$	83
6.2	Optimal $\gamma$ for different sampling rates $\lambda$	86
6.3	QAM Simulation Parameters	92
A.1	Farrow Coefficients for Linear Interpolation	108
A.2	Farrow Coefficients for Cubic Interpolation Filter	108
A.3	Farrow Coefficients for Parabolic Interpolation Filter	109
A.4	Farrow Coefficients for Vesma Interpolation Filter I	109
A.5	Farrow Coefficients for Vesma Interpolation Filter II	109

# **List of Symbols**

 $\otimes$ Convolution operator Interpolator filter parameter α Transmitted *n*-th symbol (real or complex, depending on  $a_n$ , a(n)modulation type) Transmitted *n*-th symbol at the in-phase and quadrature channels  $a_I(n), a_O(n)$ **AWGN** Additive white Gaussian noise Roll-off factor, or excess bandwidth parameter β  $B(l, k, f, T_s)$ Frequency response of the fractional interval Probability of error or bit error rate BER, P<sub>e</sub> Farrow filter coefficient  $c_l(k)$ Dirac delta-function δ() BER degradation  $D_{dR}$ Detection error due to ISI  $e_{ISI}$ Detection error due to AGWN  $e_{\eta}$ Detection error due to imperfect interpolation function  $e_h$ Error of the fractional timing estimation  $e_{\mathfrak{u}}$ Error of the symbol timing estimation  $e_{\tau}$  $E_h$ Average energy per bit Average energy per symbol  $E_{s}$  $f_l(m)$ Output at each interpolator filter branch Parameter of the parabolic interpolator filter h(t) or  $h_I(t)$ Impulse response of the interpolation function H(f) or  $H_I(f)$ Frequency response of the interpolation function Positive, real-valued step size κ AWGN portion (real or complex, depending on modulation type) η()

$\eta_I(), \eta_O()$	AWGN	portion at the	in-phase a	and quadrature char	nels

I Time interval of the interpolation function

J Cost function for interpolation filter optimization

 $\lambda$  Sampling-symbol rate ratio  $T_{svm}/T_s$ , an integer

L Degree of the interpolator filter

 $L(\mu)$  Maximum-likelihood function

M Tap length of each interpolator filter branch

 $\mu, \mu_k$  Expected timing fraction

μ Estimated timing fraction

Number of observation

 $N_o$  AWGN density

PAM Pulse-Amplitude Modulation

QAM Quadrature-Amplitude Modulation

QPSK Quadrature-Phase Shift Keying

STR Symbol-timing recovery

 $T_s, f_s$  Sampling period and frequency

 $T_{sym}, f_{sym}$  Symbol period and frequency

TED Timing-error detector

TDMA Time Division Multiple Access

x() Received signal before the interpolator

 $x_I(), x_O()$  Received signals before the interpolators at the in-phase (I) and

quadrature (Q) channels

Weighting factor (used in optimization procedure)

 $z_n$ , z(n) Detected *n*-th symbol (real or complex, depending on modulation

type)

# Chapter 1. Introduction

The work of the thesis is concerned with all-digital symbol-timing recovery (STR) techniques for burst-mode receivers. We first discuss the burst-mode communications in Section 1.1. The discussion is intended as an introduction to get the understanding of the need of such communications. Section 1.2 presents a brief survey of symbol-timing recovery techniques. Section 1.3 states the motivation for this work. Contents of each chapter and our contributions are summarized in Sections 1.4 and 1.5 respectively.

#### 1.1 Burst-Mode Communication

Early modems for data communications were first to establish reliable connections between two terminals using a *point-to-point* topology. However, user links are not always occupied all the time. For example, an Internet user usually spends most of his connection time reading a Web page or typing an email; and thus during this time, the modems at both ends of the link must maintain the connection by exchanging unuseful data which will be discarded at the receiver. Thus this results in wastes of CPU operation, transmission power and link bandwidth. As the number of subscribers has grown rapidly in these days, and due to the limitation of bandwidth availability, sharing bandwidth among users or multiple access adds another issue into the old access technology. It turns out that the continuous access mode cannot provide cost-effective connections. We require another specialized kind of modem, *a burst modem*, that can transmit and receive modulated data packets in short bursts.

Burst modems are recently required for use in time division multiple access (TDMA) systems [59, 61]. In these systems, multiple users require an essentially continuous

connection on a common channel, but the connection is provided by assigning each user a periodic time slot to transmit on a channel whose bandwidth is substantially greater than that required by any single user. A typical burst consists of preamble (containing carrier recovery, symbol-timing recovery training symbol sequences and some other system specific symbols) followed by message portion (see Figure 1.1). It can be seen that in order to increase the message data transfer efficiency of the system, the length of the training section (which is directly proportional to acquisition time) would be as short as possible.

Burst modems are commonly used today in applications such as the GSM, IS-136, and personal handy-phone system (PHS) cell phones; multimedia cable network system (MCNS) and digital audio visual council (DAVIC) cable modems; very small aperture terminals (VSAT); packet data networks like cellular digital packet data (CDPD), Ardis, Mobitex, and Reflex; and in local multipoint distribution system (LMDS) networks [61]. The design trade-offs and resulting architectures are different in each of these applications.

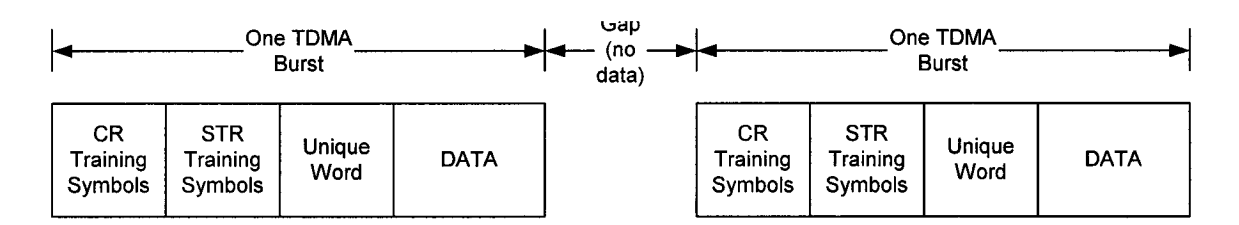


Fig. 1.1: Time Division Multiple Access (TDMA) Bursts

#### 1.2 Timing Synchronization for All-Digital Receiver

This section presents a brief survey of symbol-timing recovery (STR) algorithms and techniques.

We first consider the implementation aspects. Figure 1.2 shows three possible implementations of the existing receivers. In the analog approach (Figure 1.2-a), timing information derived from an analog circuitry is used to control the sampling clock. In the

hybrid approach (Figure 1.2-b), timing parameter is obtained from the digital processor and used to adjust the behavior of the sampling clock. The third approach first converts the signal from an analog to a digital format, and all signal processing are done in the digital domain. With digital signal processing (DSP), highly complex algorithms can be implemented for better performance and better accuracy. Reproducibility, flexibility, independence of temperature and aging are the other benefits offered by DSP. From now on, we will only consider the all-digital approach (Figure 1.2-c).

The vast number of STR estimators can be broadly categorized as either feedforward (FF) or feedback (FB) schemes. Feedforward (FF), or open-loop, estimators possess no feed-back and consequently, tend to be very well-suited for burst-mode communications. Open loop structures possess very short acquisition times and avoid hang-up complication faced by their close-loop counterparts. Hang-up is a phenomenon in FB topologies which causes them to drift aimlessly for significant periods of time before converging to a stable operating point. Occasionally, this equilibrium state differs from the true steady-state point giving rise to false lock conditions. The leading drawback of all FF estimators, however lies in their inability to track time-varying offsets, seeing how each estimate remains fixed until the FF algorithm is engaged anew. Closed-loop systems generally experience long acquisition times and may suffer from hang-up, but are extremely efficient at tracking time-varying parameters. Continuous and long burst-mode systems usually employ feedback schemes.

Parameters can be estimated independently or dependently. Joint estimation involves the optimization of the ML or maximum-a posteriori (MAP) of timing parameter and carrier offset parameter. In general, joint estimators are more complex, but perform better than independent estimators.

The feedforward estimation approach can be implemented with one of the following three types:

1 - Data aided (DA) methods exploit the knowledge of a known pattern (called a preamble) to aid timing recovery. Because preambles contain no useful user information, they decrease the overall system capacity and as a result, they should be kept as short as possible. Works in [44-48] employ the DA techniques.

- 2 Decision-directed (DD) methods resemble DA techniques except that the symbol decisions replace the preamble. Under high signal-to-noise ratio (SNR) conditions, data performance is quite good. However, at low SNR, decision errors occur frequently, and the performance is degraded. DD techniques proposed by Gardner [58] and Mueller and Muller [57] have been used in many DSL (digital subscriber loop) applications.
- 3 Non-data-aided or non-decision aided (NDA) methods require no preamble and use the data itself for estimation. NDA methods average the effects of the modulation sequence to maximize the effects of the ML function. Some works using these techniques are presented in [41, 42, and 49].

Two objectives of an all-digital receiver (Figure 1.2-c) are:

- 1 Determination of the symbol timing instant. Since the output of the demodulator must be sampled periodically at the symbol rate, at the precise sampling time instants in order to correctly recover the transmitted data, the symbol clock must be successfully obtained at the receiver. The works in [41], [46], and [47] show fast acquisition can be achieved at high sampling rates (4 or 8). Vesma et al. ([44], [45]) and Zhu et al. [43] show that timing information can be estimated at a sampling rate as low as twice the symbol rate, but with the cost in high complexity and longer acquisition time (from 32 to 64 symbols).
- 2 Determination of the value of the signal at the correct instant. Since the receiver samples the received signal at constant intervals regardless to the actual symbol clock, the value of the signal at the correct symbol instants is not available between the discrete-time samples. This problem can be solved by using interpolation. The idea of interpolation is to form an approximating continuous-time signal with the aid of the discrete-time samples, and then to evaluate the value of this signal at the desired time instant. The usual question when designing an optimal filter can be stated as, "what are the feasible considerations and how can we carry out the optimization process?" Many published works have extensively discussed the designs of the optimal interpolation filters in varied contexts. In general, they can be divided into three different classes. The first class of interpolator design consists of the time-domain methods where approximating polynomial is fitted to the discrete-time samples. Conventional Lagrange

and B-spline interpolations have been used [2 to 4, 51]. The advantage of these methods is that the filter coefficients for the Farrow structure are easily available in the closed form. In the second class, the coefficients of the Farrow structure are optimized directly in the frequency domain [7, 9, and 11]. These approaches are more flexible, and interpolation filters with better filtering and frequency-selective characteristics can be obtained. However, while they give the optimizations in the contexts of digital signal processing, they lack of considerations of other estimations in the communication systems. On the other hand, the third class of filter design was proposed mainly for considerations of estimations in the communication systems [1, 18, 19, and 39]. These methods have the drawback that they do not allow separate optimization such as data filtering which is necessary within the system.

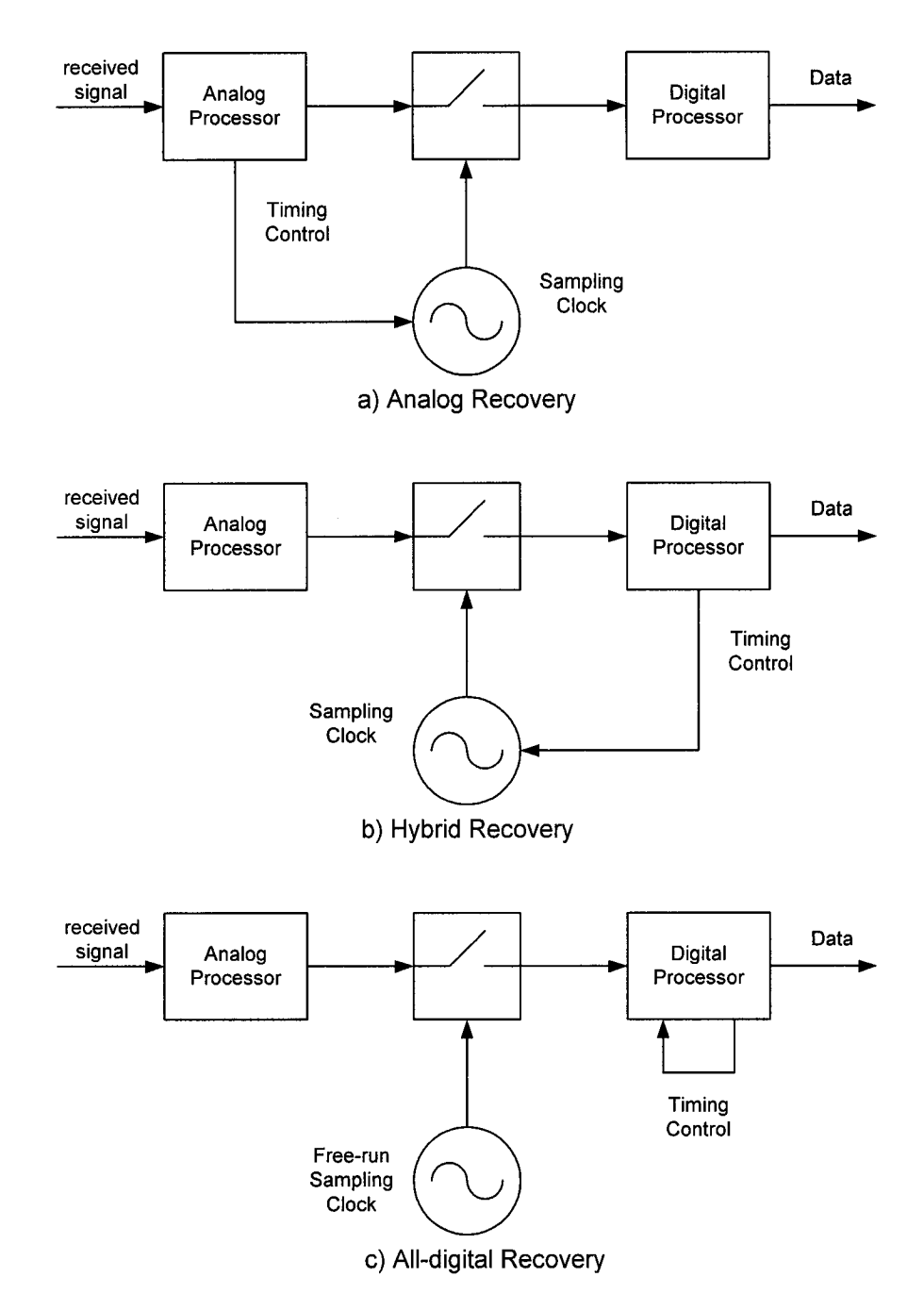


Fig. 1.2: Symbol Timing Recovery method

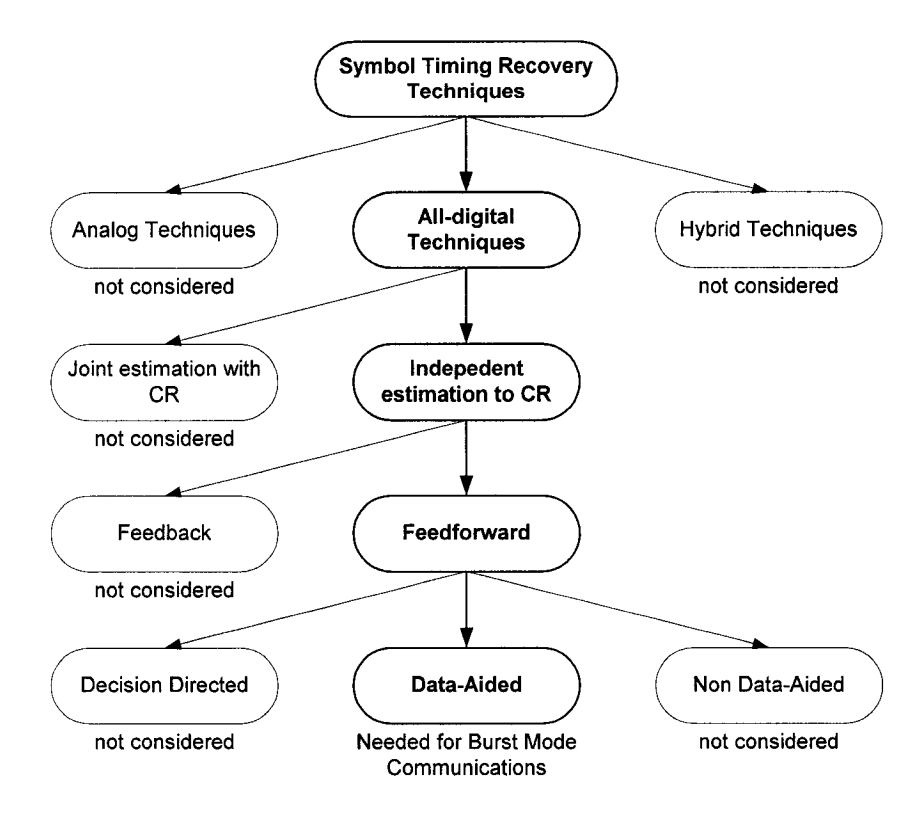


Fig. 1.3: Classification of Estimation Techniques

#### 1.3 Motivation for Research

The present study examines the efficient and low-complexity all-digital symbol-timing recovery techniques with a very short acquisition time suitable for burst-mode PAM and QAM systems. In addition, the effects of interpolation filters to the algorithm accuracy are also investigated. Optimal interpolation filters are desired to provide better signal processing while they still remain simple structures for efficient implementations. Therefore, a new and efficient synthesis of optimal interpolation filters are proposed and examined.

#### 1.4 Outline of the Thesis

The outline of the thesis is summarized as follows.

Chapter 2 explains the concept and the structure of the interpolation filters for all-digital receivers. Detailed background on interpolation filters is given and simplification of filter structure is studied. A consequent low-complexity hardware implementation can be obtained using the modified Farrow structure for the second-degree symmetric interpolator. It is proven that only M/2 coefficients are actually required, compared with 3M coefficients in the original structure.

Chapter 3 develops the theoretical backgrounds on new, all-digital symbol timing recovery techniques that employ interpolation filters. The symbol-timing estimation process, which is, in most of the cases, based on the maximum-likelihood (ML) concept, will be revised in order to improve the interpolation process. Both performance and complexity can be simultaneously considered in a joint signal detection and timing estimation process.

Chapter 4 discusses interpolation filters for symbol timing recovery (STR). The need for an interpolation filter is explained. It is shown that recent conventional interpolation filters are either not optimal, or suboptimal but not able to be implemented in on-line computation manners. A new interpolation filter methodology for minimum mean-square error (MMSE) is introduced to overcome the problems of these filters. Simulation results are included to show the performance gain.

Chapter 5 analyses the statistical performance of all-digital symbol timing recovery techniques at the sampling rate  $T_{sym}/T_s$ =2. Tracking performance for the synchronization system employing several interpolation filters are studied. Simulation results are included to show the accuracy of the theory and the analysis.

Chapter 6 generalizes the proposed timing estimation for PAM and QAM systems at higher sampling rates. The proposed feed-forward STR techniques employing interpolation filters can be applied for higher sampling rate to achieve better accuracy, with the trade-off in more hardware complexity and possible lower operated clock speed.

Results on performance versus sampling rate and preamble length can be used in design trade-off and selection of an appropriate scheme for given design requirements.

#### 1.5 Contributions of the Thesis

The contributions of this work can be summarized as follows.

- Derivation of the efficient maximum-likelihood feed-forward timing estimation algorithm for PAM and QAM systems for  $T_{sym}$  /  $T_s$  = 2 and for high sampling rate (Chapters 3 and 6).
- Derivation of the new optimum interpolation filter that minimizes the MSE of the timing estimation, and the MSE of the recovered signals in time and frequency domain (Chapter 4).
- Derivation of the modified Farrow structure to reduce the hardware complexity (Chapter 2).
- Development and performance analysis of ML-FF STR techniques for PAM and QAM systems for  $T_{sym}$  /  $T_s$  = 2 and for high sampling rates (Chapters 5 and 6).

# Chapter 2. Interpolation Filters

This chapter outlines the theoretical backgrounds and presents the efficient structures of the interpolation filters. Section 2.1 briefly presents the sampling issues and briefly reviews the reconstruction, interpolation and resampling processes in an all-digital receiver. In Section 2.2, the general structure of the polynomial-based interpolation filter is presented. Section 2.3 derives a simplified structure for symmetric polynomial-based interpolation filters suitable for low-complexity implementation. Based on the introduced structure, the complexity of different arrangements for interpolation and data filters is discussed in Section 2.4. The frequency responses of the interpolation filters are derived in Section 2.5. Section 2.6 provides concluding remarks.

# 2.1 Signal Reconstruction, Interpolation and Resampling

A modulated signal is normally transmitted over a communications medium in analog (continuous) format. In all-digital communication receivers (see Figure 1.2), the received signal from the analog front-end including antenna, RF-to-IF downconversion in case of wireless communications, is sampled and converted into a digital format by the analog-to-digital converter (ADC). In many applications requiring flexible receiver and for low jitter, the sampling clock is generated by a high-precision, low-jitter oscillator. The sampling clock frequency is fixed and may not be in synchronization with the transmitted symbol frequency and phase. The received digital signal is first processed at the sampling rate. In parallel, the STR uses received samples to derive the symbol clock

frequency and phase, and then performs both timing and amplitude adjustment to produce received signals re-sampled at the correct symbol frequency and time. Amplitude adjustment is required because the sample at the correct symbol timing instant is not available. This can be done by interpolation based on the available samples and the estimated symbol timing instant.

Figure 2.1 shows an example of a received signal and the relation between  $T_s$  and  $T_{sym}$ . The continuous curve depicts the analog received signal x(t) before sampling. The sampled values at the rate  $1/T_s$  are denoted by crosses (x). The desired samples at the symbol rate are shown by the small black circles. It is worth mentioning that the desired samples are *not* available at the sampler output and we want to reconstruct them from the available samples denoted by crosses (x). As an example, in Figure 2.1, the sampling rate  $1/T_s$  is about 1.5 times the symbol rate  $1/T_{sym}$ .

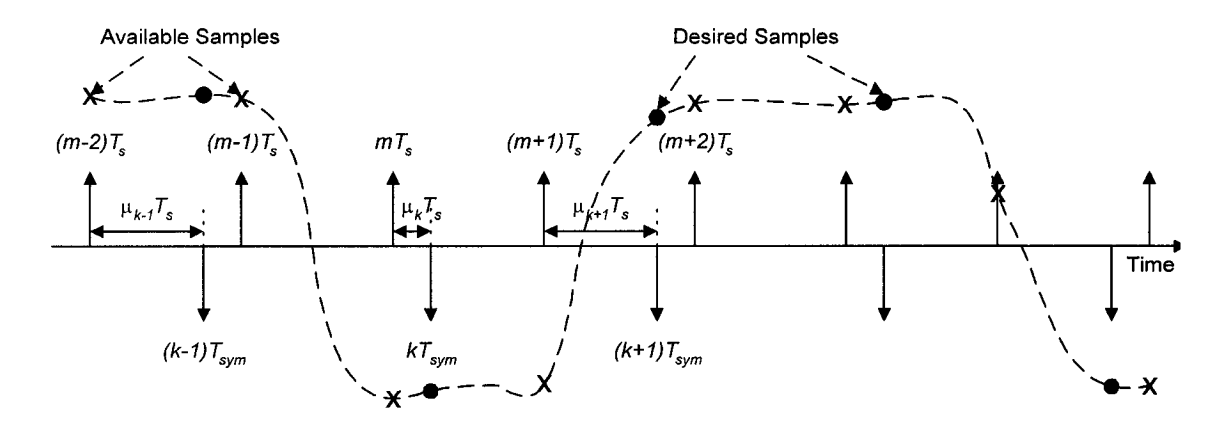


Fig. 2.1: Sample timing relations

The sampled signal  $x_d(t)$  at rate  $1/T_s$  can be represented by

$$x_d(t) = x(t) \sum_{n = -\infty}^{\infty} \delta(t - nT_s) = \sum_{n = -\infty}^{\infty} x(nT_s)\delta(t - nT_s)$$
 (2.1)

where x(t) is the analog signal before sampling and  $x(nT_s)$  are samples denoted by crosses (x).

Derivation of the desired samples at the symbol rate  $1/T_{sym}$  can be done by

reconstructing the analog signal x(t) and then re-sampling the analog signal at rate  $1/T_{sym}$ . It is well known that the reconstruction of the analog signal x(t) can be realized by filtering the sampled signal  $x_d(t)$  with a bandlimiting interpolation filter,  $h_f(t)$ , and the bandwidth of  $h_f(t)$  must be larger than or equal to that of the signal x(t).

Consider the impulse response of the interpolation filter,  $h_I(t)$ , defined in an interval [- $IT_s$ ,  $IT_s$ ] where I is an integer and can be infinity, i.e.,  $h_I(t) = 0$  for all t outside of this interval. The filtered signal can be represented as

$$y(t) = \int_{\tau = t - IT_s}^{t + IT_s} x_d(\tau) h_I(t - \tau) d\tau$$

$$= \sum_{n = -\infty}^{\infty} x(nT_s) \int_{\tau = t - IT_s}^{t + IT_s} h_I(t - \tau) \delta(\tau - nT_s) d\tau$$

$$= \sum_{n = -\infty}^{t / T_s + I} x(nT_s) h_I(t - nT_s)$$

$$= \sum_{n \ge t / T_s - I}^{t / T_s - I} x(nT_s) h_I(t - nT_s)$$
(2.2)

where,

$$\int_{\tau = t - IT_{s}}^{t + IT_{s}} \delta(\tau - nT_{s}) d\tau = \begin{cases} 1 & t - IT_{s} \le nT_{s} \le t + IT_{s} \\ 0 & otherwise \end{cases}$$

As we can observe from Figure 2.1, the interpolated output sample  $y(kT_{sym})$  is obtained by sampling y(t) at  $t = kT_{sym} = (m + \mu_k)T_s$ . Therefore,

$$y(kT_{sym}) = \sum_{n \ge m + \mu_k - I}^{m + \mu_k + I} x(nT_s)h_I((m + \mu_k - n)T_s)$$
 (2.3)

By introducing i=m-n,  $-\mu_k-I \le i \le -\mu_k+I$  or  $-I \le i \le I-1$  for  $0 \le \mu_k < 1$ , and Equation (2.3) can be simplified as

$$y(kT_{sym}) = \sum_{i=-I}^{I-1} x((m-i)T_s)h_I((\mu_k+i)T_s)$$
 (2.4)

The above equation indicates that the desired sample  $y(kT_{sym})$  can be derived by

passing the sequence  $\{x(mT_s)\}$  through an adaptive FIR filter  $h_f(mT_s)$ , and then resampling at the symbol rate  $T_{sym}$ . It also points out that at the time  $t=mT_s$ , the coefficients of the adaptive filter  $h_f(m)$  will be extracted from the interpolation function  $h_f(t)$  at  $t=(\mu_k+i)T_s$ .

For reconstruction without distortion, y(t)=x(t), the ideal interpolation filter has a simple rectangular frequency response, corresponding to the impulse response  $h_I(t)=sinc(t/T_s)$ . Figure 2.2 shows the plots of  $h_I(t)=sinc(t/T_s)$  at different timing fraction. However, this function is not practically realizable. Its time-truncated version (i.e., with a finite value of I), is proved to be the optimal function in terms of minimum mean square error (MMSE) [57].

For resampling, we need the values of  $h_I(t)$  at  $t = (\mu_k + i)T_s$  where  $(\mu_k + i)$  is a variable representing the desired resampling instant to be produced by the symbol timing recovery. It is desired to find a low-complexity digital signal processing (DSP) structure to generate  $h_I(t)$  as a function of  $(\mu_k + i)$  and to perform the interpolation/resampling process. This is the subject to be addressed in the following sections.

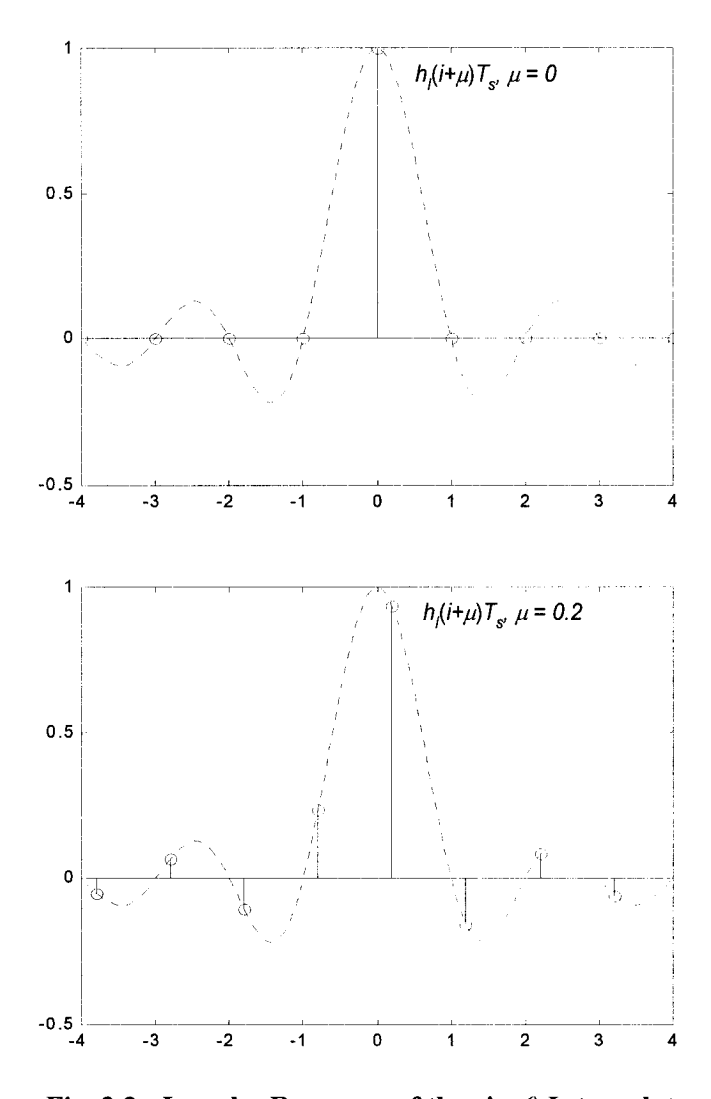


Fig. 2.2: Impulse Response of the sinc() Interpolator

## 2.2 Polynomial-based Interpolation Filters

Consider  $h_f(t)$  be approximated by a degree-L polynomial function of  $t = (\mu_k + i)T_s$ , for its simplicity, and well-developed algebraic structure,

$$h_{I}((i+\mu_{k})T_{s}) = \sum_{l=0}^{L} c_{l}(i)\mu_{k}^{l}$$
 (2.5)

Substitute into (2.4), the desired sample at  $kT_{sym}$  is

$$y(kT_{sym}) = \sum_{\substack{i=-I\\i=1\\l=1\\l=0}}^{I-1} x((m-i)T_s) \sum_{l=0}^{L} c_l(i) \mu_k^l$$

$$= \sum_{\substack{l=0\\l=0\\l=0}}^{L} \mu_k^l \sum_{i=-I}^{L} x((m-i)T_s) c_l(i)$$

$$= \sum_{l=0}^{L} \mu_k^l f_l(m)$$
(2.6)

where

$$f_{l}(m) = \sum_{i=-l}^{l-1} x((m-i)T_{s})c_{l}(i) = c_{l}(mT_{s}) \otimes x(mT_{s})$$
(2.7)

The formula shows that since  $f_l(m)$  is a result of the convolution, it can be realized as an output of a FIR filter as shown in Figure 2.3.

The result is then decomposed in further step as follows

$$y(kT_{sym}) = \sum_{l=0}^{L} \mu_k^l f_l(m)$$

$$= (...((f_L(m)\mu_k + f_{L-1}(m))\mu_k + f_{L-2}(m))\mu_k + ...)\mu_k + f_0(m)$$
(2.8)

The above equation is expressed in a Horner's relation, and can be realized by the simple DSP hardware structure initially devised by Farrow [2], as shown in Figure 2.4.

The Farrow realization, in general, requires M(L+1) coefficients, thus needs M(L+1) multiplications. In the following section, a simplified version for symmetric interpolation filter is derived.

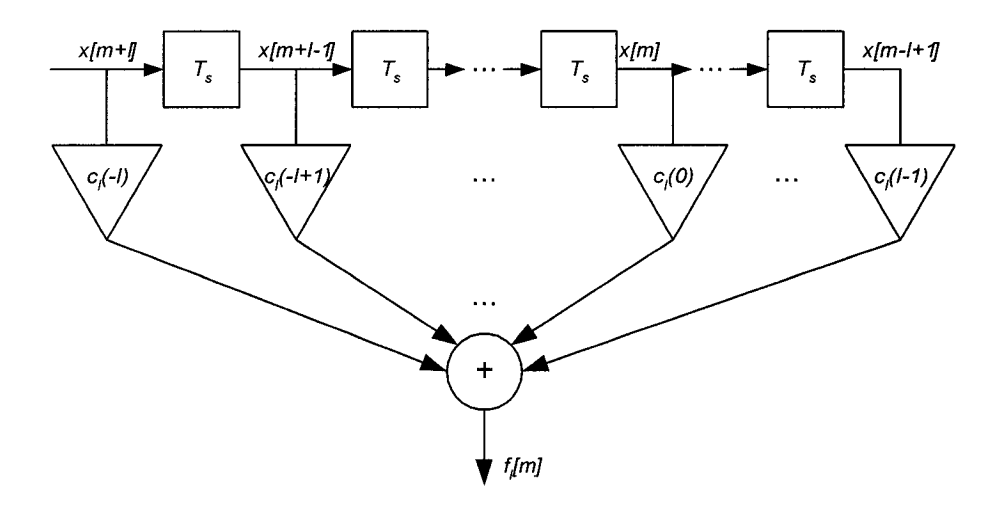


Fig. 2.3: FIR filter at the *l*-th branch

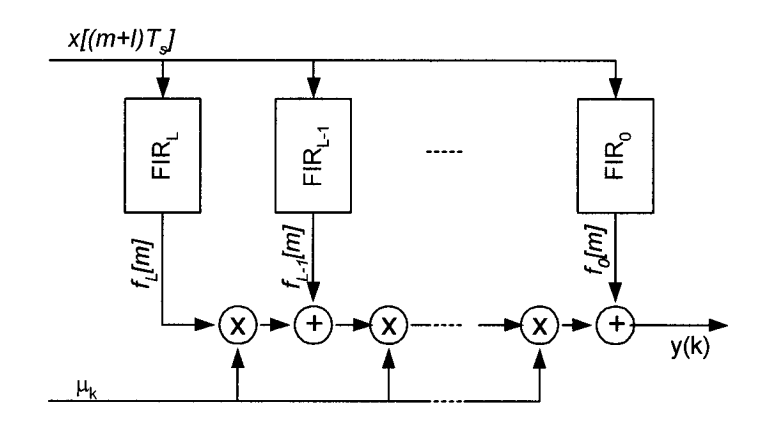


Fig. 2.4: Original Functional Diagram of the Farrow Structure

# 2.3 Symmetric Polynomial-based Interpolators

Consider an interpolation filter with an even-symmetric and real-valued impulse response  $^{1}$ , h(t),

<sup>&</sup>lt;sup>1</sup> From now on, the notation h(t) will replace  $h_1(t)$  for simplicity.

$$h_k(\mu) = h((k+\mu)T_s) = \sum_{l=0}^{L} c_l(k)\mu^l$$

For  $h(kT_s) = \delta(kT_s)$ ,

$$c_0(k) = \delta(k)$$
 (2.9)  
 $\sum_{l=0}^{L} c_l(k) = \delta(k+1)$ 

Hence,

$$c_{1}(0) + c_{2}(0) + 1 = 0$$

$$c_{1}(-1) + c_{2}(-1) = 1$$

$$c_{1}(k) + c_{2}(k) = 0, \forall (k \neq -1, 0)$$
(2.10)

or equivalently

$$c_1(k) + c_2(k) = \delta(k+1) - \delta(k)$$
 (2.11)

Due to the even symmetry,

$$h_k(\mu) = h(k+\mu) = h(-k-\mu) = h(-k-1+1-\mu) = h_{-k-1}(1-\mu), \forall (k,\mu)$$
$$\sum_{l=0}^{L} c_l(k) \mu^l = \sum_{l=0}^{L} c_l(-k-1)(1-\mu)^l, \forall (k,\mu)$$

For a second degree polynomial, three points determine the entire curve. We already know the value  $h_k(\mu) = 0$  for  $\mu = 0$  and 1. The third point will be corresponding to the value  $\mu = 1/2$ . For this, we have

$$\sum_{l=0}^{L} c_l(k) 0.5^l = \sum_{l=0}^{L} c_l(-k-1) 0.5^l$$
 (2.12)

Using the relationship (2.11), the condition (2.12) implies

$$c_2(k) = c_2(-k-1), \forall k$$
 (2.13)

$$c_1(k) = c_1(-k-1), \forall (k \neq 0, 1)$$
 (2.14)

Equations (2.11), (2.13), and (2.14) indicate that we only need to determine  $c_2(k)$ , k=0,..., (M/2-1). Thus, only M/2 unknowns are required to realize this special Farrow interpolator filter, and only M/2 multipliers are needed in hardware implementations.

Furthermore, the interpolation filter response (2.5) can be rewritten as

$$h(k + \mu) = \sum_{l} c_{l}(k) \mu^{l} = c_{0}(k) + c_{1}(k) \mu + c_{2}(k) \mu^{2}$$

$$= \delta(k) + (\delta(k+1) - \delta(k) - c_{2}(k)) \mu + c_{2}(k) \mu^{2}$$

$$= \delta(k) + (\delta(k+1) - \delta(k)) \mu + c_{2}(k) (\mu^{2} - \mu)$$
(2.15)

Equation (2.7) can be simplified as

$$f_0(m) = x(m) \tag{2.16}$$

$$f_{1}(m) = \sum_{k=-M/2}^{M/2-1} x(m-k)c_{1}(k)$$

$$= \sum_{k=-M/2}^{M/2-1} x(m-k)(\delta(k+1) - \delta(k) - c_{2}(k))$$

$$= x(m+1) - x(m) - f_{2}(m)$$
(2.17)

and

$$f_{2}(m) = \sum_{k=-M/2}^{M/2-1} x(m-k)c_{2}(k)$$

$$= \sum_{k=0}^{M/2-1} x(m-k)c_{2}(k) + \sum_{k=-M/2}^{-1} x(m-k)c_{2}(k)$$

$$= \sum_{k=0}^{M/2-1} (x(m-k) + x(m+k+1))c_{2}(k)$$

$$= \sum_{k=0}^{M/2-1} (x(m-k) + x(m+k+1))c_{2}(k)$$
(2.18)

Therefore the Farrow structure can be modified as shown in Figure 2.5 with only M/2 coefficients.

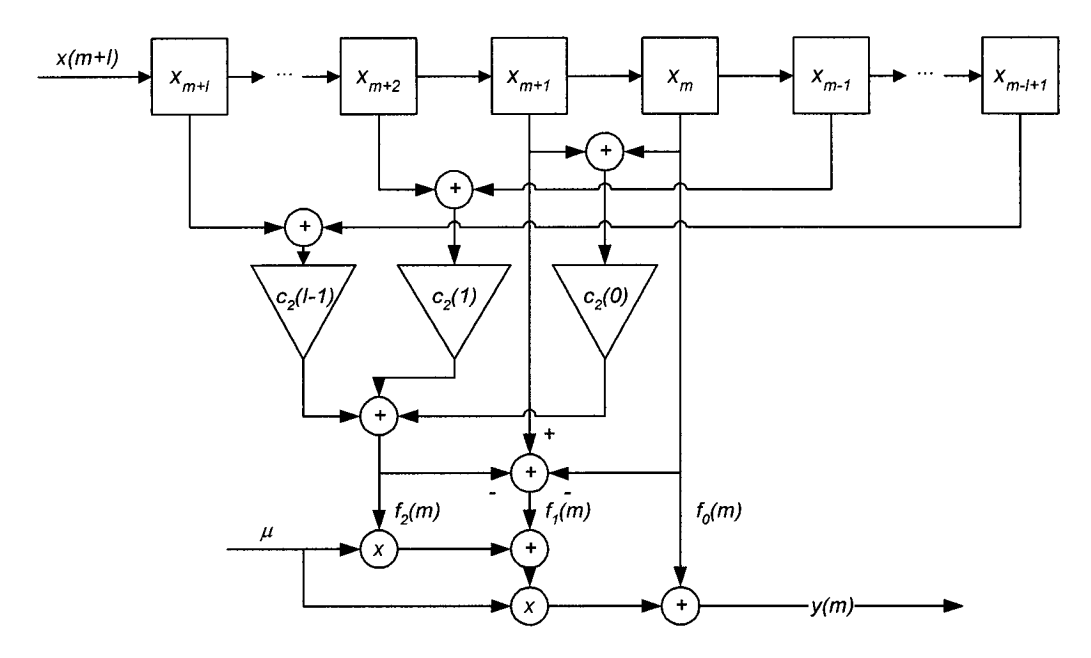


Fig. 2.5: Modified, Low-Complex Farrow Structure for L=2

# 2.4 Arrangement of Interpolation and Detection Filters and Complexity Issues

A receiver always includes filtering to reject out-of-band, unwanted noise and interference. For example, in a linear bandlimited AWGN channel, it is well known that the root raised cosine filter as an optimum detection filter [60]. Figure 2.6 illustrates the possible arrangements of the interpolation and data filters. In general, the *data* filter in this figure can represent cascaded filters for noise and interference rejection. For a linear system, the three arrangements provide the same performance. This section addresses their implementation complexity.

In Figure 2.6 (a), the data filter operates at the sampling rate prior to interpolation. In Figure 2.6 (b), the data filter follows the interpolation filter and operates at the symbol rate. In both these separate structures I & II, the data filter and the interpolation filter can be separately optimized; thus independent, simplified optimizations can be applied.

In the hope of reducing the complexity, some papers [32], [33] have considered the

combined structure in which the data filter is now combined with the interpolation filter as shown in Figure 2.6 (c). However, it is interesting to show that with the special structure proposed in the previous section, in some particular considerations, designs with lower complexity for the separate case can actually be obtained. The detailed discussions are provided in the following sections.

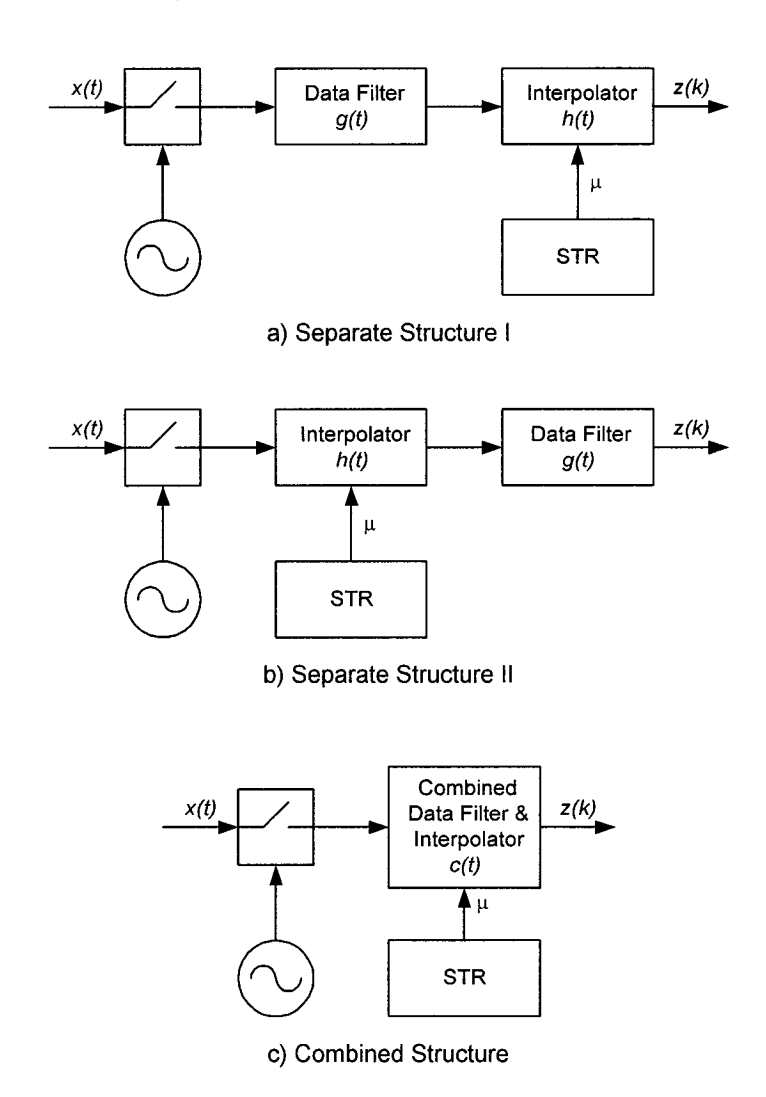


Fig. 2.6: Three different arrangements of interpolation filters

For a combined filter,

$$c(t) = h(t) \otimes g(t) \tag{2.19}$$

$$C(f) = H(f)G(f) (2.20)$$

where,

h(t), H(f)	impulse and frequency response of the interpolator
g(t), G(f)	impulse and frequency response of the data filter
c(t), C(f)	impulse and frequency response of the combined filter

If h(t) and g(t) are time-limited in  $[-I_1T_{sym}, I_1T_{sym}]$  and  $[-I_2T_{sym}, I_2T_{sym}]$  respectively, then the overall response is time-limited in  $[-(I_1+I_2)T_{sym}, (I_1+I_2)T_{sym}]$ .

#### 2.4.1 non-symmetric g(t):

In the separate case I in Figure 2.6 (a), since g(t) operates at the sampling rate  $1/T_s$ , the discrete-time implementation version of the data filter g(t) needs  $(2\lambda I_1+1)$  coefficients, where  $\lambda$  is the sampling-to-symbol rate ratio. Therefore, the total complexity for the separate case I will be  $(2\lambda I_1+1+I_2)$  coefficients.

In the separate case II in Figure 2.6 (b), g(t) operates at the symbol rate  $1/T_{sym}$ . Hence, the discrete-time implementation version of the data filter g(t) needs  $(2I_1+1)$  coefficients. The total complexity for the separate case II will be  $(2I_1+1+I_2)$  coefficients.

The combined case using the Farrow structure requires  $2(L+1)(I_1+I_2)$  coefficients.

The modified interpolator structure becomes more efficient than the combined filter when the numbers of coefficients required in the separate cases I and II are less than the one required in the combined case.

For the separate case I,

$$2\lambda I_1 + 1 + I_2 < 2(L+1)(I_1 + I_2), L \ge 2$$
(2.21)

$$2(\lambda - (L+1))I_1 + 1 < (2(L+1)-1)I_2, L \ge 2$$
(2.22)

As we can see, even with L=2, the inequality (2.22) still holds true for all  $I_1$  and  $I_2$  when  $\lambda=2$  (i.e., lowest sampling rate). For the higher sampling rates ( $\lambda>4$ ), the separate structure I can still be efficient if we can arrange the lengths of the filters so that the inequality in (2.22) is met.

For the separate structure II,

$$2I_1 + 1 + I_2 < 2(L+1)(I_1 + I_2)$$
(2.23)

$$1 < 2LI_1 + (2L+1)I_2 \tag{2.24}$$

As we can see, the inequality (2.24) holds true for all  $I_1 > 0$  and  $I_2 > 0$ . Thus the structure II is always more efficient than the combined case.

#### 2.4.2 symmetric g(t):

When the data filter g(t) is symmetric, its discrete-time implementation for the separate case I requires only  $(\lambda I_1+1)$  tap coefficients, while for the separate case II, it requires  $(I_1+1)$  tap coefficients. Therefore, the total complexity for the separate case I will be  $(\lambda I_1+1+I_2)$  coefficients, and the separate case II,  $(I_1+1+I_2)$ .

As g(t) and h(t) are both symmetric, the total response c(t) is also symmetric. Vesma [9] introduced the modified Farrow structure for symmetric interpolator to save half of the coefficients. The combined case using the Vesma-Farrow structure thus requires only  $(L+1)(I_1+I_2)$  coefficients.

For the separate structure I, in terms of complexity, the modified interpolator structure becomes more efficient than the combined filter (using Vesma-Farrow structure) when

$$\lambda I_1 + 1 + I_2 < (L+1)(I_1 + I_2)$$
 (2.25)

$$(\lambda - (L+1))I_1 + 1 < LI_2 \tag{2.26}$$

Even with L=2, the inequality (2.26) holds true for every  $I_1$  and  $I_2$  when  $\lambda=2$ . Therefore, the separate structure is more efficient with the modified Farrow structure at the lowest sampling rate. For the higher sampling rates ( $\lambda>4$ ), the separate structure can still be significantly efficient if we can arrange the lengths of the filters so that the inequality in (2.26) is met.

For the separate structure II,

$$I_1 + 1 + I_2 < (L+1)(I_1 + I_2)$$
 (2.27)

$$1 < L(I_1 + I_2) \tag{2.28}$$

As we can see, the inequality (2.28) holds true for all  $I_1 > 0$  and  $I_2 > 0$ . Thus, the structure II is always more efficient than the combined case.

### 2.5 Frequency Response of Polynomial-based Interpolation Filters

The impulse response of the polynomial-based interpolation filter can be written as

$$h_I(kT_s + t) = \sum_{l=0}^{L} c_l(k) \left(\frac{t}{T_s}\right)^l \quad \text{for } -\frac{M}{2} \le k \le \frac{M}{2} - 1$$
 (2.29)

where M is the length of the filter, L is the degree of the interpolation,  $c_l(k)$ 's are the coefficients of the Farrow structure.

The frequency response denoted by  $H_I(f)$  is

$$H_{I}(f) = \int_{-\infty}^{\infty} h_{I}(t)e^{-j2\pi ft}dt = \sum_{k=-M/2}^{M/2-1} \int_{0}^{T_{s}} h_{I}(kT_{s}+t)e^{-j2\pi f(kT_{s}+t)}dt$$

$$H_{I}(f) = \sum_{k=-M/2}^{M/2-1} \sum_{l=0}^{L} c_{l}(k) \int_{0}^{T_{s}} \left(\frac{t}{T_{s}}\right)^{l} e^{-j2\pi f(kT_{s}+t)}dt$$

$$H_{I}(f) = \sum_{k=-M/2}^{M/2-1} \sum_{l=0}^{L} c_{l}(k)e^{-j2\pi fkT_{s}}T_{s} \int_{0}^{1} t^{l} e^{-j2\pi fT_{s}t}dt$$

Define

$$B(l, k, f, T_s) = T_s e^{-j2\pi fkT_s} \int_0^1 t^l e^{-j2\pi fT_s t} dt = I(l, \alpha) T_s e^{k\alpha}$$

$$\alpha = -j2\pi fT_s t$$

$$I(n,\alpha) = \int_0^1 u^n e^{\alpha u} du = \frac{e^{\alpha}}{\alpha} - \frac{n}{\alpha} \int_0^1 u^{n-1} e^{\alpha u} du = \frac{e^{\alpha}}{\alpha} - \frac{n}{\alpha} I(n-1,\alpha)$$

where

$$I(0, \alpha) = \int_0^1 e^{\alpha u} du = \frac{e^{\alpha} - 1}{\alpha}$$

It follows that

$$I(n) = \frac{e^{\alpha}}{\alpha} \left( \sum_{i=0}^{n-1} \frac{n!(-1)^i}{\alpha^i (n-i)!} \right) + \frac{(-1)^n n!}{\alpha^n} \left( \frac{e^{\alpha} - 1}{\alpha} \right)$$

$$H_{I}(f) = \sum_{k=-M/2}^{M/2-1} \sum_{l=0}^{L} c_{l}(k)B(l, k, f, T_{s})$$
(2.30)

where

$$B(l, k, f, T_s) = T_s e^{-j2\pi fkT_s} \left( \frac{e^{-j2\pi fT_s}}{-j2\pi fT_s} \left( \sum_{i=0}^{l-1} \frac{l!(-1)^i}{(-j2\pi fT_s)^i (l-i)!} \right) + \frac{(-1)^l l!}{(-j2\pi fT_s)^l} \left( \frac{e^{-j2\pi fT_s} - 1}{-j2\pi fT_s} \right) \right)$$

$$(2.31)$$

Equations (2.30) and (2.31) are true for all polynomial-based filters.

For the specific case of second-order symmetric polynomial filters, their frequency response can be further simplified as follows,

$$\begin{split} H_I(f) &= c_0(0)B(0,0) + \sum_{k=-M/2}^{M/2-1} c_1(k)B(1,k) + \sum_{k=-M/2}^{M/2-1} c_2(k)B(2,k) \\ &= B(0,0) + \sum_{k=-M/2}^{M/2-1} (\delta(k+1) - \delta(k) - c_2(k))B(1,k) + \sum_{k=-M/2}^{M/2-1} c_2(k)B(2,k) \\ &= B(0,0) + B(1,-1) - B(1,0) + \sum_{k=-M/2}^{M/2-1} (B(2,k) - B(1,k))c_2(k) \end{split}$$

$$= B(0,0) + B(1,-1) - B(1,0) + \sum_{k=0}^{M/2-1} (B(2,k) - B(1,k))c_{2}(k)$$

$$+ \sum_{k=-M/2}^{-1} (B(2,k) - B(1,k))c_{2}(k)$$

$$= B(0,0) + B(1,-1) - B(1,0) + \sum_{k=0}^{M/2-1} (B(2,k) - B(1,k))c_{2}(k)$$

$$+ \sum_{k=0}^{M/2-1} (B(2,-k-1) - B(1,-k-1))c_{2}(-k-1)$$

$$= B(0,0) + B(1,-1) - B(1,0)$$

$$= B(0,0) + B(1,-1) - B(1,0)$$

$$+ \sum_{k=0}^{M/2-1} (B(2,-k-1) - B(1,-k-1) + B(2,k) - B(1,k))c_{2}(k)$$

$$(2.32)$$

where we adopted the following abbreviation,  $B(l, k) = B(l, k, f, T_s)$ 

#### 2.6 Conclusion

Based on the general Farrow structure of polynomial-based interpolators, a simplified version for symmetric cases was derived. The modified structure only needs M/2 coefficients as compared to a requirement of 3M coefficients in the original structure. With this modified structure, it is shown that a separate arrangement with an interpolation filter followed by a symmetric data filter operating at the symbol rate is the most efficient one in terms of complexity. This separate arrangement is much simpler than the combined interpolation and data filter structure proposed in [32] and [33]. The frequency response of the interpolation filter was derived to be used in the optimization process in Chapter 4.

# Chapter 3. Digital STR Employing Interpolation Filters

This chapter develops the theoretical backgrounds for the proposed all-digital symbol timing recovery techniques that employ interpolation filters.

#### 3.1 General Structures

Figure 3.1 shows a simplified block diagram of a typical all-digital receiver with emphasis on the symbol timing recovery (STR). The received digital signal is first processed at the sampling rate. In parallel, the STR uses received samples to derive the symbol clock frequency and phase, and then performs both timing and amplitude adjustment to produce received signals re-sampled at the correct symbol frequency and time. The timing adjustment can be done by a combined feedforward estimation and feedback tracking structure as shown in Figs. 3.1 and 3.2.

The feedforward timing estimator (FF-TE) block in Fig. 3.2 is one of the main subjects of this work to be discussed in detail in the subsequent sections. Its function is to estimate the correct symbol timing instant  $\mu$ . Performance of this block can be represented by its estimation accuracy and time required to achieve the accurate estimate. Estimation accuracy can be further represented by the mean squared error (MSE) for various channel signal-to-noise ratios. The time required to achieve the accurate estimate can be called acquisition time and is an important parameter for burst transmission of packets. Short acquisition time needs short overhead bits and hence offers high

transmission efficiency, especially for short data packets/cells. For this reason, fast feedforward estimation technique is preferred. In systems using long bursts with considerable variation in symbol timing frequency and phase over the burst interval, tracking and correction of timing error is necessary by using a feedback timing error detector (FB-TED) block as shown in Fig. 3.2. Many good algorithms, such as Muller and Mueller, Gardner feedback symbol timing recovery [57, 58], can be used to implement this FB-TED block. The correct timing instant is the angle of the symbol clock signal and hence a linear function of the estimated frequency and phase. It is generated by the parameter updater in forms of a numerically controlled oscillator (NCO) as shown in Fig. 3.3. Figure 3.4 illustrates the operation of the STR by a finite-state diagram with 4 states: search, lock, unlock, and normal.

The STR starts in its *search* state by looking for the preamble from the received sequence and derives the timing instant by using a feedforward estimation scheme. When the timing instant has been established, the STR gets in its *lock* state. The acquisition process is assumed to be finished and the timing information  $\mu$  is loaded to the NCO. The feedforward estimator is then de-selected and the feedback tracking loop is kicked in by the MUX in Fig. 3.3 in the *normal* state during the information part of the burst.

In the *normal* state, the value of  $\mu$  is updated with the timing error  $e_k$  provided from the TED. The updated value is kept to be in the range [0, 1] by the *mod-1* operator. If it becomes negative, the *mod-1* operator will add 1 to the value and flag *overflow=1* for one period. If the value becomes larger than 1, the *mod-1* operator will reduce it by 1, and flag *overflow=1* for one period. The design shown in Fig. 3.3 is for the case of  $T_{sym}$  about twice  $T_s$ . Hence, the down-sampler produces the sample at symbol rate  $(1/T_{sym})$  by selecting one of the two samples at the sampling rate  $(1/T_s)$ . The selection of this odd or even sample is controlled by the *mod-2* operator based on the status of the updated value of  $\mu$ .

The end of the Tx burst is detected either by its length or power detection to reactivate the feedforward estimator during the *unlock* state. The cycle of 4 states is continued.

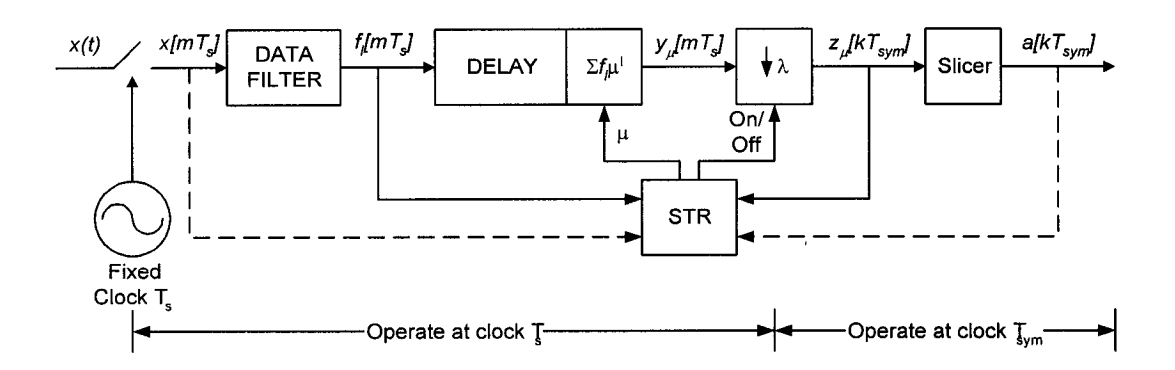


Fig. 3.1: Simplified block diagram of an all-digital receiver

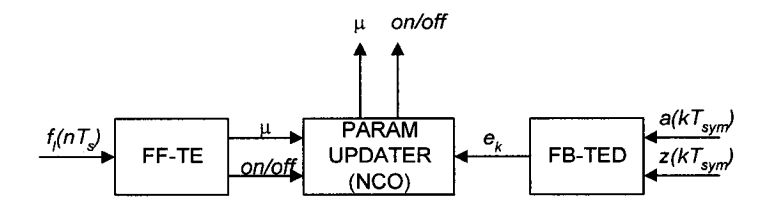


Fig. 3.2: Components of the symbol-timing recovery block

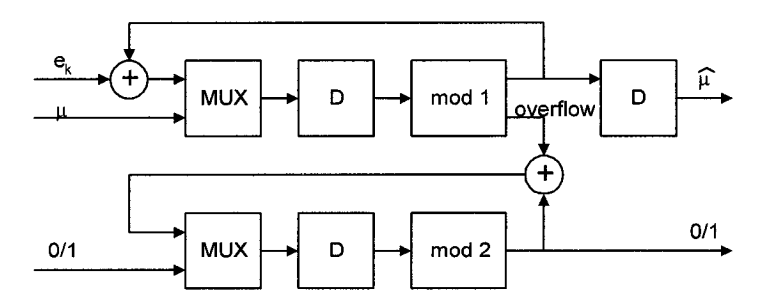


Fig. 3.3: A simple parameter updater

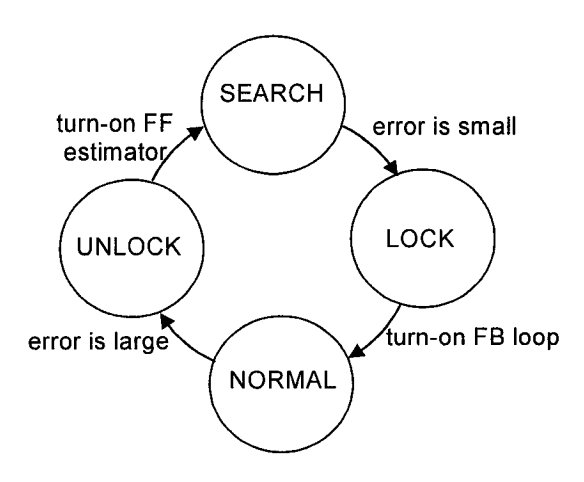


Fig. 3.4: A simple control state diagram

#### 3.2 Representation of Received Baseband Signals

We consider a baseband component received from a pulse-amplitude modulated (PAM) transmitter. The main system assumptions are summarized in Table 3.1. The baseband component received at the matched filter output is given by

$$x(t) = \sum_{n} a_{n}g(t - \tau + nT_{sym}) + \frac{\eta(t)}{\sqrt{E_{h}}}$$
(3.1)

where

 $a_n$ : Baseband transmitted symbol, which is a known symbol used in the preamble for timing estimation, and a random symbol in the information part.

 $T_{sym}$ : Symbol period.

au: Unknown symbol phase or time delay due to either channel delay or sampling clock;  $0 \le au < T_{sym}$ .

g(t): Baseband pulse. In most practical design, this pulse is the impulse response of a raised cosine filter [59],

$$g(t) = \frac{\sin(\pi t/T_{sym})}{\pi t/T_{sym}} \frac{\cos(\beta \pi t/T_{sym})}{1 - (2\beta t/T_{sym})^2}$$

where  $\beta$  is the roll-off factor.

 $\eta(t)$ : Filtered noise after the matched filter, i.e., root raised-cosine filter. In most cases, it is modeled as an additive Gaussian noise.

 $E_b$ : Bit energy.

A typical received PAM signal burst is shown in Figure 3.5.

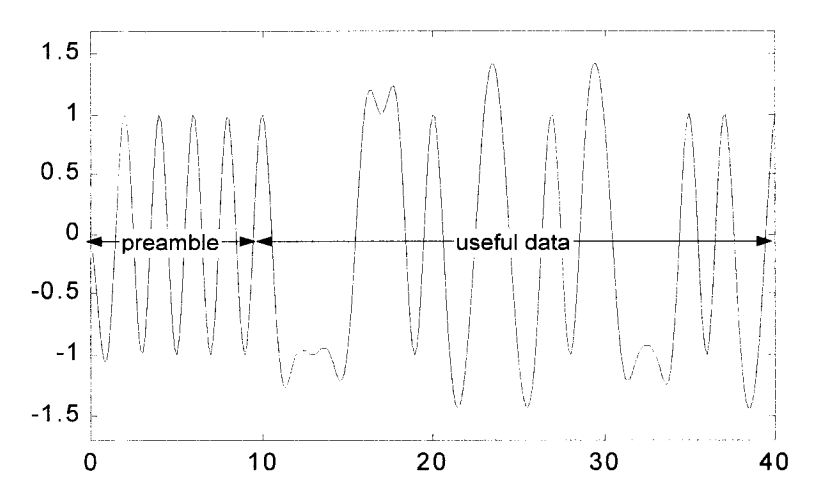


Fig. 3.5: Typical PAM-2 burst

In this chapter, we assume the symbol rate is known and the sampling interval is  $T_s = 0.5T_{sym}$ . However, the symbol phase is unknown, but constant during burst. In most practice, the difference in frequency between the sampling and transmitted symbol clocks is within a required tolerance, e.g., 0.01% [49].

1 Data is transmitted in burst-mode, and modulated in PAM signal.
2 Pulse shaping filter is a raised cosine filter
3 AWGN channels
4 Known signal sampling rate (T<sub>sym</sub>/T<sub>s</sub>) is close to 2
5 Symbol Clock phase is unknown, but constant during bursts

Table 3.1: Assumptions for the proposed STR

For the sake of simplicity in synchronizer's operation, in all cases the baseband pulse

g(t) can be approximated as [59, Chapter 2.2.3]

$$g(t) = \begin{cases} (1/2)(1 + \cos(\pi t/T_{sym})) \text{ for } |t| < T_{sym} \\ 0 \text{ otherwise} \end{cases}$$
(3.2)

We can verify that, for the alternative input sequence  $a_n = (-1)^n$ , the signal portion in (3.1) becomes

$$x(t) = \sum_{n} (-1)^{n} g(t - \tau - nT_{sym})$$

$$= \sum_{2n} g(t - \tau - 2nT_{sym}) - \sum_{2n+1} g(t - \tau - (2n+1)T_{sym})$$

$$= \frac{1}{2} (1 + \cos(\pi(t - \tau)/T_{sym})) - \frac{1}{2} (1 + \cos(\pi(t - \tau + T_{sym})/T_{sym}))$$

$$= \cos(\pi(t - \tau)/T_{sym})$$

Therefore, the received signal can be simplified as

$$x(t) = \cos\left(\frac{\pi(t-\tau)}{T_{sym}}\right) + \frac{\eta(t)}{\sqrt{E_b}}$$
(3.3)

#### 3.3 Maximum-Likelihood Estimation Technique

The received signal in Equation (3.1) is sampled at rate  $1/T_s$  to produce a sampled version

$$x(kT_s) = \sum_{m_1} a_{m_1} g(kT_s - \tau - m_1 T_{sym}) + \frac{\eta(kT_s)}{\sqrt{E_b}}$$
 (3.4)

where  $\tau$  is the unknown timing delay  $(0 \le \tau < T_{sym})$  to be determined. We limit the discussions to the case  $T_{sym}/T_s = \lambda$ , where  $\lambda$  is an integer. The timing delay can be

expressed as

$$\tau = iT_s + \mu T_s \tag{3.5}$$

$$0 \le i < \lambda$$
, and  $0 \le \mu < 1$  (3.6)

where i is an integer timing interval and  $\mu$  is a timing fraction. Therefore, the samples can be given by

$$x(kT_s) = \sum_{m_1} a_{m_1} g(kT_s - m_1 T_{sym} - iT_s - \mu T_s) + \frac{\eta(kT_s)}{\sqrt{E_h}}$$
(3.7)

The target of this work is to find the unknown timing delay  $\tau$ , or equivalently the timing fraction  $\mu$ . The discrete version is then passed through an interpolation filter  $h_{\hat{\mu}}(kT_s) = h((k+\hat{\mu})T_s)$  in order to reconstruct the signal at the estimated timing instant  $\hat{\mu}$ . The reconstructed signal output (without noise) will be

$$y((k+\hat{\mu})T_s) = \sum_{m_2} x((k-m_2)T_s)h_{\hat{\mu}}(m_2T_s)$$

$$= \sum_{m_1} \sum_{m_2} a_{m_1} g(kT_s - m_2T_s - m_1T_{sym} - iT_s - \mu T_s)h_{\hat{\mu}}(m_2T_s)$$
(3.8)

Given that the symbol detection will need to down-sample the sequence  $y((k+m)T_s)$  with the rate of  $\lambda$  at the correct timing delay, the output after the downsampler at time instant  $\hat{\tau} = (i + \hat{\mu})T_s$  will be

$$z(nT_{sym} + \hat{\tau}) = z(n\lambda T_s + iT_s + \hat{\mu}T_s) = y(((n\lambda + i) + \hat{\mu})T_s) + \frac{\eta(nT_{sym})}{\sqrt{E_b}}$$
(3.9)

Substituting (3.7) and (3.8) into (3.9), we obtain

$$z_{n}(\hat{\tau}) = \sum_{m_{1}} \sum_{m_{2}} a_{m_{1}} g(n\lambda T_{s} - m_{1} T_{sym} - (m_{2} + \mu)) h_{\mu}(m_{2} T_{s}) + \frac{\eta(n T_{sym})}{\sqrt{E_{b}}}$$

$$= \sum_{m_1} \sum_{m_2} a_{m_1} g((n-m_1) T_{sym} - (m_2 + \mu) T_s) h_{\mu}(m_2 T_s) + \frac{\eta(n T_{sym})}{\sqrt{E_b}}$$

In the ideal case, if h(t) is an interpolation function, and timing information can be

recovered such that  $\hat{\tau} = \tau$  or equivalently  $\hat{\mu} = \mu$ , then

$$\sum_{m_2} g((n-m_1)T_{sym} - (m_2 + \mu)T_s) h_{\hat{\mu}}(m_2T_s) \Big|_{\hat{\mu} = \mu} \cong g(nT_{sym} - m_1T_{sym})$$

$$|z_n(\hat{\tau})|_{\hat{\tau} = \tau} \cong \sum_{m_1} a_{m_1} g(nT_{sym} - m_1 T_{sym}) + \frac{\eta(nT_{sym})}{\sqrt{E_b}} = a_n + e_{\eta}$$

For an impulse response g(t) satisfying the ISI-free (Nyquist) conditions, i.e.,  $g(kT_{sym})=1$  for k=0 and =0 for non-zero k, the detected symbol at the timing instant  $\hat{\tau}$  will be

$$z(nT_{SVm} + \hat{\tau}) = z_n(\hat{\tau}) = a_n + e_{ISI}(\Delta \tau) + e_h(\hat{\tau}) + e_n$$
 (3.10)

where,  $\Delta \tau = \tau - \hat{\tau}$  denotes the timing error;  $e_h(\hat{\tau})$  denotes the imperfection interpolation error caused by the interpolation function h(t);  $e_{ISI}(\Delta \tau)$  denotes the inter-symbol interference (ISI) error due to the imperfection of timing estimation; and  $e_{\eta}$  denotes the error due to the AWGN. If exact timing and perfect interpolation filter can be obtained,  $e_h(\hat{\tau})$  and  $e_{ISI}(\Delta \tau)$  are negligible. Therefore, for the sake of simplicity, we can assume only Gaussian noise  $e_{\eta}$  would contribute towards the performance of the symbol detection process.

Assuming  $\hat{\tau} = \tau$  for perfect synchronization, an optimal detection is to recover the sequence  $a = \{a_0, a_1, ..., a_{N-1}\}$  from the noisy sequence  $z(\tau) = \{z_0(\tau), z_1(\tau), ..., z_{N-1}(\tau)\}$  with minimum error probability. Therefore, given that a sequence of N symbols is transmitted, the detection process can be summarized as

$$\max(p(\boldsymbol{a}|\boldsymbol{z}(\tau))) = \max \frac{p(\boldsymbol{z}(\tau)|\boldsymbol{a})p(\boldsymbol{a})}{p(\boldsymbol{z}(\tau))} = \max(p(\boldsymbol{z}(\tau)|\boldsymbol{a}))$$
(3.11)

in which we assume equally probable data sequence, and the distribution of  $z(\tau)$  is independent to the detection process. The data-aided maximum likelihood (ML) timing estimation is

$$L(\tau)_{DA} = max(p(z(\tau)|a))$$

$$= max \left( \left( \frac{1}{\sqrt{2\pi}\sigma} \right)^{N} \exp \left( -\frac{1}{2\sigma^{2}} \| \boldsymbol{z}(\tau) - \boldsymbol{a} \|^{2} \right) \right)$$

$$= max(-\|\mathbf{z}(\tau) - \mathbf{a}\|^2)$$

$$= max(-\sum_{n=0}^{N-1} z_n^2(\tau) + 2\sum_{n=0}^{N-1} a_n z_n(\tau) - \sum_{n=0}^{N-1} a_n^2)$$

Since the sequence  $\{a_n\}$  is known, and  $\{z_n(\tau)\}$  is independent of the detection process, we can simplify the maximum-likelihood (ML) equation as

$$L(\tau)_{DA} = \max(\sum_{n=0}^{N-1} a_n z_n(\tau)) = \max(\boldsymbol{a} \cdot \boldsymbol{z}(\tau))$$
(3.12)

#### 3.4 Derivation of the Proposed Algorithm

This section presents the timing estimation algorithm based on (3.12). Because most receivers now preferably operate at the lowest sampling rate, in this section, the feedforward, ML timing estimation algorithm is only discussed for the sampling rate of 2 and PAM systems. However, the algorithm is applicable to higher sampling rates and QAM systems, and will be discussed in Chapter 6.

Recall that the output of the interpolation filter is a function of  $\hat{\mu}$ .

$$y_{\hat{\mu}}[n] = \sum_{l=0}^{L} f_{l}[n] \hat{\mu}^{l} = \sum_{l=0}^{L} \sum_{m=-M/2}^{M/2-1} c_{l}(m) x [n-m] \hat{\mu}^{l}$$
(3.13)

Following from (3.9), the output after the downsampling of 2 will be,

$$z_{\Omega}[n] = y_{\Omega}[2n+i] \tag{3.14}$$

where i = 0 or 1. Therefore, the ultimate goals of an interpolation-based STR are:

- 1. To detect in which sampling interval, a correct symbol detection can be taken. This will be corresponding to finding the appropriate value of i (0 or 1).
- 2. To detect the correct timing information  $\mu$  for best signal reconstructing from the interpolation filter.

These two goals will be proceeded with the optimal criterion as described next.

Substituting (3.13) and (3.14) into (3.12), the ML function for the *i*-th sampling interval is

$$L_{i}(\hat{\mu}) = \sum_{n=0}^{N-1} a_{n} \sum_{l=0}^{L} f_{l}[2n+i]\hat{\mu}^{l}$$

$$= \sum_{l=0}^{L} \hat{\mu}^{l} \left( \sum_{n=0}^{N-1} a_{n} f_{l}[2n+i] \right)$$

$$= \sum_{l=0}^{L} \hat{\mu}^{l} E[a_{n} f_{l}[2n+i]]$$
(3.15)

Since the alternative sequence,  $a[n]=(-1)^n$ , is applied as the training symbols in order to improve the estimation process (Section 5.2), the likelihood function becomes

$$L_{i}(\hat{\mu}) = \sum_{l=0}^{L} \hat{\mu}^{l} E[(-1)^{n} f_{l}[2n+i]]$$
(3.16)

With the structure shown in Figure 3.1, for every symbol period  $T_{sym}=2T_s$ , the STR algorithm will generally generate two values of  $\hat{\mu}_1$  and  $\hat{\mu}_2$  for the time intervals  $[2k, 2k+1]T_s$  and  $[2k+1, 2k+2]T_s$  respectively. However, there exists only one maximum point for (3.16) in  $[2k, 2k+2]T_s$  (Section 5.2), which corresponds only to either  $\hat{\mu}_1$  or  $\hat{\mu}_2$ . This raises the question, "What is the appropriate method to select the correct  $\hat{\mu}$ ?" Some authors ([44]) suggested that the correct  $\hat{\mu}$  would be the one that gives a greater value of  $L_i(\hat{\mu})$ . However, this requires one more step of complex computation of  $L_i(\hat{\mu})$ . This section presents another approach that can directly give the value of  $\hat{\mu}$  without computing  $L_i(\hat{\mu})$ .

Second-order polynomial is used to approximate the likelihood function in (3.16) for its simplicity. The main disadvantage of using second-order polynomials is that, in general, a low-order polynomial cannot offer a reconstruction quality as good as higher order polynomials. However, as to be shown in Section 5.2, second-order interpolators can offer as good signal quality as the third-order one in reconstructing the sine waveforms. Furthermore, as shown Section 2.3, symmetric second-order interpolators

order polynomials is that their single maximum or minimum points are very simple to calculate. Higher order polynomials usually have more than one extreme points and the solutions require highly complex implementation. Furthermore, as to be shown in Section 5.2, for the likelihood function (3.16), there exists one and only one maximum point in the entire  $[2k, 2k+2]T_s$  intervals. Thus, the second-order polynomial is the simplest and best approximation.

By letting the derivative of the ML function equal to zero, we can find the maximum value of the ML function, i.e.,

$$\frac{\partial}{\partial \hat{\mu}} L_i(\hat{\mu}) \Big|_{\hat{\mu} = \mu} = \sum_{l=1}^2 l \hat{\mu}^{l-1} E[a_n f_l[2n+i]] \Big|_{\hat{\mu} = \mu} = 0$$
(3.17)

The solution of this equation is the estimated timing phase information,

$$\hat{\mu}[i] = -\frac{\sum_{n=0}^{N-1} ((-1)^n f_1[2n+i])}{\sum_{n=0}^{N-1} ((-1)^n f_2[2n+i])} \approx -\frac{E[(-1)^n f_1[2n+i]]}{2E[(-1)^n f_2[2n+i]]}$$
(3.18)

Because there exists one and only one extreme in the interval  $[2n, 2n+2]T_s$ , n=0,1,..., the estimation at the extreme infers that: if at the interval  $[2n, 2n+1]T_s$ , we get the maximum, i.e.,  $0 \le \hat{\mu}[0] \le 1$ , then the value of  $\hat{\mu}[1]$  calculated during the interval  $[2n+1, 2n+2]T_s$  must be the extreme point of the interval  $[2n, 2n+1]T_s$ , i.e.,  $\hat{\mu}[1] \notin [0, 1]$ . Theoretically, we want to have the distance between estimated values as far as possible so that under noise contribution, the detection algorithm will result in only one distinct correct estimated timing. Thus, the necessary condition for good decision-making is

$$|\hat{\mu}[0] - \hat{\mu}[1]| \ge 1 \tag{3.19}$$

It has been shown that for the raised cosine filter impulse response g(t), and the transmitted alternating  $\{+A, -A\}$  data sequence, the output of the matched filter at the receiver can be represented as a cosine waveform with the Gaussian noise component

 $\eta(t)$ , i.e., for  $T_{sym}=2T_s$ ,

$$x(t) = \cos\left(\frac{\pi}{2}\left(\frac{t}{T_s} - \mu\right)\right) + \frac{\eta(t)}{\sqrt{E_b}}$$
 (3.20)

where  $\mu$  is *uniformly* distributed in [0,1). Figure 3.6 shows the continuous output example when  $\mu$ =0.3. The discrete signal at every sampling period  $nT_s$  is

$$x[n] = \cos\left(\frac{\pi}{2}(n-\mu)\right) + \frac{\eta[n]}{\sqrt{E_h}}$$
(3.21)

where we ignore the time unit  $T_s$  in the expression of x[n].

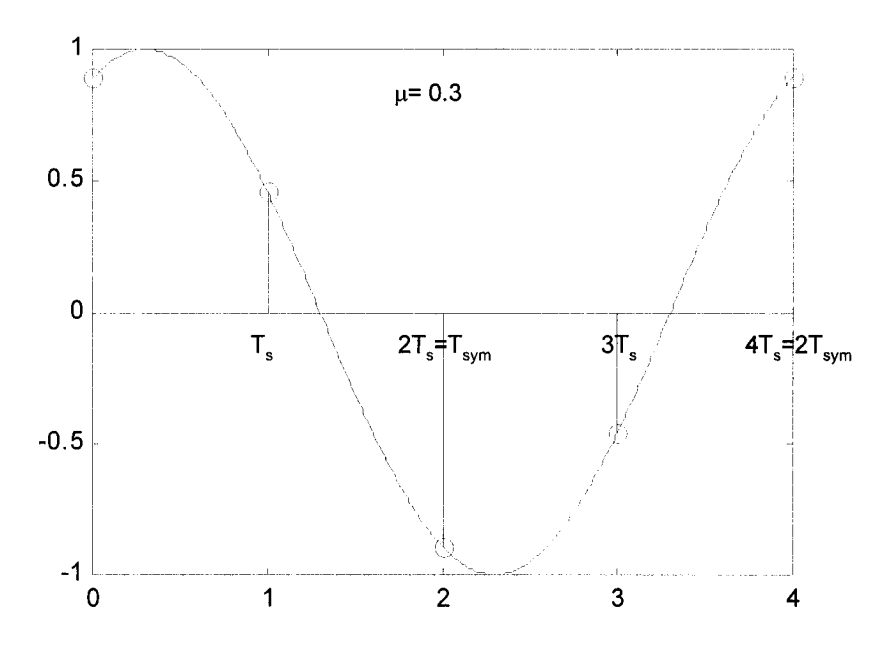


Fig. 3.6: Cosine wave at sampling points

Recall that,

$$f_{l}[2n+i] = \sum_{m=-M/2}^{M/2-1} x[2n+i-m]c_{l}(m)$$
(3.22)

Substituting (3.21) into (3.22), we have

$$E[(-1)^{n} f_{l}[2n+i]] \cong E\left[(-1)^{n} \sum_{m=-M/2}^{M/2-1} \left(\cos\left(\frac{\pi}{2}(2n+i-m-\mu)\right) + \frac{\eta[2n+i-m]}{\sqrt{E_{b}}}\right) c_{l}(m)\right]$$

$$E[(-1)^{n} f_{l}[2n+i]] \cong \sum_{m=-M/2}^{M/2-1} c_{l}(m) E\Big[(-1)^{n} \cos\Big(\frac{\pi}{2}(2n+i-m-\mu)\Big)\Big]$$
(3.23)

where  $E[\eta[n]] \cong 0$ 

$$E[(-1)^{n} f_{l}[2n+i]] \cong \sum_{m=-M/2}^{M/2-1} c_{l}(m) \cos\left(\frac{\pi}{2}(i-m-\mu)\right)$$
(3.24)

Therefore, for the case of no noise or high SNR, the timing phase estimation in (3.18) converges to

$$\hat{\mu}[i] \to -\frac{\sum_{m=-M/2}^{M/2-1} c_1(m) \cos\left(\frac{\pi}{2}(i-m-\mu)\right)}{2\sum_{m=-M/2}^{M-1} c_2(m) \cos\left(\frac{\pi}{2}(i-m-\mu)\right)}$$
(3.25)

For the sake of simplicity in measuring the error, one should remove the ambiguity that the decision interval  $iT_s$  might cause. By examining the waveform of x(t) in Fig. 3.6, we can see that the maximum point lies in the interval  $[0, T_s]$ ; thus the ML algorithm must choose this as a valid interval, i.e., i=0. The timing estimation error (normalized to  $T_{sym}$ ) can be given as

$$e_{\tau} = \frac{T_s}{T_{sym}} \left( \mu + \frac{\sum_{m=-M/2}^{M/2-1} c_1(m) \cos\left(\frac{\pi}{2}(-m-\mu)\right)}{\sum_{m=-M/2}^{M/2-1} c_2(m) \cos\left(\frac{\pi}{2}(-m-\mu)\right)} \right)$$
(3.26)

This approximation is in general form which can be applied for any structure of interpolation filters. In the next section, we will introduce an alternative, simpler version of  $e_{\tau}$  for the separate interpolation filters. This general form can be used to study the

boundary of the error of the estimation or to provide constraints on the design of second order polynomial interpolation filters with respect to (3.19) and to minimize the MSE of the timing estimation.

### 3.5 MSE in symbol-timing estimation of some secondorder interpolators

Equation (3.26) is used to compute the MSE in timing estimation of the following interpolation filters.

- 1 The piece-wise parabolic interpolation filter with  $\gamma = 0.5$ .
- 2 The piece-wise parabolic interpolation filter with  $\gamma = 0.45$ .
- 3- Vesma's optimal interpolation filter I for M = 4 (Table A.4) [13].
- 4- Vesma's optimal interpolation filter II for M = 6 (Table A.5) [13].

Interpolation Filters	MSE
Parabolic with $\gamma = 0.5$	2.7x10 <sup>-4</sup>
Parabolic with $\gamma = 0.45$	0.8x10 <sup>-4</sup>
Vesma Interpolation Filter I	8.9x10 <sup>-4</sup>
Vesma Interpolation Filter II	1.0x10 <sup>-4</sup>

Table 3.2: MSE of timing estimation

The results in Table 3.2 indicate that the Vesma Interpolation Filter I yields the highest MSE. The parabolic with 4 tap-length ( $\gamma$ =0.45) has a better MSE than Vesma's Filter II with 6 tap-length.

The above results motivate a further investigation on how to optimize the Lagrange parabolic filters to achieve the minimum MSE for timing estimation.

Following from (3.25), the estimation of  $\mu$  for the second-order Lagrange interpolator

is evaluated as

$$\hat{\mu}[i] \cong -\frac{(1-2\gamma)\cos\left(\frac{\pi}{2}(i-\mu)\right) - (1+2\gamma)\sin\left(\frac{\pi}{2}(i-\mu)\right)}{4\gamma\left(\cos\left(\frac{\pi}{2}(i-\mu)\right) - \sin\left(\frac{\pi}{2}(i-\mu)\right)\right)}$$
(3.27)

or

$$\hat{\mu}[i] \cong \frac{1}{2} - \frac{\sin\left(\frac{\pi}{2}(i-\mu)\right) + \cos\left(\frac{\pi}{2}(i-\mu)\right)}{4\gamma\left(\cos\left(\frac{\pi}{2}(i-\mu)\right) - \sin\left(\frac{\pi}{2}(i-\mu)\right)\right)}$$
(3.28)

$$\hat{\mu}[i] \cong \frac{1}{2} - \frac{1}{4\gamma} \tan\left(\frac{\pi}{2}\left(i - \mu + \frac{1}{2}\right)\right) \tag{3.29}$$

The symbol timing estimation error, normalized to  $T_{sym}$ , is given as

$$e_{\tau} = \frac{T_s}{T_{svm}} (\mu - \hat{\mu}) = \frac{1}{2} \left( \mu - \frac{1}{2} + \frac{1}{4\gamma} \tan \left( \frac{\pi}{2} \left( \frac{1}{2} - \mu \right) \right) \right)$$
 (3.30)

The variance of this timing estimation error is

$$VAR[e_{\tau}] = \frac{1}{32\gamma^2} \left(\frac{4}{\pi} - 1\right) - \frac{1.4863}{4\gamma\pi^2} + \frac{1}{24}$$
 (3.31)

and its plot is shown in Figure 3.7. The S-curves for two cases,  $\gamma = 0.5$  and  $\gamma_{optimal} = 0.4536$ , are plotted in Figure 3.8.

We will have to verify the condition given in (3.19):

$$|\hat{\mu}[0] - \hat{\mu}[1]| = \frac{1}{4\gamma} \left| \tan\left(\frac{\pi}{2}\left(-\mu - \frac{1}{2}\right)\right) - \tan\left(\frac{\pi}{2}\left(-\mu + \frac{1}{2}\right)\right) \right|$$
(3.32)

$$= \frac{1}{4\gamma} \left| \tan\left(\frac{\pi}{2}\left(-\mu + \frac{1}{2}\right)\right) + \frac{1}{\tan\left(\frac{\pi}{2}\left(-\mu + \frac{1}{2}\right)\right)} \right| \ge \frac{1}{2\gamma}$$
 (3.33)

where  $\left| a + \frac{1}{a} \right| \ge 2$ ,  $\forall (a \in R)$ .

Therefore the given condition can be always satisfied when  $1/(2\gamma) > 1$ , or  $\gamma < 1/2$ . Thus the optimal value also satisfies the condition given in (3.19).

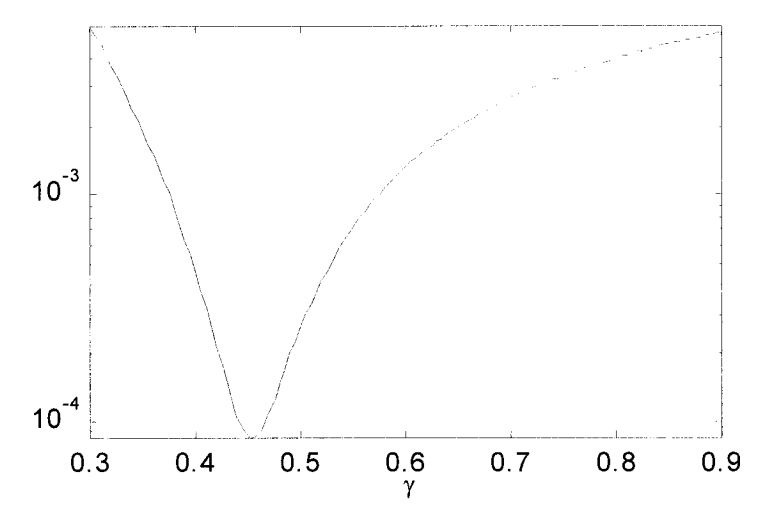


Fig. 3.7: MSE of timing function versus  $\gamma$ .

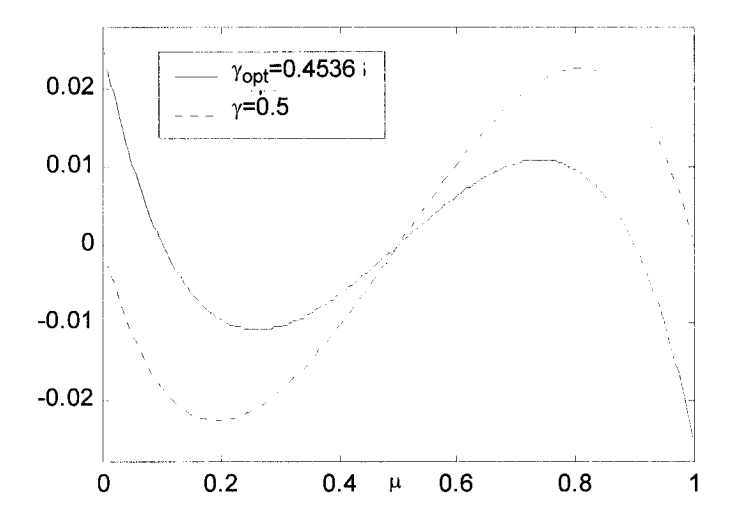


Fig. 3.8: Symbol Timing Error versus  $\mu$ .

#### 3.6 Estimation of Symbol Frequency

The proposed algorithm in Section 3.4 was presented with an assumption that  $T_{sym}/T_s$  is an integer. In practice, this ratio  $(T_{sym}/T_s)$  is rarely an exact integer. In the case of non-integer  $T_{sym}/T_s$ , the proposed algorithm will be applied first, and other successive estimates are needed at later steps to track the fluctuation of the symbol frequency with time.

Define the following relationship

$$\frac{T_{sym}}{T_s} = \lambda + \Delta\lambda \tag{3.34}$$

where,  $\lambda$  is an integer, and  $\Delta\lambda$  is fractional. Assume at the *m*-th and *n*-th sampling time, we measure the *k*-th and *l*-th symbol time (Figure 3.9),

$$kT_{svm} = (m + \mu_k)T_s \tag{3.35}$$

$$lT_{sym} = (n + \mu_l)T_s \tag{3.36}$$

For P = n - m and Q = l - k, it is easy to show that

$$\Delta \lambda_{l,k} = \frac{P}{Q} + \frac{1}{Q} (\mu_l - \mu_k) - \lambda \tag{3.37}$$

In the case of single step or Q=l-k=1, the equation can be simplified as

$$\Delta \lambda_k = P_k + (\mu_{k+1} - \mu_k) - \lambda \tag{3.38}$$

We notice that the result in (3.37) is the average of (3.38) over the window size Q:

$$\Delta \lambda_{l, k} = E[\Delta \lambda_{k}] \tag{3.39}$$

Equations (3.37) to (3.39) can be used to estimate the symbol frequency fraction and we need to correct the estimated timing with this fraction.

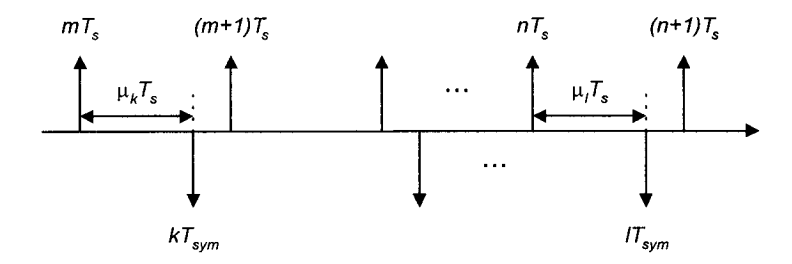


Fig. 3.9: Samples at different estimate time

#### 3.7 Conclusion

We have presented a new symbol timing recovery scheme (STR) for asynchronous data receivers for the case of  $T_{sym}/T_s$ =2. The general structure and theoretical background of the proposed STR scheme are discussed. Timing errors were formulated for further analysis and simulation. Moreover, performance of some second-order interpolators applied to the proposed algorithm is investigated. Techniques to estimate and correct frequency error were discussed. As implementation is concerned, computations are greatly reduced: only short simple averaging filters and one simple division are required. This implies lower complexity and faster operations for hardware implementation.

# Chapter 4. Optimal Interpolation Filters for Digital STR

The main objective of an interpolation/resampling filter is to reproduce the samples of an analog signal at the *desired* instants with no or minimum distortion from a given sampled version. As discussed, if the original analog signal is bandlimited then a rectangular filter with bandwidth slightly larger than that of the signal is a good choice. However, using an FIR implementation of sampled signal, the impulse response of the interpolation filter needs be truncated in time. Furthermore, for a simple structure of the interpolator/resampler using polynomial approximation, the actual implementation is deviated from the rectangular filter shape.

Designing *optimum* interpolation filters for a certain objective has been discussed in the literature. Bucket and Moeneclaey [39] showed how to optimize the piece-wise parabolic interpolation filter to minimize the output BER in the assumption of correctly established symbol timing. Various filter design methodologies aim to minimize the mean-square error (MSE) at the output of the receiver [1], [19], [49] or the output BER [39]. It is expected that the MSE in timing estimation is indirectly made small [49, Chapter 3.2.3]. Other papers [2]-[13] presented different optimization approaches in the context of digital signal processing without consideration of communication aspects.

The optimization algorithm presented in this chapter takes into consideration the *desired* filter shape in terms of both time-domain and frequency-domain responses and the timing estimation performance. Desired time-domain and frequency-domain responses are derived from a particular system design requirements in out-of-band interference and noise suppression.

This chapter is organized as follows. Section 4.1 proposes the joint cost function, including the MSE in (i) matching the desired impulse response of the filter g(t), (ii) matching the desired frequency response of the filter G(f), and (iii) symbol timing estimation. Section 4.2 provides an efficient algorithm to search for optimal interpolator coefficients in order to minimize the proposed cost function. Section 4.3 presents the performance evaluation of the proposed algorithm by simulations. For low complexity, we will focus on integer sampling rate and second-order polynomial-based Farrow structure.

#### 4.1 Proposed Cost Function

The time-domain and frequency-domain responses of the interpolation filter are h(t), and H(f), respectively. They will be designed to match the *desired* time-domain and frequency-domain responses, g(t) and G(f), which are often symmetric. The MSE in time and frequency domains are defined as

$$E[e_{time}^2] = \oint (h(t) - g(t))^2 dt \tag{4.1}$$

$$E[e_{freq}^{2}] = \oint (H(f) - G(f))^{2} df$$
 (4.2)

Notice that we define the operations in (4.1), (4.2) for certain ranges of interest.

The MSE in STR is <sup>1</sup>

$$E[e_{STR}^2] \propto (\rho - \rho_{opt})^2 \tag{4.3}$$

<sup>&</sup>lt;sup>1</sup> The derivation of the MSE in STR will be presented in Chapters 6.

where

$$\rho_{opt} = -\frac{\sin\left(\frac{\pi}{2\lambda}\right)}{2\alpha_{opt}} \tag{4.4}$$

$$\rho = \sum_{k=0}^{M/2-1} c_2(k) \cos\left(\frac{\pi}{\lambda} \left(k + \frac{1}{2}\right)\right)$$
 (4.5)

We propose the cost function

$$J = w_{time} E[e_{time}^{2}] + w_{freq} E[e_{freq}^{2}] + w_{STR} E[e_{STR}^{2}]$$
 (4.6)

whereas  $e_{time}$ ,  $e_{freq}$  and  $e_{STR}$  are denoted for the time-, and frequency-domain error and timing detection error; and  $w_{time}$ ,  $w_{freq}$  and  $w_{STR}$  are their corresponding weighting factors.

The proposed cost function is essentially a generalization of the DSP design filter approach in [13] and the filter optimization process for STR in Chapters 5 and 6. Letting  $w_{STR}$ =0 will result similar filters as in [13], while the optimal interpolators presented in Chapter 5, and 6 are the solutions of (4.6) for  $w_{time}$ =0 and  $w_{freq}$ =0.

#### 4.2 Algorithm Derivation

The cost function (4.6) can be applied to a general interpolator. Its gradient is

$$\nabla_{m} J = \frac{\partial J}{\partial c_{2}(m)}$$

$$= w_{time} \frac{\partial}{\partial c_{2}(m)} E[e_{time}^{2}] + w_{freq} \frac{\partial}{\partial c_{2}(m)} E[e_{freq}^{2}] + w_{STR} \frac{\partial}{\partial c_{2}(m)} E[e_{STR}^{2}]$$
(4.7)

where k = 0, 1,..., M/2-1. The cost function J attains its optimum value, all the elements of the gradient operator must be simultaneously equal to zero, as shown by,

$$\nabla_m J = 0, \quad m = 0, 1, ..., M/2 - 1$$
 (4.8)

Under this set of conditions, the filter is said to be optimum in the mean-squared-error

sense.

We focus on the second-order polynomial for the interpolation filter for its simple structure in the following derivation.

From the definition (4.1), the time-domain criteria is

$$\frac{\partial}{\partial c_2(m)} E[e_{time}^2] = \int_{-M/2}^{M/2} 2(h(t) - g(t)) \frac{\partial}{\partial c_2(m)} h(t) dt$$

$$= \sum_k \int_0^1 2(h(k+\mu) - g(k+\mu)) \frac{\partial}{\partial c_2(m)} h(k+\mu) d\mu$$

$$\frac{\partial}{\partial c_2(m)} h(k+\mu) = (\mu^2 - \mu) \delta(m-k)$$
(4.9)

Therefore.

$$\frac{\partial}{\partial c_2(m)} E[e_{time}^2] = \sum_k \int_0^1 2(h(k+\mu) - g(k+\mu))(\mu^2 - \mu)\delta(m-k)d\mu$$

$$= 2 \int_0^1 (h(m+\mu) - g(m+\mu))(\mu^2 - \mu)d\mu$$

$$= 2 \int_0^1 (\delta(m) + (\delta(m+1) - \delta(m))\mu + c_2(m)(\mu^2 - \mu) - g(m+\mu))(\mu^2 - \mu)d\mu$$

$$= 2 \left(\frac{1}{30}c_2(m) - \frac{1}{12}(\delta(m) + \delta(m+1)) - \int_0^1 g(m+\mu)(\mu^2 - \mu)d\mu\right) \tag{4.10}$$

Following (4.2), the frequency-domain criteria is

$$\frac{\partial}{\partial c_2(m)} E[e_{freq}^2] = \int 2(H(f) - G(f)) \frac{\partial}{\partial c_2(m)} H(f) df$$
 (4.11)

$$\frac{\partial}{\partial c_2(m)} H(f) = B(2, -m-1) - B(1, -m-1) + B(2, m) - B(1, m)$$
 (4.12)

From (4.3) to (4.5), the STR criteria is

$$\frac{\partial}{\partial c_2(m)} E[e_{STR}^2] = 2(\rho - \rho_{opt}) \frac{\partial \rho}{\partial c_2(m)}$$
(4.13)

Therefore, the cost function can be rewritten as follows,

$$\begin{split} &\nabla_{m} J = 0 \\ &= 2w_{time} \left(\frac{1}{30}c_{2}(m) - \frac{1}{12}(\delta(m) + \delta(m+1)) - \int_{0}^{1}g(m+\mu)(\mu^{2} - \mu)d\mu\right) \\ &+ 2w_{freq} \mathfrak{q} \left(B(0,0) + B(1,-1) - B(1,0) - G(f) + \sum_{k=0}^{M/2-1} (B(2,-k-1) - B(1,-k-1) + B(2,k) - B(1,k))c_{2}(k)\right) \frac{\partial}{\partial c_{2}(m)} H(f)df \\ &+ 2w_{STR} \left(\sum_{k=0}^{M/2-1}c_{2}(k)\cos\left(\frac{\pi}{\lambda}(k+\frac{1}{2})\right) - \rho_{opt}\right)\cos\left(\frac{\pi}{\lambda}(m+\frac{1}{2})\right) \\ &= -2w_{time} \left(\frac{1}{12}(\delta(m) + \delta(m+1)) + \int_{0}^{1}g(m+\mu)(\mu^{2} - \mu)d\mu\right) \\ &+ 2w_{freq} \mathfrak{q} \left(B(0,0) + B(1,-1) - B(1,0) - G(f)\right) \frac{\partial}{\partial c_{2}(m)} H(f)df \\ &- 2w_{STR}\rho_{opt}\cos\left(\frac{\pi}{\lambda}(m+\frac{1}{2})\right) + \sum_{k=0}^{M/2-1}c_{2}(k) \\ &\left[2w_{time}\frac{\delta(m-k)}{30} + 2w_{STR}\cos\left(\frac{\pi}{\lambda}(k+\frac{1}{2})\right)\cos\left(\frac{\pi}{\lambda}(m+\frac{1}{2})\right) \\ &+ 2w_{freq} \mathfrak{q} \left(B(2,-k-1) - B(1,-k-1) + B(2,k) - B(1,k)\right) \frac{\partial H(f)}{\partial c_{2}(m)} df \right] \end{split}$$

Equation (4.14) can be expressed in a compact vector form,

$$\nabla_m J/2 = B(m) + A(m)X$$

$$= w_{time}B_{time}(m) + w_{freq}B_{freq}(m) + w_{STR}B_{STR}(m) + (w_{time}A_{time}(m) + w_{freq}A_{freq}(m) + w_{STR}A_{STR}(m))X$$

$$(4.15)$$

The vectors in (4.15) are defined as follows

$$A_{time}(m) = [A_{k, time}(m)] = \frac{\delta(m-k)}{30}$$
 (4.16)

$$A_{freq}(m) = [A_{k,freq}(m)] = \oint ((B(2,-k-1)-B(1,-k-1) + B(2,k)-B(1,k))(B(2,-m-1)-B(1,-m-1)+B(2,m)-B(1,m)))df$$
(4.17)

$$A_{STR}(m) = \left[A_{k,STR}(m)\right] = \cos\left(\frac{\pi}{\lambda}\left(k + \frac{1}{2}\right)\right)\cos\left(\frac{\pi}{\lambda}\left(m + \frac{1}{2}\right)\right)$$
(4.18)

$$X = [c_2(0), c_2(1), ..., c_2(M/2 - 1)]^T$$
(4.19)

$$B_{time}(m) = -\left(\frac{1}{12}(\delta(m) + \delta(m+1)) + \int g(m+\mu)(\mu^2 - \mu)d\mu\right)$$
(4.20)

$$B_{freq}(m) = \oint ((B(0,0) + B(1,-1) - B(1,0) - G(f))$$

$$(B(2,-m-1) - B(1,-m-1) + B(2,m) - B(1,m)))df$$
(4.21)

$$B_{STR}(m) = -\rho_{opt} \cos\left(\frac{\pi}{\lambda} \left(m + \frac{1}{2}\right)\right)$$
 (4.22)

Therefore, the Farrow coefficients are the solution X of the equation,

$$AX_{opt} + B = 0 (4.23)$$

$$\boldsymbol{X}_{ont} = -\boldsymbol{A}^{-1}\boldsymbol{B} \tag{4.24}$$

where, A = [A(m)], and B = [B(m)]

In some cases, the matrix A may be nearly singular, thus a deepest descent algorithm can be used to obtain the desired solution. The solution at time (n+1) is computed by using the following recursive relation,

$$X_{n+1} = X_n + \kappa[-\nabla J_n] \tag{4.25}$$

$$\nabla J_n = AX_n + B \tag{4.26}$$

where n is denoted for recursive time, and  $\kappa$  is a positive real-valued constant (step size).

#### 4.3 Design Examples

This section presents a design example for the case M = 4, L = 2. The desired impulse response is g(t)=sinc(t). In this example, we assume that the received baseband signal is shaped by a raised-cosine filter with an roll-off factor of 0.35, and then sampled at 2, 4, and 8 times faster than the symbol rate<sup>1</sup>. Because the sampling process introduces replicated frequency images centered at  $kf_s$ , in designing the optimum interpolation filter, we aim to suppress as much as possible such alias. Consider  $f_s$  normalized to 1. The signal frequency band is  $[0, 0.35f_{sym}]$ , while the images to be suppressed fall in the frequency bands  $[1-0.35f_{sym}, 1+0.35f_{sym}]$  and  $[2-0.35f_{sym}, 2]$ . Therefore, the desired frequency responses would be 1, 0, and 0 in the frequency band of interest  $[0, 0.35f_{sym}]$ ,  $[1-0.35f_{sym}, 1+0.35f_{sym}]$  and  $[2-0.35f_{sym}, 2]$ , respectively. For comparison, we carried out the filter designs for two objectives:

- I) Minimum MSE for STR only, and
- II) Minimum MSE for time-domain, frequency-domain responses, and STR.

The design parameters and objectives are summarized in Table 4.1.

Simulations with the parameters summarized in Table 4.2 are used to compare the performance of the obtained filters and two other interpolators:

- The Vesma's interpolator type I (Table A.4);
- The regular piece-wise parabolic interpolator ( $\gamma$ =0.5);

As discussed in Section 2.3, the modified Farrow structure for this new interpolator requires only 1 or 2 coefficients and multipliers. The optimum filter coefficients for the Farrow structure of the new interpolators are listed in Tables 4.4 and 4.3, respectively.

<sup>&</sup>lt;sup>1</sup> The integer rates are considered because they are used in the next sections. Non-integer rate might require another simulation setup.

Table 4.1: Design parameters

#### **Design parameters**

desired impulse response: g(t) = sinc(t); desired frequency responses: 1 for  $[0, 0.35f_{sym}]$ , 0 for  $[1-0.35f_{sym}, 1+0.35f_{sym}]$ , and  $[2-0.35f_{sym}, 2]$ ,

M = 4, L = 2

Sampling rates  $T_{sym}/T_s = 2$ , 4, and 8

Objectives: I) minimize MSE for STR only; II) minimize MSE jointly in time, frequency, and STR

**Table 4.2: Simulation Assumptions** 

Simulation Parameters		
PAM signal		
signal shaped by a root raised-cosine filter with a roll-off factor of 0.35		
Sampling rates $T_{sym}/T_s = 2$ , 4, and 8		
Ideal channel		
Perfect timing synchronization		

Table 4.3: Filter Coefficients for the Optimal Interpolators Type I

;	$c_2(i)$		
	$T_{sym}/T_s=2$	$T_{sym}/T_s=4$	$T_{sym}/T_s=8$
0	-0.4536	-0.2867	-0.2585
1	0.4536	-0.2867	0.2585

Table 4.4: Filter Coefficients for the Optimal Interpolators Type II

Three comparison criteria were considered, and the results are summarized in Tables 4.5 to 4.7, and plotted in Figures 4.1 to 4.4.

- a) Symbol Timing Estimation Error: The MSE of the symbol timing estimation for different interpolators are shown in Tables 4.5 to 4.7. As mentioned in Chapters 3, 5, and 6, these measurements show whether an interpolator is suitable to the proposed feedforward STR scheme. From Chapters 5, and 6, it is evident that only the new optimal interpolators can attain the minimum MSE of the symbol timing estimation.
- b) ISI Error: Non-ideal interpolator causes intersymbol interference (ISI) even at the perfect timing points. The MSE of the ISI error is measured at the decision points, between the recovered values and the expected values. Figure 4.1 shows the MSE of the four interpolators for various values of  $\mu$ , while Tables 4.5 to 4.7 gives the numerical values of the maximum ISI that occur at  $\mu = 0.5$ . The simulations show that the new interpolators have the best performance.
- c) Maximum image attenuation: This performance criteria is to measure the capability of reducing the effect of the frequency image. Figures 4.2 to 4.4 show the spectrum that demonstrate the behavior of the four interpolators to PAM signals shaped by a raised-cosine filter with a roll-off factor of 0.35. As observed in the results in Tables 4.5 to 4.7, the new interpolators provide an excellent image rejection.

Table 4.5: MSE of STR and ISI, and Maximum Image Attenuation  $(T_{svm}/T_s = 2)$ 

	MSE(e <sub>STR</sub> )	Max MSE(e <sub>ISI</sub> )	Max Image Attenuation (dB)
Vesma's method for <i>M</i> =4, L=2	8.9x10 <sup>-4</sup>	67x10 <sup>-4</sup>	-28.7

Table 4.5: MSE of STR and ISI, and Maximum Image Attenuation  $(T_{sym}/T_s = 2)$ 

	MSE(e <sub>STR</sub> )	Max MSE(e <sub>ISI</sub> )	Max Image Attenuation (dB)
Regular Interpolator	2.7x10 <sup>-4</sup>	31x10 <sup>-4</sup>	-29.5
Optimal Interpolator Type I	8x10 <sup>-5</sup>	15x10 <sup>-4</sup>	-31.6
Optimal Interpolator Type II	8x10 <sup>-5</sup>	8x10 <sup>-4</sup>	-32.8

Table 4.6: MSE of STR and ISI, and Maximum Image Attenuation  $(T_{sym}/T_s=4)$ 

	MSE(e <sub>STR</sub> )	Max MSE(e <sub>ISI</sub> )	Max Image Attenuation (dB)
Vesma's method for <i>M</i> =4	9.6x10 <sup>-6</sup>	5.31x10 <sup>-3</sup>	-32.8
Regular Interpolator	9.4x10 <sup>-4</sup>	9.04x10 <sup>-4</sup>	-39.1
Optimal Interpolator Type I	9.7x10 <sup>-7</sup>	3.86x10 <sup>-6</sup>	-55.5
Optimal Interpolator Type II	9.7x10 <sup>-7</sup>	1.96x10 <sup>-6</sup>	-56.1

Table 4.7: MSE of STR and ISI, and Maximum Image Attenuation  $(T_{sym}/T_s = 8)$ 

	MSE(e <sub>STR</sub> )	Max MSE(e <sub>ISI</sub> )	Max Image Attenuation (dB)
Vesma's method for <i>M</i> =4	2.3x10 <sup>-3</sup>	9.37x10 <sup>-3</sup>	-32.8
Regular Interpolator	3.0x10 <sup>-4</sup>	7.75x10 <sup>-5</sup>	-51.4
Optimal Interpolator Type I	1.43x10 <sup>-8</sup>	1.07x10 <sup>-8</sup>	-75.9
Optimal Interpolator Type II	1.43x10 <sup>-8</sup>	1.03x10 <sup>-8</sup>	-76.1

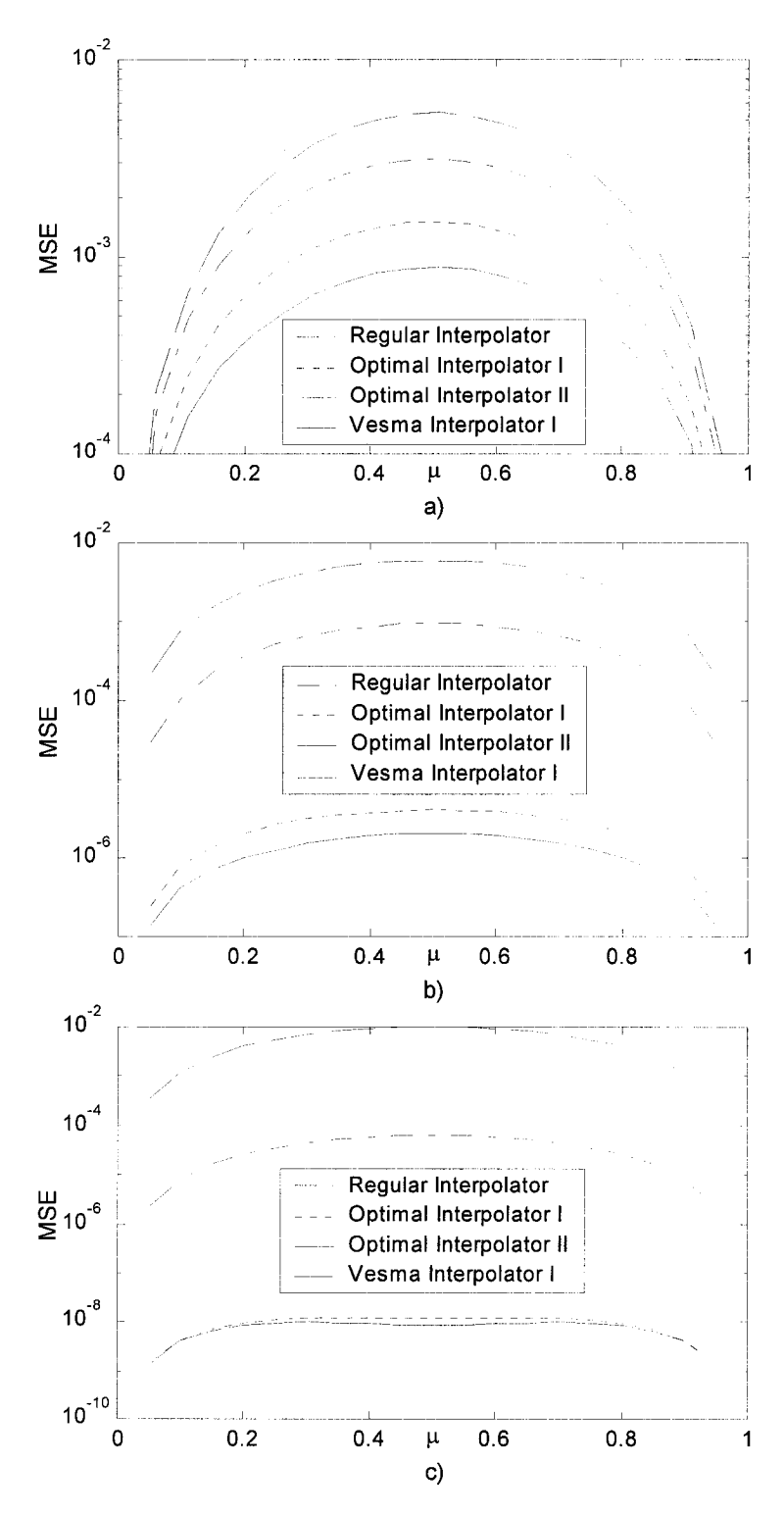


Fig. 4.1: MSE (ISI) at the decision points when  $T_{sym}/T_s$  is equal to a) 2, b) 4, c) 8

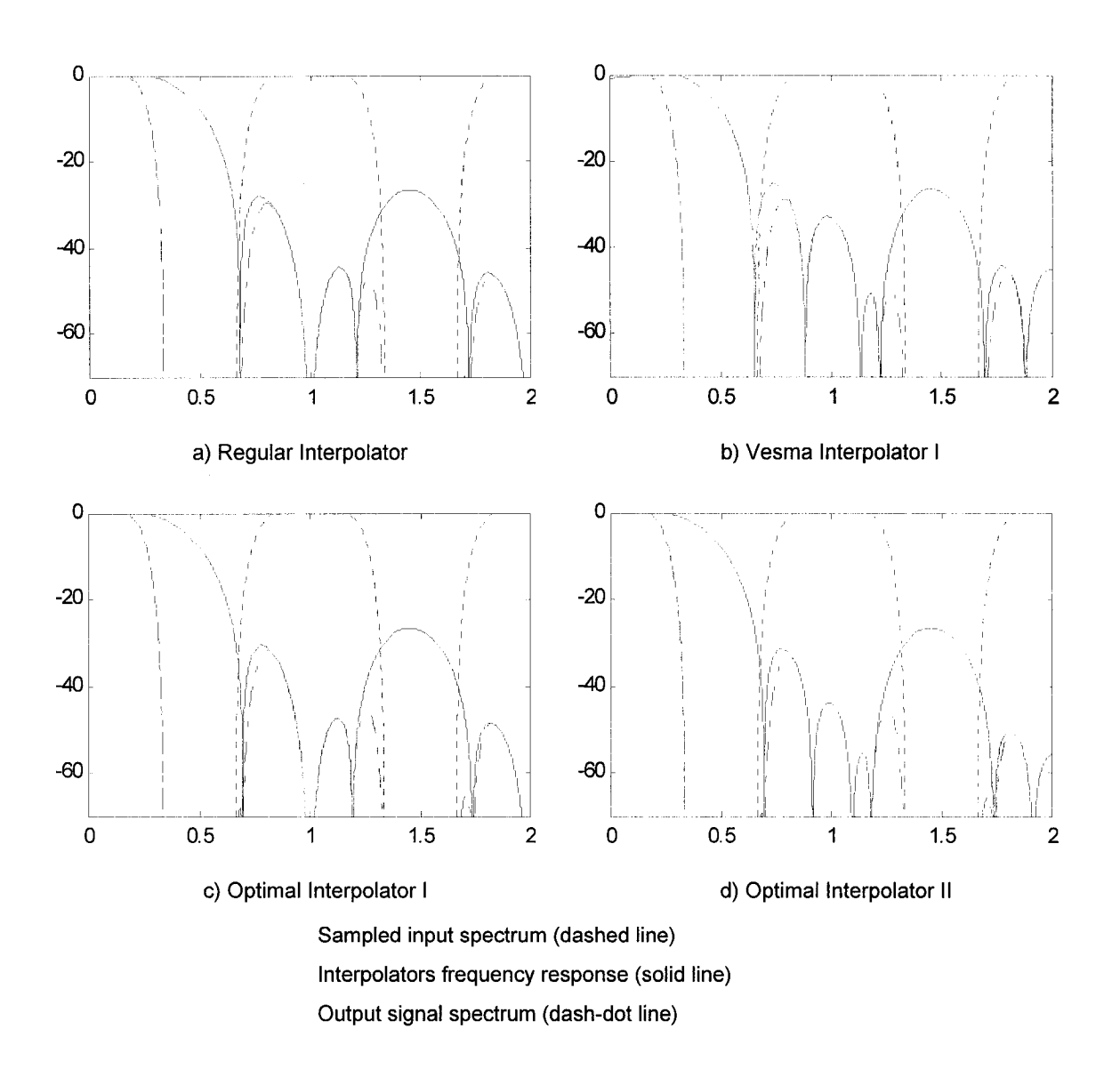


Fig. 4.2: Frequency responses of four interpolators  $(T_s/T_{sym}=2)$ 

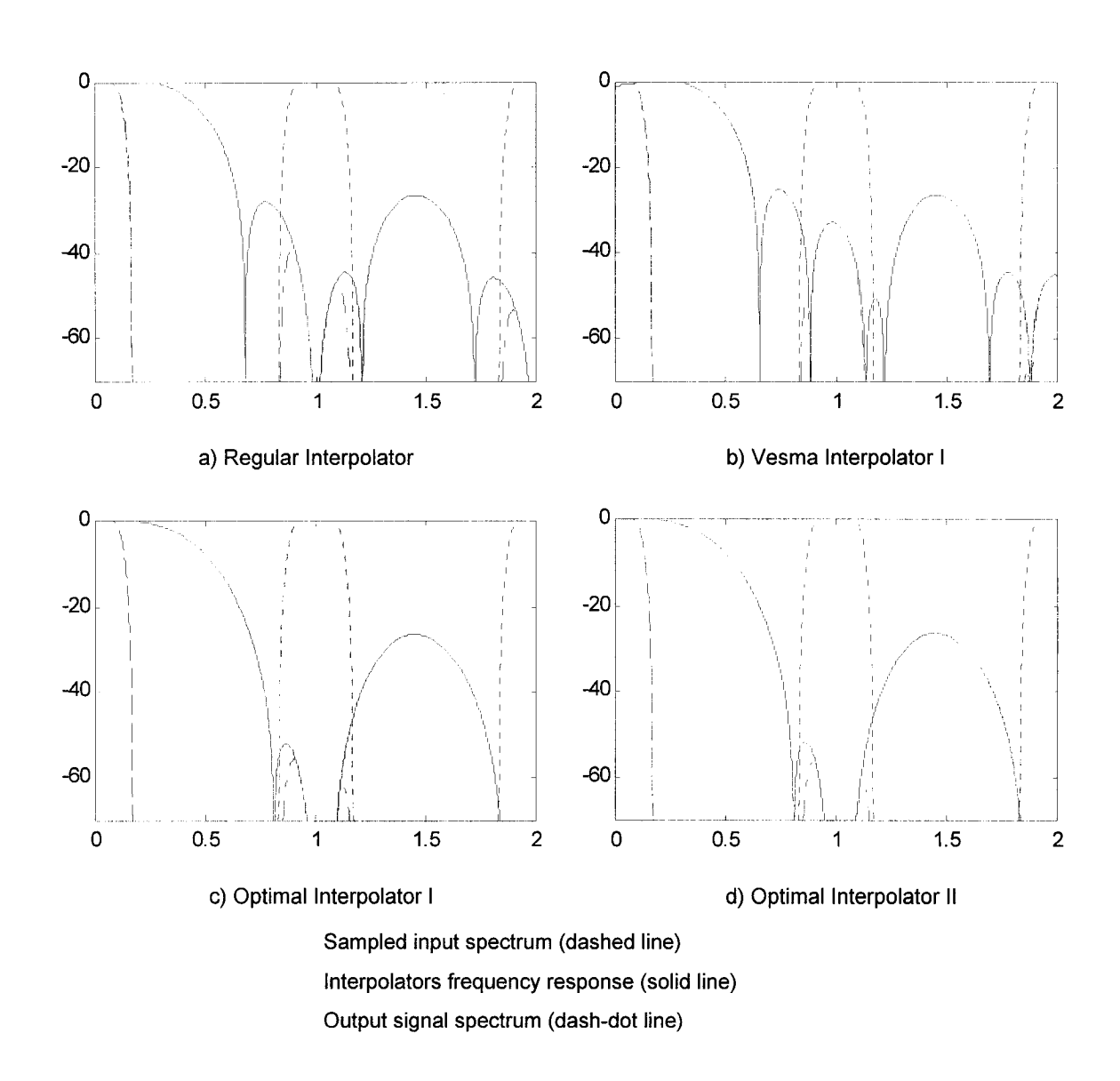


Fig. 4.3: Frequency responses of four interpolators  $(T_s/T_{sym}=4)$ .

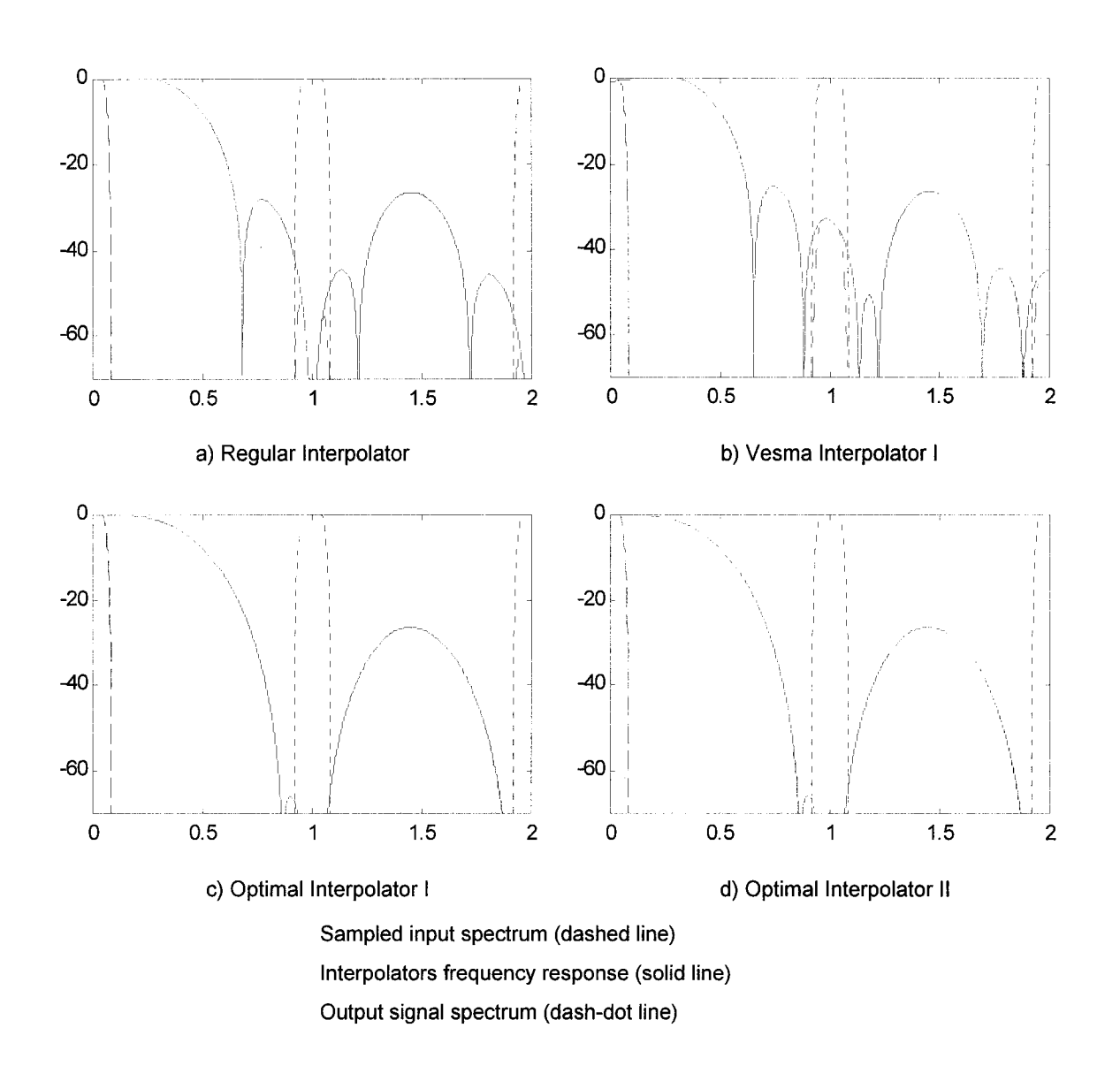


Fig. 4.4: Frequency responses of four interpolators  $(T_s/T_{sym}=8)$ .

#### 4.4 Conclusion

A new optimal, efficient filter design synthesis for interpolation filters is presented. The proposed cost function takes into consideration the desired time and frequency responses as well as the timing error, suitable for practical design objectives. Illustrative filter design examples are given and their performance are compared with that of other similar interpolators with a similar complexity. Simulation results show that the new interpolators outperform others. A resulting low-complexity hardware implementation can be obtained using the modified Farrow structure for the second-order polynomial, symmetric interpolator. It confirmed that only M/2 coefficients is actually required, as compared to M(L+1) coefficients in the original structure. The significant reduction in complexity of the modified structure allows a better interpolation performance with longer filter lengths.

# Chapter 5. Performance of Proposed STR Employing Interpolators

This chapter presents the performance analysis of the new feed-forward symbol timing estimation technique that employs interpolators proposed in Chapter 3.

# 5.1 Bias and Variance of Symbol Timing Estimator

The interpolated sample values can be different from the actual ones due to the non-ideal characteristics of the interpolation filter even if correct timing is assumed. Therefore, if the non-ideal interpolated samples are used to reproduce timing information, this information will not be exact. It is of course desirable to have zero bias and very small variance in timing estimation. Fortunately, through the analysis and some intensive experimental results, we will show that it is possible to achieve such goal.

# 5.1.1 Bias in timing estimation

Consider the estimated timing value close to the actual one. This assumption is usually valid for some appropriate interpolation filters. We can then approximate the ML function with its truncated Taylor version as follows:

$$L(\hat{\mu}) \cong L(\mu) + (\hat{\mu} - \mu)L'(\mu) + \frac{1}{2}(\hat{\mu} - \mu)^2 L''(\mu)$$
 (5.1)

The ML function becomes maximum when

$$\hat{\mu} - \mu \cong -\frac{L'(\mu)}{L''(\mu)} \tag{5.2}$$

Given the condition for the estimated value in (3.17), the expression in (5.2) is equal to zero, and this proves that the timing estimation process is nearly unbiased.

#### 5.1.2 Variance of the timing estimation error

The timing estimation error can be found as

$$e_{\tau} = -\frac{T_s}{T_{sym}} \frac{L'(\mu)}{L''(\mu)} = \frac{\mu}{2} + \frac{\sum_{n=0}^{N-1} (-1)^n f_1[2n+i]}{4\sum_{n=0}^{N-1} (-1)^n f_2[2n+i]}$$

$$e_{\tau} = \frac{\sum_{n=0}^{N-1} (-1)^n (2\mu f_2[2n+i] + f_1[2n+i])}{4\sum_{n=0}^{N-1} (-1)^n f_2[2n+i]}$$

Since the error is very small, the denominator varies very slowly compared to the numerator. We can safely replace the denominator by its mean. Thus the symbol timing error function can be rewritten as

$$e_{\tau} = \frac{\sum_{n=0}^{N-1} (-1)^n (2\mu f_2[2n+i] + f_1[2n+i])}{E\left[4\sum_{n=0}^{N-1} (-1)^n f_2[2n+i]\right]}$$

$$E[e_{\tau}^{2}] = \frac{E\left[\left(\sum_{n=0}^{N-1} (-1)^{n} (2\mu f_{2}[2n+i] + f_{1}[2n+i])\right)^{2}\right]}{16\left(E\left[\sum_{n=0}^{N-1} (-1)^{n} f_{2}[2n+i]\right]\right)^{2}}$$

$$E[e_{\tau}^{2}] = \frac{4\mu^{2}R_{2,2} + 4\mu R_{1,2} + R_{1,1}}{16\left[E\left[\sum_{n=0}^{N-1} (-1)^{n} f_{2}[2n+i]\right]^{2}}$$
(5.3)

where

$$E\left[\sum_{n=0}^{N-1} (-1)^n f_l[2n+i]\right] = N \sum_{m=M/2}^{M/2-1} c_l(m) \cos\left((i-m-\mu)\frac{\pi}{2}\right)$$
 (5.4)

and

$$R_{l, l'} = E\left[\left(\sum_{n=0}^{N-1} (-1)^{n} f_{l}[2n+i]\right) \left(\sum_{n'=0}^{N-1} (-1)^{n'} f_{l'}[2n'+i]\right)\right]$$

$$= E\left[\sum_{n=0}^{N-1} \sum_{n'=0}^{N-1} (-1)^{n+n'} f_{l}[2n+i] f_{l'}[2n'+i]\right]$$

$$= E\left[\sum_{n=0}^{N-1} \sum_{n'=0}^{N-1} (-1)^{n+n'} \sum_{m=-M/2}^{M/2-1} \sum_{m'=-M/2}^{M/2-1} c_{l}(m) c_{l'}(m')\right]$$

$$x(2n+i-m)x(2n'+i-m')$$

$$= \sum_{m=-M/2}^{M/2-1} \sum_{m'=-M/2}^{M/2-1} c_{l}(m)c_{l'}(m')R_{X}$$
(5.5)

where

$$R_{X} = E \left[ \sum_{n=0}^{N-1} \sum_{n'=0}^{N-1} (-1)^{n+n'} x(2n+i-m) x(2n'+i-m') \right]$$

$$= E \left[ \left( N \cos \left( \frac{\pi}{2} (i - m - \mu) \right) + \sum_{n=0}^{N-1} \frac{\eta (2n + i - m)}{\sqrt{E_b}} (-1)^n \right) \right. \\ \times \left( N \cos \left( \frac{\pi}{2} (i - m' - \mu) \right) + \sum_{n'=0}^{N-1} \frac{\eta (2n' + i - m')}{\sqrt{E_b}} (-1)^{n'} \right) \right]$$

$$= N^2 \cos \left( \frac{\pi}{2} (i - m - \mu) \right) \cos \left( \frac{\pi}{2} (i - m' - \mu) \right) + \frac{\sigma_{\eta}^2}{E_b} \sum_{n'=0}^{N-1} \delta[n - n', m - m']$$
(5.6)

Thus,

$$4\mu^{2}R_{2,2} + 4\mu R_{1,2} + R_{1,1}$$

$$= N^{2} \left( \sum_{m = -M/2}^{M/2 - 1} (2\mu c_{2}(m) + c_{1}(m)) \cos\left(\frac{\pi}{2}(i - m - \mu)\right) \right)^{2}$$

$$+ N \frac{\sigma_{\eta}^{2}}{E_{b}} \sum_{m = -M/2}^{M/2 - 1} (2\mu c_{2}(m) + c_{1}(m))^{2}$$

Therefore, it can be shown that the error in (5.3) can be expressed in terms of two independent error components: the error due to algorithm precision  $e_A$  and the error due to the Gaussian noise  $e_N$ , i.e.,

$$E[e_{total}^{2}] = E[e_{A}^{2}] + E[e_{N}^{2}]$$
(5.7)

where

$$E[e_A^2] = \frac{1}{4} \left( \frac{\sum_{m = -M/2}^{M/2 - 1} c_1(m) \cos\left((-m - \mu)\frac{\pi}{2}\right)}{\sum_{m = -M/2}^{M/2 - 1} c_2(m) \cos\left((-m - \mu)\frac{\pi}{2}\right)} \right)^2$$

$$(5.8)$$

and

$$E[e_N^2] = \frac{1}{32N} \left( \frac{N_o}{E_b} \right) \frac{\sum_{m = -M/2}^{M/2 - 1} (2\mu c_2(m) + c_1(m))^2}{\sum_{m = -M/2}^{M/2 - 1} c_2(m) \cos\left(\frac{\pi}{2}(-m - \mu)\right)^2}$$
(5.9)

## 5.1.3 Minimum mean square error (MMSE)

This section simplifies Equation (5.8) for a symmetric second-order polynomial-based interpolation filter; and then derives the minimum mean square error (MMSE) of the proposed algorithm precision.

Recall the relationships in (2.11), (2.13), and (2.14), the numerator of Equation (5.8) can be re-expressed as

$$M/2 - 1 \sum_{m = -M/2} c_1(m) \cos\left((-m - \mu)\frac{\pi}{2}\right)$$

$$= \left(-\sum_{m = -M/2}^{M/2 - 1} c_2(m) \cos\left((-m - \mu)\frac{\pi}{2}\right) - \cos\left((-\mu)\frac{\pi}{2}\right) + \cos\left((1 - \mu)\frac{\pi}{2}\right)\right)$$

$$= -\sum_{m = -M/2}^{M/2 - 1} c_2(m) \cos\left((-m - \mu)\frac{\pi}{2}\right) - \sqrt{2} \sin\left(\left(\frac{1}{2} - \mu\right)\frac{\pi}{2}\right)$$

and the denominator can be re-written as

$$\sum_{m=-M/2}^{M/2-1} c_2(m) \cos\left((-m-\mu)\frac{\pi}{2}\right)$$

$$= \sum_{m=0}^{M/2-1} \left(c_2(m) \cos\left((-m-\mu)\frac{\pi}{2}\right) + c_2(-m-1) \cos\left((m+1-\mu)\frac{\pi}{2}\right)\right)$$

$$= \sum_{m=0}^{M/2-1} c_2(m) \left(\cos\left((-m-\mu)\frac{\pi}{2}\right) + \cos\left((m+1-\mu)\frac{\pi}{2}\right)\right)$$

$$= 2 \sum_{m=0}^{M/2-1} c_2(m) \left( \cos \left( \left( \frac{1}{2} - \mu \right) \frac{\pi}{2} \right) \cos \left( \left( m + \frac{1}{2} \right) \frac{\pi}{2} \right) \right)$$

$$= 2\cos\left(\left(\frac{1}{2} - \mu\right)\frac{\pi}{2}\right) \sum_{m=0}^{M/2-1} c_2(m)\cos\left(\left(m + \frac{1}{2}\right)\frac{\pi}{2}\right)$$

Therefore, Equation (5.8) can be simplified as

$$E[e_A^2] = \frac{1}{4} \left( \mu - \frac{1}{2} - \frac{\sqrt{2} \tan\left(\left(\frac{1}{2} - \mu\right)\frac{\pi}{2}\right)}{4\sum_{m=0}^{M/2 - 1} c_2(m) \cos\left(\left(m + \frac{1}{2}\right)\frac{\pi}{2}\right)} \right)^2$$
 (5.10)

By defining the constant term  $\alpha$  as

$$\alpha = \left(-\frac{1}{\sqrt{2}}\right) \sum_{m=0}^{M/2-1} c_2(m) \cos\left(\left(m + \frac{1}{2}\right) \frac{\pi}{2}\right)$$
 (5.11)

we obtain

$$E[e_A^2] = \frac{1}{4} \left( \mu - \frac{1}{2} + \frac{1}{4\alpha} \tan\left( \left( \frac{1}{2} - \mu \right) \frac{\pi}{2} \right) \right)^2$$
 (5.12)

The derived timing error for the general second-order polynomial with tap length of M in (5.12) is analogous to the case for the simple polynomial interpolation filter in (3.30). Thus all results obtained from (3.30) can be applied here.

There are two important points we can draw from (5.12):

- 1. We can achieve the minimum MSE of timing estimation for all interpolation filter at MSE =  $8.458 \times 10^{-5}$ . This is the limit for the proposed techniques at  $T_{sym}/T_s$ =2.
- 2. An interpolation filter that has minimum timing estimation satisfies

$$\frac{-1}{\sqrt{2}} \sum_{m=0}^{M/2-1} c_2(m) \cos\left(\left(m + \frac{1}{2}\right) \frac{\pi}{2}\right) \cong \alpha_{opt} = 0.4536$$
 (5.13)

This condition is very useful to establish filter design constraints to be discussed in the other section.

#### 5.1.4 Bounds for Gaussian Noise Contributed Error

The Cauchy-Schwarz inequality shows that

$$\left(\sum_{m} c_2(m) \cos\left(\frac{\pi}{2}(m+\mu)\right)\right)^2 \le \sum_{m} c_2^2(m) \sum_{m} \cos^2\left(\frac{\pi}{2}(m+\mu)\right)$$
(5.14)

Given that

$$\sum_{m=-M/2}^{M/2-1} \cos^2\left(\frac{\pi}{2}(m+\mu)\right) = \frac{M}{2}\left(\sin^2\left(\frac{\pi}{2}\mu\right) + \cos^2\left(\frac{\pi}{2}\mu\right)\right) = \frac{M}{2},$$

we get

$$\left(\sum_{m=-M/2}^{M/2-1} c_2(m) \cos\left(\frac{\pi}{2}(m+\mu)\right)\right)^2 \leq \frac{M}{2} \sum_{m=-M/2}^{M/2-1} c_2^2(m).$$

The numerator in (5.9) is a second-order polynomial with respect to  $\mu$ . It is easy to find the minimum value  $A_{min}$  of this polynomial, such that

$$\sum_{m = -M/2}^{M/2 - 1} (2\mu c_2(m) + c_1(m))^2 \ge A_{min}$$
 (5.15)

where

$$A_{min} = \sum_{m = -M/2}^{M/2 - 1} c_1^2(m) - \frac{\left(\sum_{m = -M/2}^{M/2 - 1} c_1(m)c_2(m)\right)^2}{\sum_{m = -M/2}^{M/2 - 1} c_2^2(m)}$$

$$(5.16)$$

Therefore,

$$E[e_N^2] \ge \frac{A_{min}}{\left(\sum_{m = -M/2}^{M/2 - 1} c_2^2(m)\right) 16MN(E_b/N_o)}$$
(5.17)

Inequality (5.14) imposes loose conditional bounds due to the lack of information of

the interpolation filters' coefficients. The equality occurs when

$$c_2(m)\cos\left(\frac{\pi}{2}(m+\mu)\right) = f(\mu), \forall m$$
 (5.18)

or a looser condition is

$$c_2(m)\cos\left(\frac{\pi}{2}\left(m+\frac{1}{2}\right)\right) = const, \,\forall m \tag{5.19}$$

Only few interpolation filters can meet this requirement. It can be verified that the second-order Lagrange interpolation filter is one of them, thus it can achieve the bound in (5.17), and provides efficient estimation. For ones that do not satisfy the requirement, it is difficult to judge how far the error variance can be from the lower bound given in (5.17).

# 5.2 Alternative Interpretation and Acquisition Time

This section first gives an alternative explanation for the proposed technique in searching the eye-opening instant of the waveform and in noise filtering. While the ML approach infers optimality, the analogous approach shows the nature of the proposed technique and many important results that might not be very obvious when explained by the ML intuition. Acquisition time and preamble sequence length will be examined by using this approach.

The DA-STR problem raises the simple question, "In a noise-free environment, what is the shortest known sequence  $\{a_k\}$  that can give us enough information to correctly recover the timing on the received waveform?" The simple answer would be 2, and the sequence would be  $\{+1, -1\}$ . As random noise is concerned, it has equivalent effects on any sequences  $\{a_k\}$ . Thus we can infer that for a technique that can reduce the effect of random noise within a very short block of symbols, the alternative sequence  $\{+1, -1\}$  would be one of the shortest sequences that can give best information for estimating the timing of the received signal. This conclusion is valid when noise suppression is involved within the STR technique; and we can prove that it is possible to achieve such desirable shortest sequence with the proposed technique.

Consider the alternative sequence  $\{+1, -1\}$  used as the reference information. For the raised-cosine filter, g(t), the output of the receiver matched filter can be represented as a sine-wave with the noise component  $\eta(t)$ . Therefore at every sampling period  $nT_s$ ,

$$x[n] = \cos\left(\frac{\pi}{2}(n-\mu)\right) + \frac{\eta[n]}{\sqrt{E_b}}$$
 (5.20)

where we omit the time unit  $T_s$  in the expression for simplicity.

Now the noise term is ignored for a moment. Using the interpolation filter as an oversampling device, for a given sample period  $T_s$ , we are virtually able to reconstruct the whole sine-wave x(t) within that period. Figure 5.1 shows the reconstruction of a sine-wave using several interpolation filters.

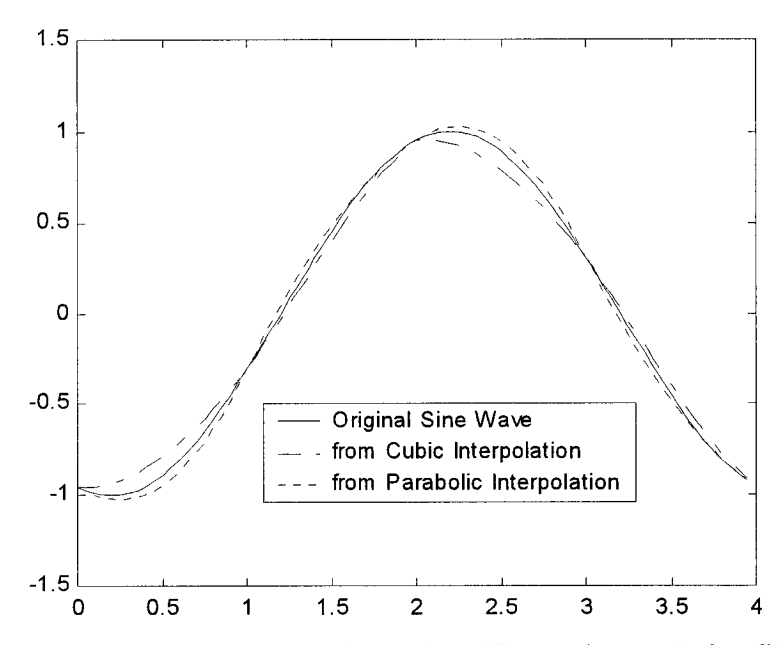


Fig. 5.1: Sine wave reconstruction using different interpolation filters

Having the reconstructed waveform, one can search for the optimal value of  $\mu$  corresponding to the position of the maximum value. From Figure 5.1, one can easily claim that the waveform obtained from the cubic interpolation does not have the extreme points and its maximum location occurs far away from the correct one, thus both extreme and maximum searching will not work. This emphasizes that interpolation filters have a great impact on making decision in the searching algorithm.

Searching process is often complex; however it is quite simple for the case of a second-order polynomial. The recovered signal from a second-order polynomial based interpolation filter is

$$y_{\mu}(n) = \sum_{l=0}^{2} \hat{f}_{l}[n] \mu^{l}$$
 (5.21)

Its extremum points are located at

$$\hat{\mu} = -\frac{\hat{f}_1[n]}{2\hat{f}_2[n]} \tag{5.22}$$

When additive noise is concerned, the output at the filter banks can be represented as

$$f_{l}[n] = \hat{f}_{l}[n] + \eta_{l}[n] \tag{5.23}$$

For a zero-mean noise term  $\eta_l(n)$ , it can be removed by averaging  $f_l[n]$ . However, it is easy to verify that,

$$\hat{f}_{l}[n] = -\hat{f}_{l}[n+2] \tag{5.24}$$

$$E[f_l[n]] = 0 (5.25)$$

Thus we cannot simply average the value of  $f_l[n]$ . In fact, for fixed  $\mu$ ,

$$(-1)^{n}\hat{f}_{t}[2n+i] = (-1)^{n+1}\hat{f}_{t}[2(n+1)+i] = const$$
 (5.26)

thus

$$E[(-1)^{n}\hat{f}_{l}[2n+i]] = (-1)^{n}\hat{f}_{l}[2n+i]$$
 (5.27)

Thus the correct way is to average the value of  $(-1)^n f_l[2n]$ ; and the detection now becomes,

$$\hat{\mu} = -\frac{E[(-1)^n f_1[2n+i]]}{2E[(-1)^n f_2[2n+i]]} = -\frac{\hat{f}_1[2n+i]}{2\hat{f}_2[2n+i]}$$
(5.28)

We notice that due to a similarity in (5.22) and (5.28), with the appropriate interpolation

filter, the reconstructed waveform  $y_{\mu}(n)$  should have a sinusoidal shape; so does the maximum likelihood function.

The estimation process obtained in (5.28) is exact to the proposed one (3.18) in Chapter 3. We observe the following facts:

- 1. The alternative {+1, -1} sequence is the best choice for a possibly shortest preamble. At high SNR, or with proper noise filtering, we can obtain a preamble block as short as 4.
- 2. With an appropriate interpolation filter, for any symbol interval, the ML function is close to the cosine wave-shape with the guaranteed existence of the unique global maximum location in the entire symbol interval.
- 3. The selected sequence also simplifies the STR implementation and analysis.

# 5.3 BER Degradation

This section devotes a short discussion of the impact of the proposed STR technique on the bit error rate (BER) degradation.

The BER degradation is defined as an increase in signal to noise ratio  $E_s/N_o$ , required to maintain the same BER as the case without synchronization error [59, Chapter 7.3]. For a small value of timing error, the BER degradation (in dB) of PAM signals is approximated by

$$D_{dB} = -10 \times \log \left(\frac{\sigma^2}{\sigma_0^2}\right) \cong \frac{10}{\ln(10)} \left(A(\beta) + \frac{1}{\sigma_0^2} B(\beta)\right) VAR(e_{\tau})$$
 (5.29)

where  $\sigma_o$  is the solution of

$$BER_o = \frac{2(M-1)}{M\log 2(M)} Q \left( \sqrt{\frac{3}{(M^2-1)\sigma_o^2}} \right)$$
 (5.30)

and the constant A and B are defined as [59, Chapter 7.3],

$$A(\beta) = -g''(0)T_{sym}^2 = \frac{\pi^2}{3} + (\pi^2 - 8)\beta^2$$
 (5.31)

$$B(\beta) = \sum_{m = -\infty}^{\infty} (g'(mT_{sym})T_{sym})^2 = 2\sum_{m = 1}^{\infty} \frac{\cos^2(\pi\beta m)}{m^2(1 - (2\beta m)^2)^2}$$
(5.32)

Since the value of each term in the above series decreases with  $m^8$ , we can approximate the value of B with a few terms.

Figures (5.2) and (5.3) show the simulation results on of the BER degradation of the proposed technique for two typical interpolation filters in 2-PAM and 4-PAM signals. We also observe that the BER degradation does not always decrease as the BER decreases (or SNR increases). The following derivation will provide an explanation.

Recall that because the timing error usually contains two terms: one related to the SNR due to noise contribution, and the other independent of SNR and due to the algorithm precision, the BER degradation can be rewritten as,

$$D_{dB} = \frac{10}{\ln(10)} \left( A(\beta) + \frac{2E_s}{N_o} B(\beta) \right) (e_A^2 + e_N^2)$$

$$= \frac{10}{\ln(10)} \left( A + 2B \frac{E_s}{N_o} \right) \left( C + D \frac{N_o}{E_s} \right)$$

$$= \frac{10}{\ln(10)} \left( AC + 2BD + 2CB \frac{E_s}{N_o} + AD \frac{N_o}{E_s} \right)$$
(5.33)

The equation implies that depending on whether AD or 2BC is dominant, the BER degradation can increase or decrease with respect to the SNR  $E_s/N_o$ . It has a lower bound

$$D_{dB} \ge \frac{10}{\ln(10)} (AC + 2BD + 2\sqrt{2ABCD}) = \frac{10}{\ln(10)} (\sqrt{AC} + \sqrt{2BD})^2$$
 (5.34)

The equality occurs when,

$$\frac{E_s}{N_o} = \sqrt{\frac{AD}{2BC}} \tag{5.35}$$

In [59, Chapter 7.3], it is mentioned that a good STR should yield  $D_{dB}$  about 0.2dB. Most data-aided feedforward techniques mainly suffer from the algorithm precision and can only meet this requirement with a relatively long preamble. However, by using a feedback mechanism to track the information after using the feedforward for parameter acquisition, this requirement would be released or relaxed.

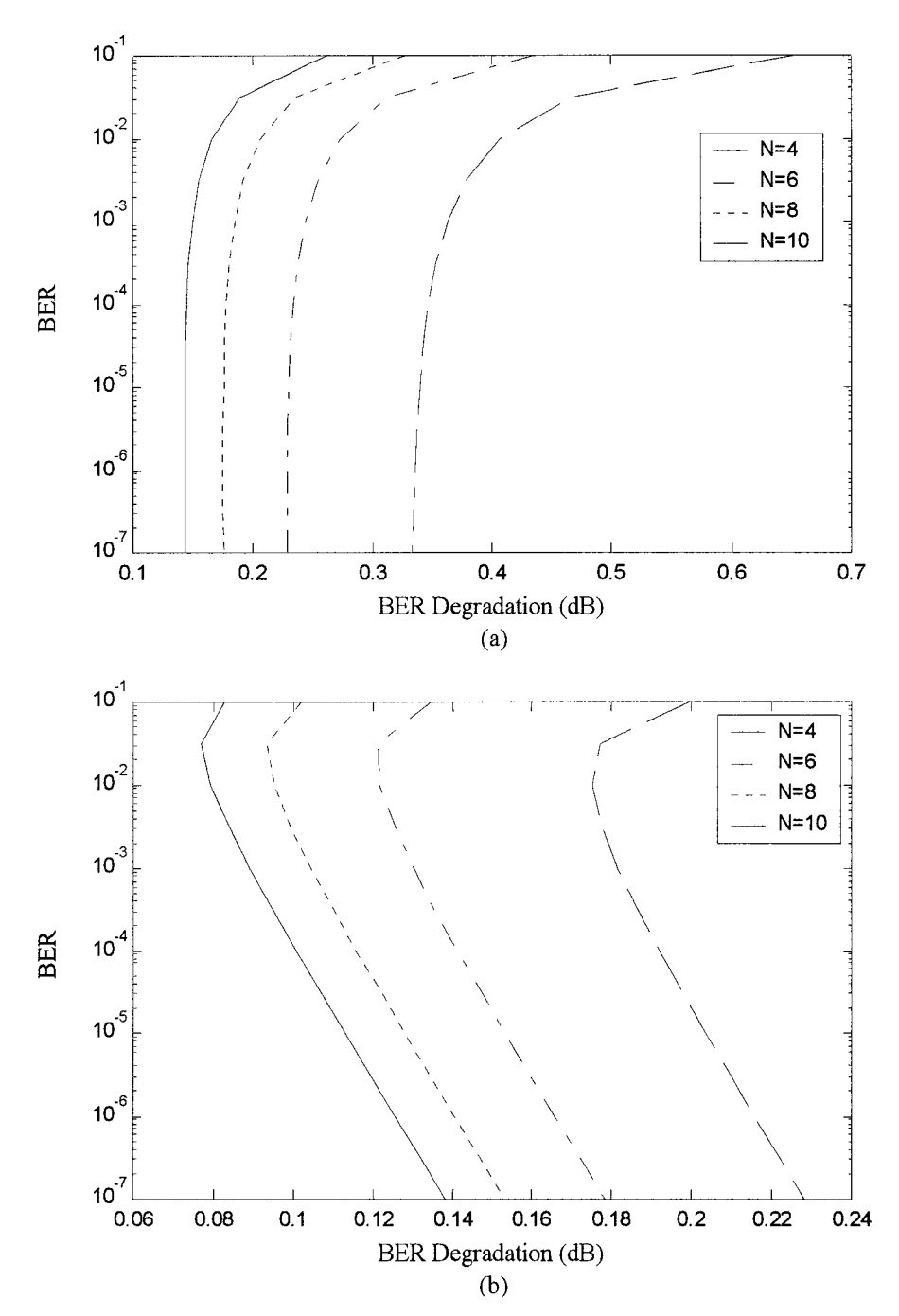


Fig. 5.2: BER Degradation for Parabolic Interpolation Filter: (a) 2-PAM (b) 4-PAM

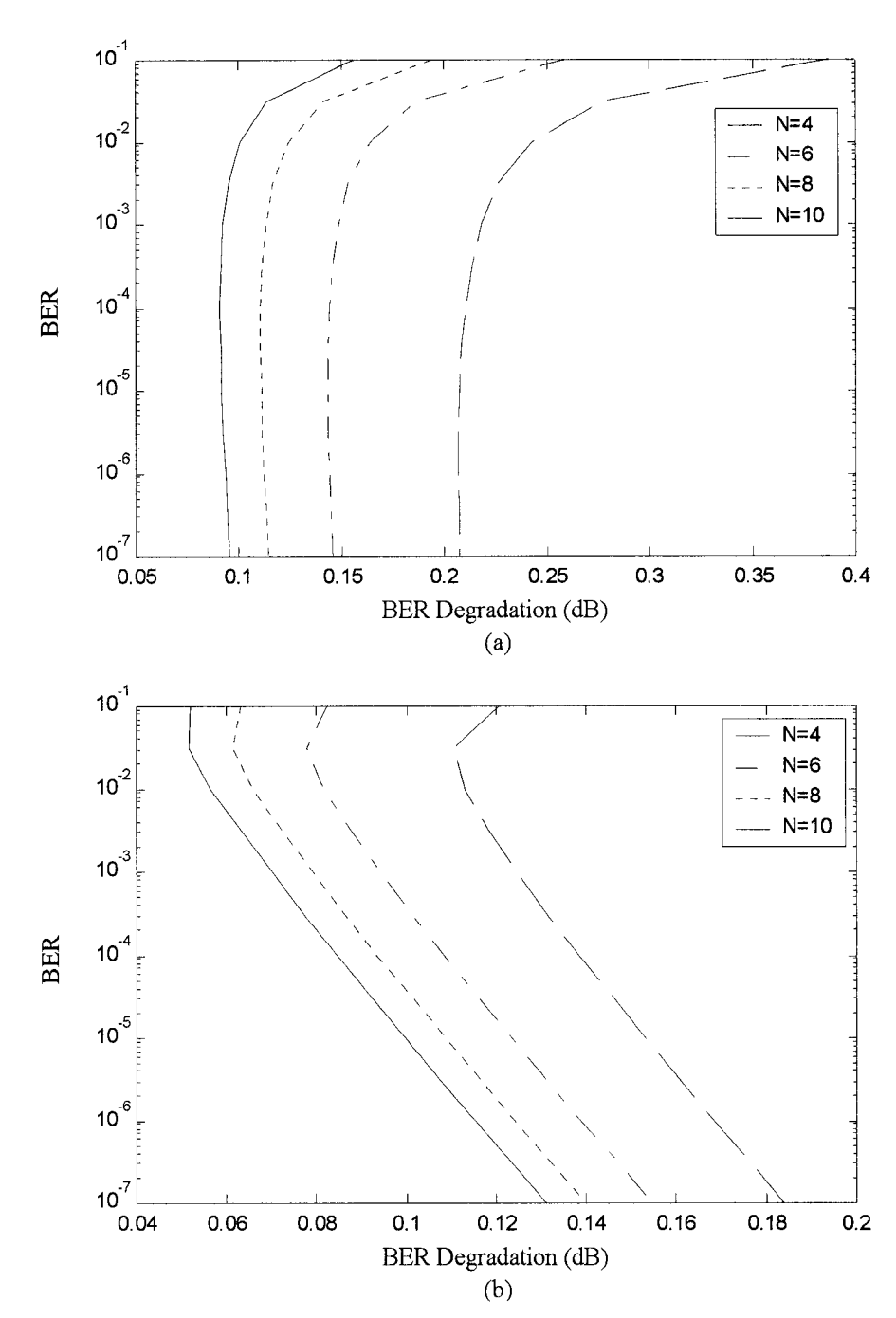


Fig. 5.3: BER Degradation for Vesma's Interpolator-Type II: (a) 2-PAM (b) 4-PAM

#### 5.4 Simulation Results

Numerical results obtained by using the analytical expressions in the previous section show that the timing information can be recovered with a preamble as short as 4 symbols. This has been confirmed by detailed simulation studies.

Table 5.1 summarizes the parameters used in the simulations:

1	Short burst mode transmission		
2	Alternative sequence {+1,-1} as preamble		
3	Raised cosine filter with 35% roll-off		
4	AWGN channel		
5	Signal Sampling rate near to 2 (+/-0.0001)		
6	Unknown symbol phase		
7	$E_b/N_o = 5dB$ , 15dB and 25dB		
8	Experimental interpolation filters are Vesma's interpolation filter II (M=6), Optimal Parabolic (γ=0.4536, M=4)		

Table 5.1: Simulations' Parameters

Figures 5.4 and 5.5 illustrate the convergence behavior of the timing estimator (TE) for two different interpolation filters in the presence of AWGN. The timing error measurement is started when the first preamble symbol enters in the averaging filters. As seen from the graphs, the estimations converge to the timing errors as the whole preamble sequences fit inside the filters. The estimated values are better for higher signal-to-noise ratio (SNR). For low SNR ( $E_b/N_o$ =5dB), short preambles (i.e., N=4, 6) cannot provide adequate estimated values. Longer preamble length (i.e., N=10 or greater) should be used to provide better accuracy. For high SNR ( $E_b/N_o$ =15dB or so), the simulations show that it is possible to obtain small estimation error with a very short preamble length (N=4). The convergence behaviors are very similar for all the other fractional delay values.

Timing error variances of the proposed STR for two interpolators are shown in Figures 5.6 and 5.7. The simulation results of the Vesma interpolation filter are far from the bounds, and those of the proposed optimal interpolation filter are very close to their theoretical bounds. It is because the optimal filter satisfies the condition (5.14), but the

other does not. It also points out that the optimal interpolation with a shorter filter length can provide the same performance as Vesma's interpolator with a longer filter length.

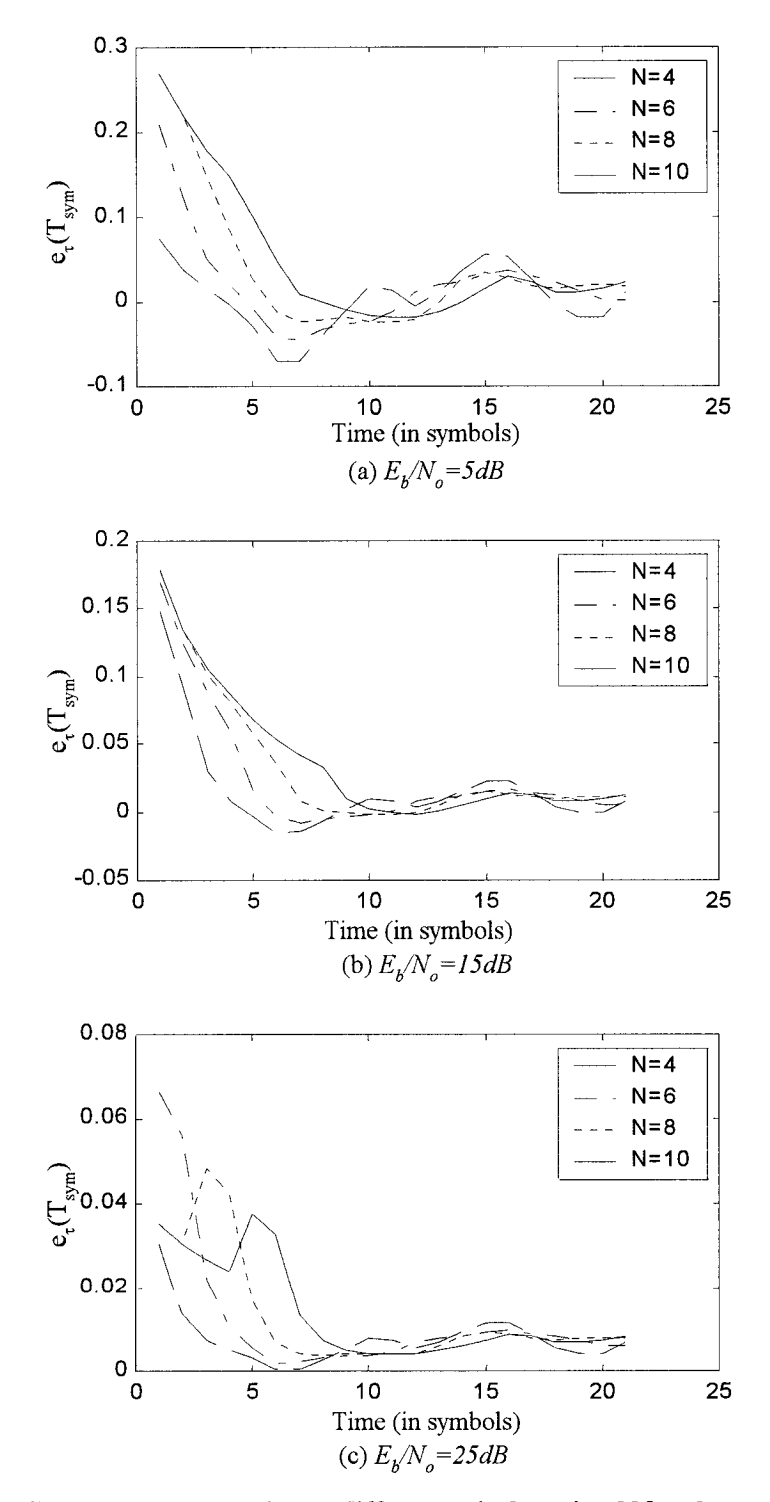


Fig. 5.4: Convergence behavior at different window size N for the parabolic filter

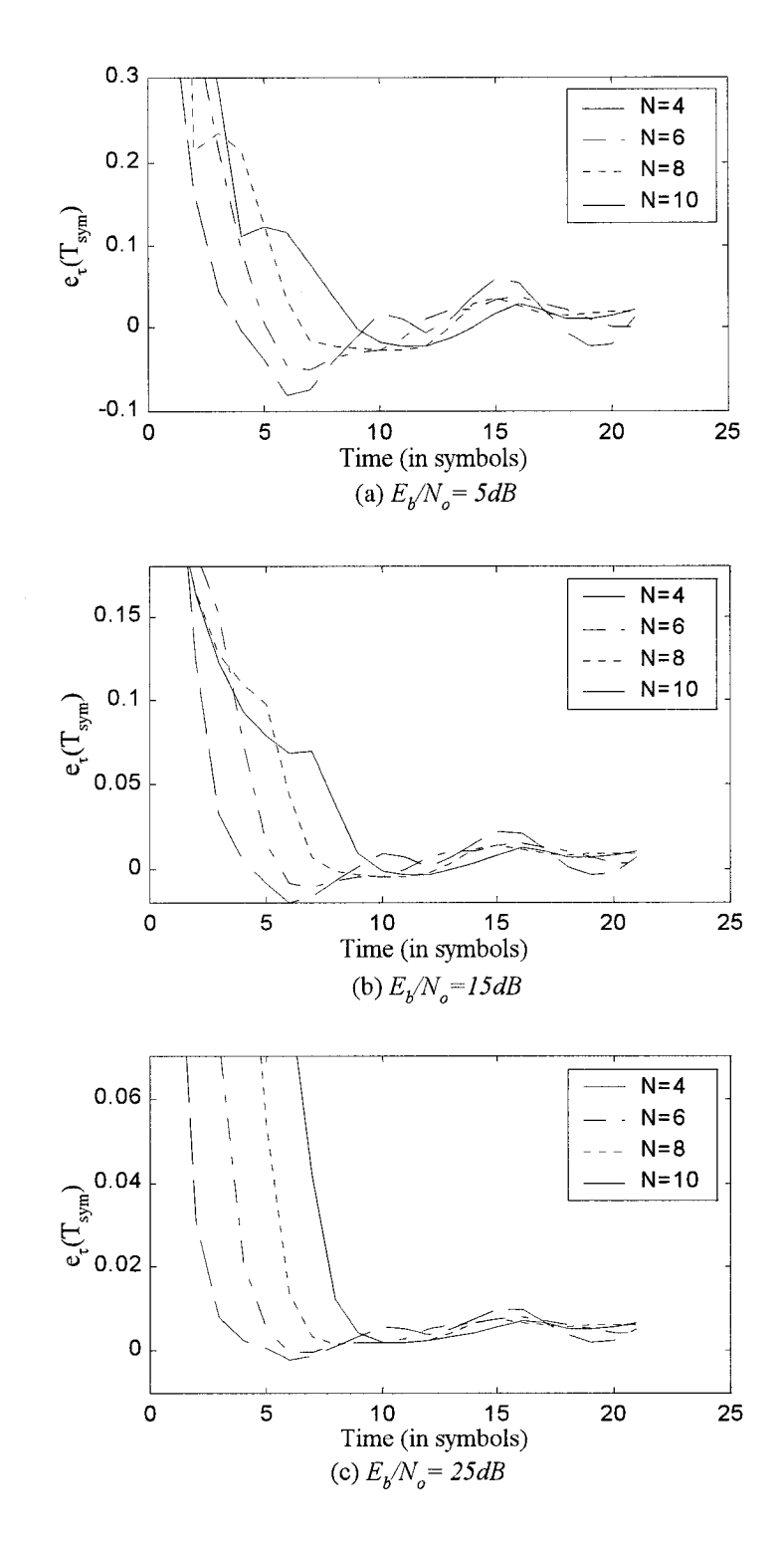


Fig. 5.5: Convergence behavior at different window size N for Vesma filter Type II

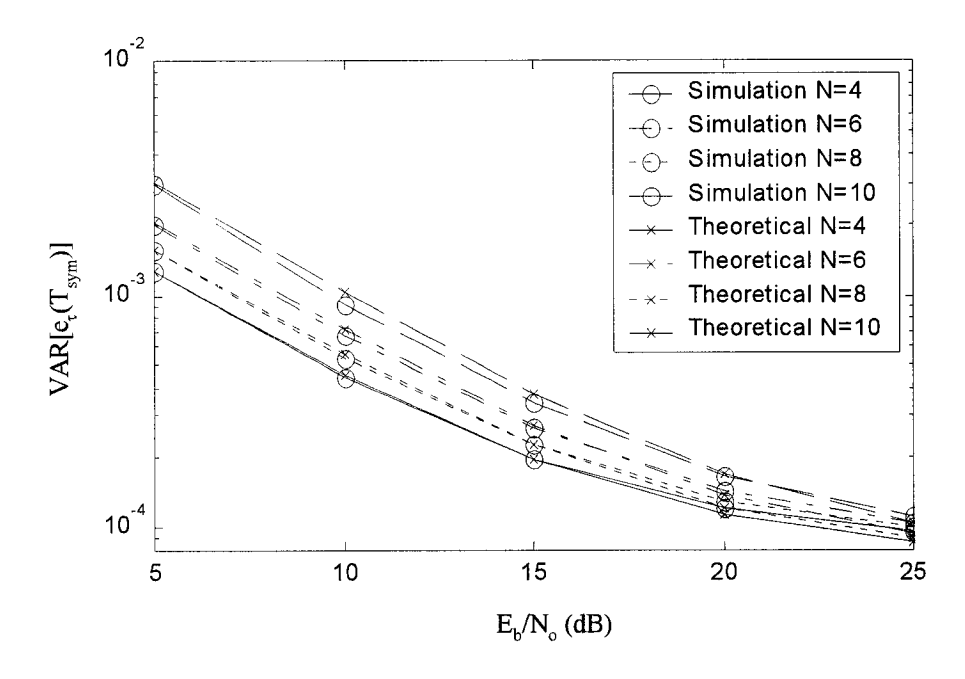


Fig. 5.6: Symbol Timing Error Variance for Parabolic Interpolation Filter

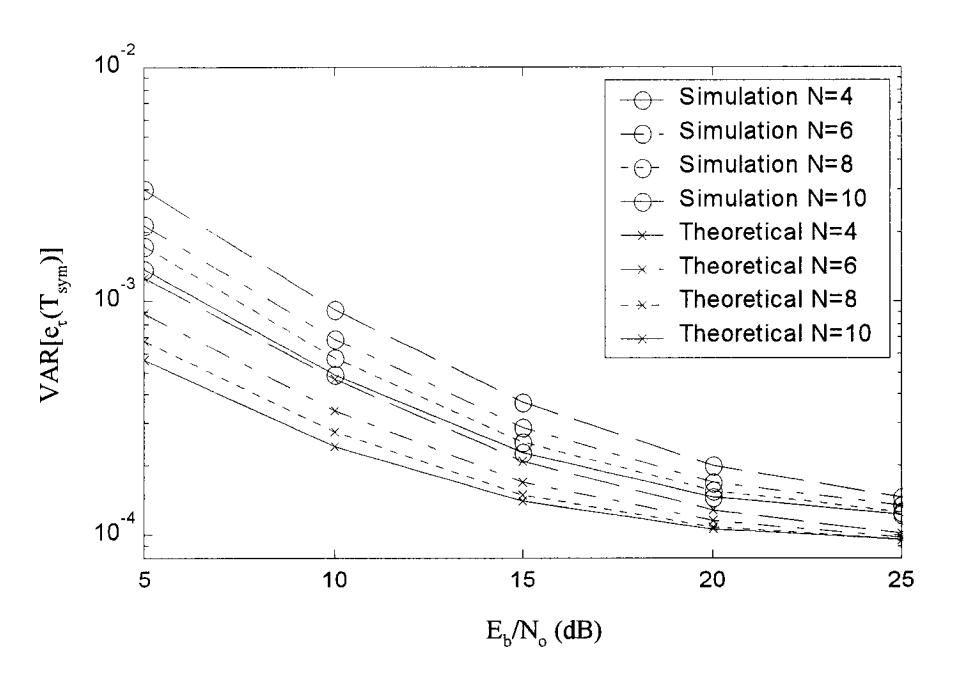


Fig. 5.7: Symbol Timing Error Variance for Vesma Interpolation Filter II.

#### 5.5 Conclusion

We have analyzed the performance of the proposed symbol timing recovery scheme for the case of  $T_{sym}/T_s$ =2. Timing estimation error variance is greatly reduced with the alternative  $\{-1, +1\}$  preamble, and with the appropriate interpolation filters. As predicted, the simulations show that short preambles help in rapid synchronization because of shorter length, but are susceptible to multipath and noise. Due to the particular interpolation filter and the aid of the particular preamble, rapid estimation convergence can be obtained with as low as 4 symbols. A bound on the estimation error variance has been derived. Simulation results are close to this bound.

# Chapter 6. STR Techniques in Systems using Oversampling

Sampling at the lowest rate is normally desired in DSP implementation in order to reduce the operation speed and possibly complexity. As a rule of thumbs, doubling the sampling rate will double the complexity and slow down the operation clock by a factor of 2. However, for low-capacity transmission applications in which the operation speed is not a concern, sampling at high rates provides more samples per symbol interval for possible performance improvement. This chapter examines the performance of the proposed techniques for PAM and QAM systems using oversampling. The analytical results can be used for trade-off between performance and complexity/speed.

# 6.1 PAM Systems using Oversampling

This section is an extension of the techniques presented in Chapters 3 and 5 for PAM systems. The techniques are revised to be suitable to higher sampling rates.

# 6.1.1 Maximum-Likelihood Algorithm for Timing Estimate

Approaches used in the previous chapter can be applied for the case of  $T_{sym}/T_s = \lambda > 2$ . The examined cosine wave is sampled as shown in Figure 6.1.

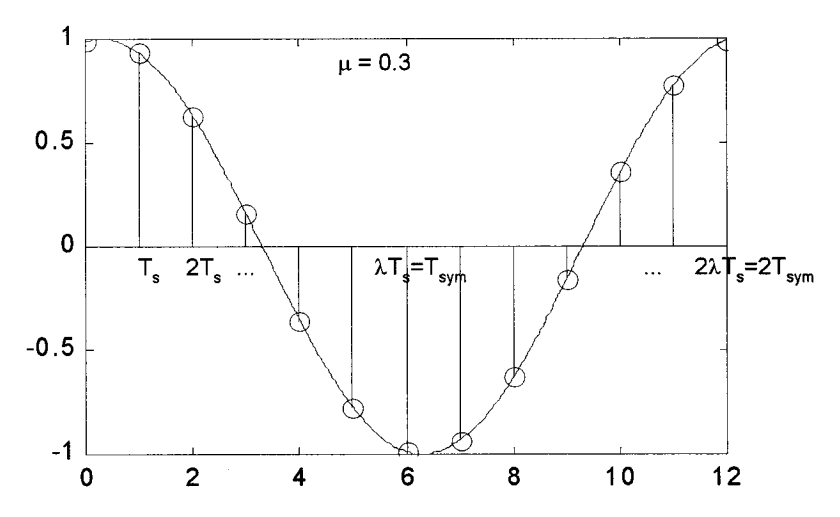


Fig. 6.1: Cosine wave at general sampling rate (for  $\mu = 0.3$ )

It can easily be verified that

$$x[n] = \cos\left(\frac{\pi}{\lambda}(n-\mu)\right) + \frac{\eta[n]}{\sqrt{E_s}}$$
 (6.1)

A similar formula resulting from ML estimation of timing fraction is given as

$$\hat{\mu}[i] = -\frac{b}{2a} = -\frac{\sum_{n=0}^{N-1} ((-1)^n f_1[\lambda n + i])}{\sum_{n=0}^{N-1} ((-1)^n f_2[\lambda n + i])} \approx -\frac{E[(-1)^n f_1[\lambda n + i]]}{2E[(-1)^n f_2[\lambda n + i]]}$$
(6.2)

For noiseless or high SNR, the estimate converges to

$$\hat{\mu}[i] \rightarrow -\frac{\sum_{m=-M/2}^{M-1} c_1(m) \cos\left(\frac{\pi}{\lambda}(i-m-\mu)\right)}{2\sum_{m=-M/2}^{M-1} c_2(m) \cos\left(\frac{\pi}{\lambda}(i-m-\mu)\right)}$$
(6.3)

### 6.1.2 Variance of Error due to Algorithm Precision

The general timing estimation error, normalized to  $T_{sym}$ , can be written as

$$e_{A} = \frac{1}{\lambda} \begin{bmatrix} \frac{M/2 - 1}{\sum_{m = -M/2}^{M/2 - 1} c_{1}(m) \cos\left(\frac{\pi}{\lambda}(-m - \mu)\right)}{\sum_{m = -M/2}^{M/2 - 1} c_{2}(m) \cos\left(\frac{\pi}{\lambda}(-m - \mu)\right)} \\ 2 \sum_{m = -M/2}^{M/2 - 1} c_{2}(m) \cos\left(\frac{\pi}{\lambda}(-m - \mu)\right) \end{bmatrix}$$
(6.4)

For symmetric interpolation filters,

$$\sum_{m=-M/2}^{M/2-1} c_1(m) \cos\left((i-m-\mu)\frac{\pi}{\lambda}\right)$$

$$= -\sum_{m=-M/2}^{M/2-1} c_2(m) \cos\left((i-m-\mu)\frac{\pi}{\lambda}\right) - \cos\left((i-\mu)\frac{\pi}{\lambda}\right) + \cos\left((i+1-\mu)\frac{\pi}{\lambda}\right)$$

$$= -\sum_{m=-M/2}^{M/2-1} c_2(m) \cos\left((i-m-\mu)\frac{\pi}{\lambda}\right) - 2\sin\left((i-\mu+\frac{1}{2})\frac{\pi}{\lambda}\right) \sin\left(\frac{\pi}{2\lambda}\right)$$

where

$$\sum_{m=-M/2}^{M/2-1} c_2(m) \cos\left((i-m-\mu)\frac{\pi}{\lambda}\right)$$

$$= \sum_{m=0}^{M/2-1} \left(c_2(m) \cos\left((i-m-\mu)\frac{\pi}{\lambda}\right) + c_2(-m-1) \cos\left((i+m+1-\mu)\frac{\pi}{\lambda}\right)\right)$$

$$= \sum_{m=0}^{M/2-1} c_2(m) \left(\cos\left((i-m-\mu)\frac{\pi}{\lambda}\right) + \cos\left((i+m+1-\mu)\frac{\pi}{\lambda}\right)\right)$$

$$= 2\cos\left(\left(i+\frac{1}{2}-\mu\right)\frac{\pi}{\lambda}\right) \sum_{m=0}^{M/2-1} c_2(m) \cos\left(\left(m+\frac{1}{2}\right)\frac{\pi}{\lambda}\right)$$

Therefore, the estimated timing fraction is

$$\hat{\mu}_{i} = \frac{1}{2} + \frac{\sin\left(\frac{\pi}{2\lambda}\right)\tan\left(\left(i + \frac{1}{2} - \mu\right)\frac{\pi}{\lambda}\right)}{2\sum_{m=0}^{M/2-1} c_{2}(m)\cos\left(\left(m + \frac{1}{2}\right)\frac{\pi}{\lambda}\right)}$$
(6.5)

Introducing the constant term  $\alpha$ 

$$\alpha = -\frac{\sin\left(\frac{\pi}{2\lambda}\right)}{2\sum_{m=0}^{M/2-1} c_2(m)\cos\left(\left(m + \frac{1}{2}\right)\frac{\pi}{\lambda}\right)}$$
(6.6)

we can obtain

$$\hat{\mu}[i] = \frac{1}{2} - \alpha \tan\left(\left(i + \frac{1}{2} - \mu\right) \frac{\pi}{\lambda}\right) \tag{6.7}$$

and the error of the timing estimation in (6.4) can be simplified as

$$e_A = \frac{1}{\lambda} \left( \mu - \frac{1}{2} + \alpha \tan \left( \left( \frac{1}{2} - \mu \right) \frac{\pi}{\lambda} \right) \right)$$
 (6.8)

The values of  $\alpha$  with different  $\lambda$  are shown in Table 6.1.

It can be shown that

$$E[e_A^2] = \int_0^1 \frac{1}{\lambda^2} \left( \mu - \frac{1}{2} + \alpha \tan \left( \left( \frac{1}{2} - \mu \right) \frac{\pi}{\lambda} \right) \right)^2 d\mu = \int_{-x_o}^{x_o} \frac{\lambda}{\pi^3} (x + \beta \tan(x))^2 dx$$

$$= A\beta^2 - 2B\beta + C \tag{6.9}$$

where

$$\beta = \frac{\pi \alpha}{\lambda} = \frac{B}{A}, \text{ and } x_o = \frac{\pi}{2\lambda}$$

$$A = \frac{2\lambda}{\pi^3} \int_0^{x_o} \tan^2(x) dx = \frac{2\lambda}{\pi^3} (\tan(x_o) - x_o)$$

$$B = \frac{2\lambda}{\pi^3} \int_0^{x_o} x \tan(x) dx \approx \frac{2\lambda}{\pi^3} \int_0^{x_o} \tan^2(x) dx = A, \text{ for small } x_o$$

$$C = \frac{1}{12\lambda^2}$$

Therefore, at a high sampling rate  $\lambda$ ,  $\beta$  will approach 1, thus an approximately linear relationship can be given as

$$\alpha_{opt} = \frac{\lambda}{\pi} \tag{6.10}$$

As we can see in Table 6.1, the approximation becomes accurate for sampling rates higher than 4. Figure 6.2 shows the decrement of MSE of the estimated timing as the sample rate  $\lambda$  increases. As we can see the error is reduced dramatically as  $\lambda$  increases at the expense of increased complexity and operation speed.

Table 6.1: Optimal  $\alpha$  for different sampling rate  $\lambda$ 

λ	Actual a <sub>opt</sub>	<b>Approximated</b> α <sub>opt</sub>	Approximation Error
2	0.5511	0.6366	15.51%
3	0.9007	0.9549	6.02%
4	1.2332	1.2732	3.25%
5	1.5597	1.5915	2.04%
6	1.8835	1.9099	1.40%
7	2.2056	2.2282	1.02%
8	2.5267	2.5465	0.78%

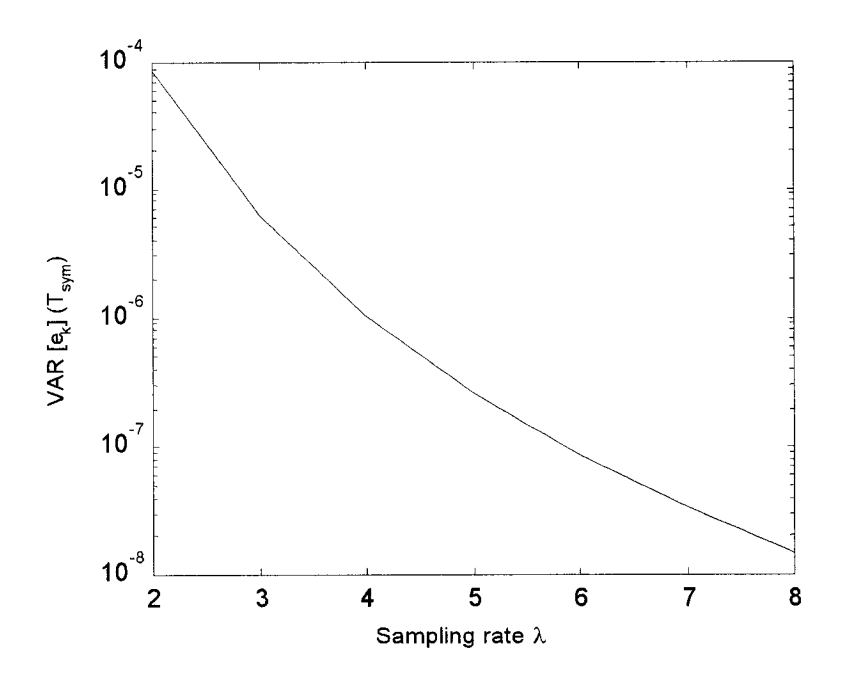


Fig. 6.2: MSE of Estimated Timing versus Sampling Rate  $\lambda$ 

### 6.1.3 AWGN Contribution

Using the same approach as in the previous chapter, we derive the variance of the error due to the Gaussian noise as

$$E[e_N^2] = \frac{\sigma_{\eta}^2}{4\lambda^2 N E_s} \frac{\sum_{m = -M/2}^{M/2 - 1} (2\mu c_2(m) + c_1(m))^2}{\sum_{m = -M/2}^{M/2 - 1} c_2(m) \cos(\frac{\pi}{\lambda}(-m - \mu))^2}$$
(6.11)

The Cauchy-Schwarz inequality shows that

$$\left(\sum_{m=-M/2}^{M/2-1} c_2(m) \cos\left(\frac{\pi}{\lambda}(-m-\mu)\right)\right)^2 \leq \sum_{m=-M/2}^{M/2-1} c_2^2(m) \sum_{m=-M/2}^{M/2-1} \cos^2\left(\frac{\pi}{\lambda}(-m-\mu)\right)$$

We can approximate the  $\cos^2(x)$  term by its average value,

$$\int_0^1 \cos^2\left(\frac{\pi}{\lambda}(-m-\mu)\right) d\mu = \frac{1}{2} + \sin\left(\frac{\pi}{\lambda}\right) \cos\left(\frac{2\pi}{\lambda}(m+\frac{1}{2})\right)$$

$$\sum_{m=-M/2}^{M/2-1} \cos^2\left(\frac{\pi}{\lambda}(-m-\mu)\right) = \frac{M}{2} + \sin\left(\frac{\pi}{\lambda}\right) \sum_{m=-M/2}^{M/2-1} \cos\left(\frac{2\pi}{\lambda}(m+\frac{1}{2})\right)$$

Therefore,

$$E[e_N^2] \ge \frac{1}{\frac{M}{2} + \sin(\frac{\pi}{\lambda})} \sum_{n = -M/2}^{M/2 - 1} \cos(\frac{2\pi}{\lambda} (m + \frac{1}{2})) \frac{A_{min}}{\sum_{m = -M/2}^{M/2 - 1} c_2^2(m)} \frac{1}{8\lambda^2 N(E_s/N_o)}$$
(6.12)

where

$$A_{min} = \sum_{m = -M/2}^{M/2 - 1} c_1^2(m) - \frac{\left(\sum_{m = -M/2}^{M/2 - 1} c_1(m)c_2(m)\right)^2}{\sum_{m = -M/2}^{M/2 - 1} c_2^2(m)}$$

$$m = -M/2$$

For  $\lambda = 2$  or  $M = k\lambda$ ,

$$\sum_{m=-M/2}^{M/2-1} \cos\left(\frac{2\pi}{\lambda}\left(m+\frac{1}{2}\right)\right) = 0$$

and the bound can be simplified as

$$E[e_N^2] \ge \frac{1}{4\lambda^2 MN(E_s/N_o)} \frac{A_{min}}{\sum_{m=-M/2}^{M/2-1} c_2^2(m)}$$
(6.13)

which is consistent with the results obtained in the previous section.

We have noticed that the above lower bound can be applied for any second-order polynomial interpolation filters.

### 6.1.4 Case-Study: Optimal Lagrange Parabolic Interpolators

In this section, we focus our discussion on the proposed STR algorithm using the Lagrange second-order interpolation filters with M=4. Bucket and Moeneclaey [39] introduced a filter optimization approach based on a BER degradation criteria. We will mathematically show in this case of study the similar results, which were obtained in [39]. Kim ([49]) showed that minimizing MSE at the symbol detector is very much equivalent to minimizing the MSE at the timing estimation. Thus, they all infer the generality of our proposed method over the one proposed in [39].

Applying (6.6) to the Lagrange second-order polynomial interpolation filter, where

$$c_2(-2) = -c_2(-1) = -c_2(0) = c_2(1) = \gamma$$

we obtain

$$\alpha_{opt} = -\frac{\sin\left(\frac{\pi}{2\lambda}\right)}{2\gamma\left(-\cos\left(\frac{\pi}{2\lambda}\right) + \cos\left(\frac{3\pi}{2\lambda}\right)\right)} = \frac{1}{4\gamma\sin\left(\frac{\pi}{\lambda}\right)} \to \frac{\lambda}{\pi}$$
 (6.14)

Thus the parameter of the optimal Lagrange second-order polynomial interpolation filter for minimizing the symbol timing estimation error are computed as

$$\gamma_{opt} = \frac{1}{4\alpha_{opt}\sin(\frac{\pi}{\lambda})} \to \frac{1}{4\frac{\lambda}{\pi}\sin(\frac{\pi}{\lambda})} = 0.25; \text{ for } \lambda \text{ is large}$$
(6.15)

The optimum  $\gamma$  converges to 0.25 at a high sampling rate. Table 6.2 shows the optimal values of  $\gamma$  corresponding to several values of  $\lambda$ . The approximated values are obtained using the linear approximation of  $\alpha$  (Eq. 6.10).

λ	<b>Actual</b>	<b>Approximated</b>	Approximation
	γ <sub>opt</sub>	γ <sub>opt</sub>	Error
2	0.4536	0.3927	13.43%

λ	Actual <sup>Y</sup> opt	<b>Approximated</b> γ <sub>opt</sub>	Approximation Error
3	0.3205	0.3023	5.68%
4	0.2867	0.2777	3.15%
5	0.2727	0.2672	2.00%
6	0.2655	0.2618	1.38%
7	0.2612	0.2586	1.01%
8	0.2585	0.2565	0.77%

Table 6.2: Optimal  $\gamma$  for different sampling rates  $\lambda$ 

The MSE of the timing estimation for the optimal interpolation filters with  $\lambda = 2$ , 4, and 8 are plotted in Figures 6.3, 6.4, and 6.5. As one can expect from the analysis, the lower bounds can be reached for the case of  $M = k\lambda = 4$ , i.e.,  $\lambda = 2$  and 4. This is confirmed by the plots in Figures 6.3, 6.4. For higher sampling rates, the equality cannot be held, so that the actual variance is not close to the bound as shown in Figure 6.5.

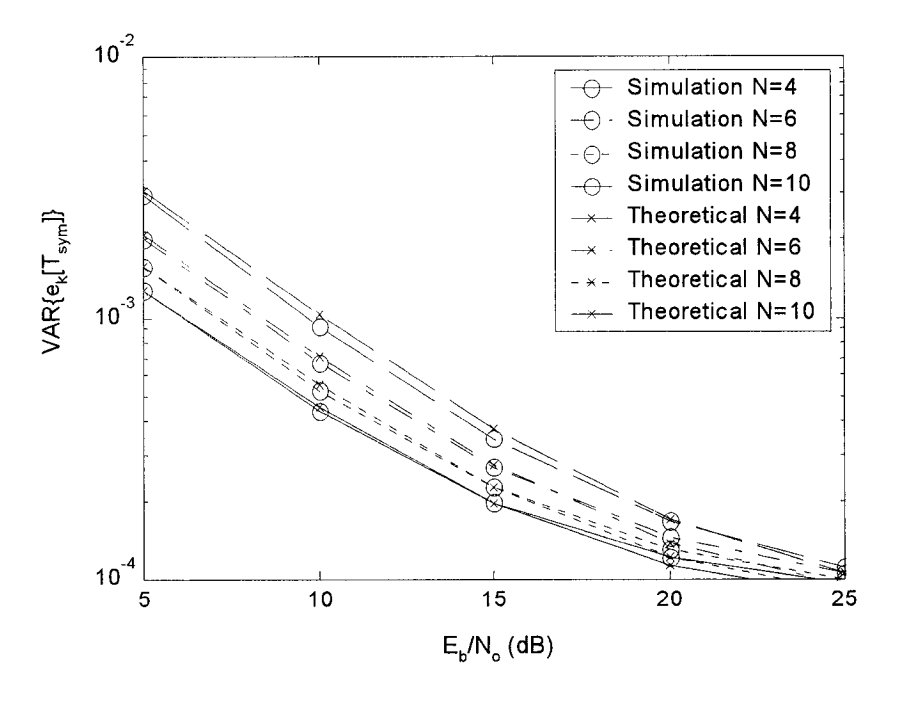


Fig. 6.3: Symbol Timing Error Variance ( $\lambda$ =2)

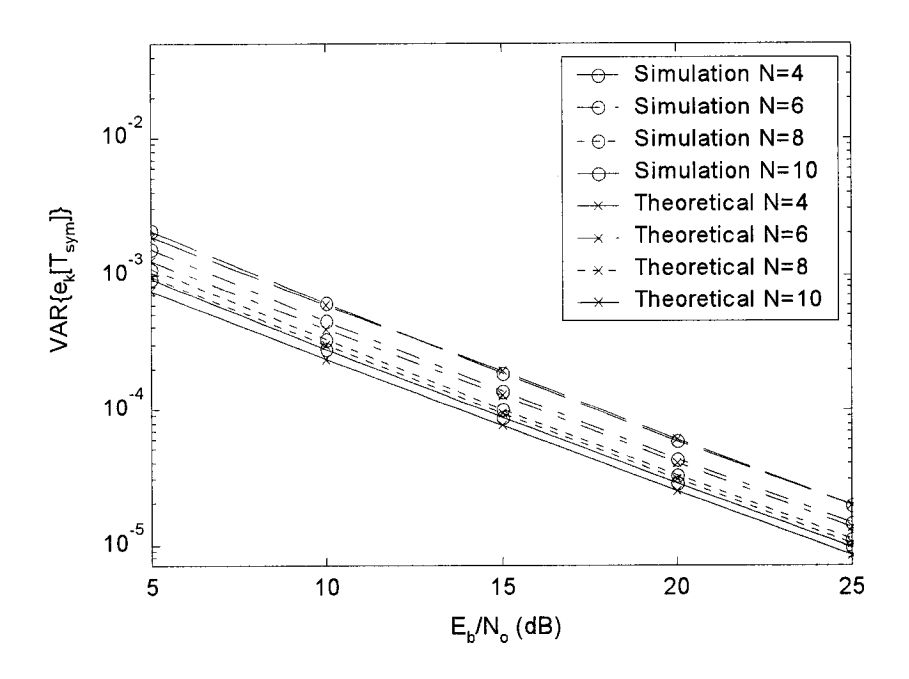


Fig. 6.4: Symbol Timing Error Variance ( $\lambda$ =4)

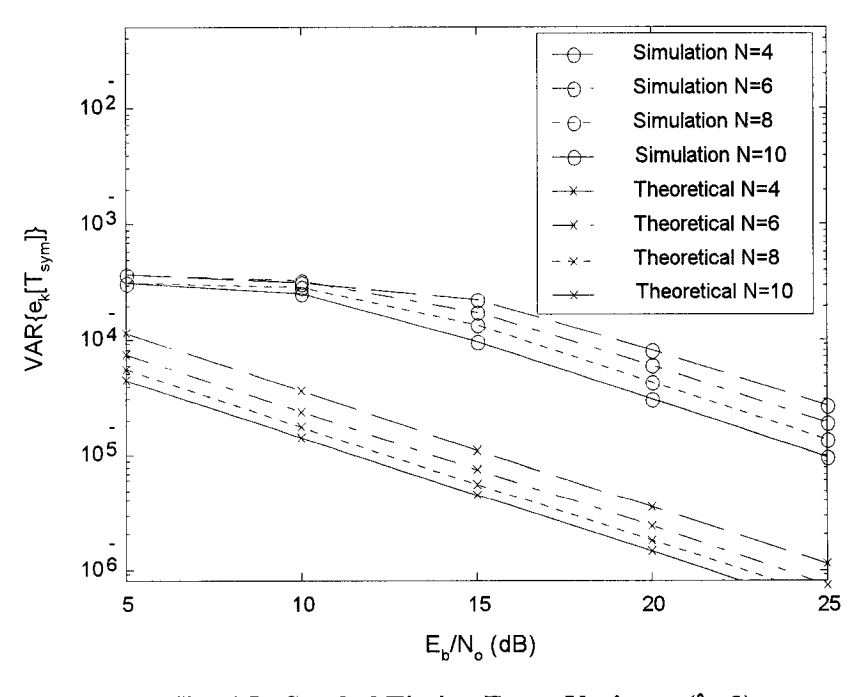


Fig. 6.5: Symbol Timing Error Variance ( $\lambda$ =8)

# 6.2 QAM Systems using Oversampling

The proposed technique can be modified to suit very well the QAM systems, which are widely used in many applications. This section gives a brief description of joint estimation algorithms of I and Q channels to improve the performance of the timing estimation. The analysis and simulations show a 3dB improvement with the new joint estimation scheme.

## 6.2.1 Algorithm Derivation

The ML function used for QAM signals can be refined as follows [59]

$$L(\hat{\mu}) = max \left( \Re \left[ \sum_{n=0}^{N-1} a^*(n) z_{\hat{\mu}}(n) \right] \right)$$
 (6.16)

where

 $\Re$ : real part of the number.

$$a(n) = a_I(n) + ja_Q(n)$$
 is the transmitted sequence and  $a^*(n) = a_I(n) - ja_Q(n)$ .

Since,

$$z_{\hat{\mu}}(n) = y_{\hat{\mu}}(\lambda n + i) = y_{\hat{\mu}, I}(\lambda n + i) + jy_{\hat{\mu}, Q}(\lambda n + i)$$

$$= \sum_{l=0}^{L} (f_{l, I}[\lambda n + i] + jf_{l, Q}[\lambda n + i])\hat{\mu}^{l}$$
(6.17)

The ML function can be rewritten as

$$L(\hat{\mu}) = \max \left( \Re \left[ \sum_{n=0}^{N-1} (a_I(n) - ja_Q(n)) \sum_{l=0}^{L} (f_{l,l}[\lambda n + i] + jf_{l,Q}[\lambda n + i]) \hat{\mu}^l \right] \right)$$

$$= \max \left( \sum_{l=0}^{L} \sum_{n=0}^{N-1} (a_{l}(n) f_{l,l}[\lambda n + i] + a_{Q}(n) f_{l,Q}[\lambda n + i]) \hat{\mu}^{l} \right)$$

$$= \max \left( \sum_{l=0}^{L} E[a_{l}(n) f_{l,l}[\lambda n + i] + a_{Q}(n) f_{l,Q}[\lambda n + i]] \hat{\mu}^{l} \right)$$
(6.18)

For the same reasons as given in the previous sections, we consider only the secondorder polynomial. The function is maximum when its derivative equals zero. Therefore,

$$\frac{\mathrm{d}}{\mathrm{d}\hat{\mu}}L(\hat{\mu})\big|_{\hat{\mu}=\mu} = \sum_{l=1}^{2}l\hat{\mu}^{l-1}E[a_{I}(n)f_{l,I}[\lambda n+i] + a_{Q}(n)f_{l,Q}[\lambda n+i]] = 0$$
 (6.19)

The estimated timing information is given by

$$\hat{\mu}[i] = -\frac{\sum_{N=0}^{N-1} (-1)^n (f_{1,I}[\lambda n + i] + f_{1,Q}[\lambda n + i])}{2\sum_{n=0}^{N-1} (-1)^n (f_{2,I}[\lambda n + i] + f_{2,Q}[\lambda n + i])}$$
(6.20)

$$= \frac{E[(-1)^{n}(f_{1,I}[\lambda n+i]+f_{1,Q}[\lambda n+i])]}{2E[(-1)^{n}(f_{2,I}[\lambda n+i]+f_{2,Q}[\lambda n+i])]}$$

which is very similar to the expression for PAM signals.

# 6.2.2 Variance of Error due to Algorithm Precision

The error due to algorithm precision for QAM systems is the same for PAM systems,

$$e_{A, QAM} = e_{A, PAM} = \frac{1}{\lambda} \left( \frac{\sum_{\substack{M/2-1 \\ M/2-1}}^{M/2-1} c_1(m) \cos\left(\frac{\pi}{\lambda}(-m-\mu)\right)}{\sum_{\substack{M/2-1 \\ M/2-1}}^{M/2-1} c_2(m) \cos\left(\frac{\pi}{\lambda}(-m-\mu)\right)} \sum_{\substack{m=-M/2}}^{M/2-1} c_2(m) \cos\left(\frac{\pi}{\lambda}(-m-\mu)\right) \right)$$
(6.21)

For symmetric interpolation filters, we have simplified expression as follows

$$e_{A, QAM} = e_{A, PAM} = \frac{1}{\lambda} \left( \mu - \frac{1}{2} + \alpha \tan \left( \left( \frac{1}{2} - \mu \right) \frac{\pi}{\lambda} \right) \right)$$
 (6.22)

#### 6.2.3 AWGN Contribution

A similar approach is used in the analysis of the effect of AWGN on QAM systems. The bound on the error due to noise is

$$E[e_N^2] \ge \frac{1}{\frac{M}{2} + \sin(\frac{\pi}{\lambda}) \sum_{n = -M/2}^{M/2 - 1} \cos(\frac{2\pi}{\lambda} (m + \frac{1}{2})) \sum_{m = -M/2}^{M/2 - 1} c_2^2(m)} \frac{\sigma_{\eta}^2}{16E_s \lambda^2 N}$$

where

$$A_{min} = \sum_{m = -M/2}^{M/2 - 1} c_1^2(m) - \frac{\left(\sum_{m = -M/2}^{M/2 - 1} c_1(m)c_2(m)\right)^2}{\sum_{m = -M/2}^{M/2 - 1} c_2^2(m)}$$

$$= -M/2$$

$$\sigma_{\eta}^2 = \sigma_{\eta, I}^2 + \sigma_{\eta, Q}^2 = N_o$$

Therefore

$$E[e_N^2] \ge \frac{1}{\frac{M}{2} + \sin(\frac{\pi}{\lambda})} \sum_{n = -M/2}^{M/2 - 1} \cos(\frac{2\pi}{\lambda} (m + \frac{1}{2})) \sum_{m = -M/2}^{M/2 - 1} c_2^2(m)^{16E_s \lambda^2 N}$$
(6.23)

For  $\lambda = 2$  or  $M = k\lambda$ , the bound can be simplified as

$$E[e_N^2] \ge \frac{1}{8\lambda^2 MN(E_s/N_o)} \frac{A_{min}}{\sum_{m=-M/2} c_2^2(m)}$$
(6.24)

Comparing the bounds for  $M^2$ -QAM systems in (6.23) and (6.24) with the bounds for M-PAM systems in (6.12) and (6.13), we observe 3dB improvement for the joint

estimation in QAM systems.

#### **6.2.4** Simulation Results

This section investigates the proposed STR techniques for 4-QAM systems at the following sampling rates:  $T_{sym}/T_s = 2$ , 4, and 8. For all simulations in this section, we assume a short burst, and a raised-cosine shaping filter with a roll-off factor of 0.35. The preamble is an alternative  $\{A, -A\}$  sequence with length N. The performance of the proposed technique is evaluated in terms of the error variance of the estimated symbol timing and the ISI at the receiver output. The considered parameters are summarized in Table 6.3.

Short-burst transmission

4-QAM systems

Alternative sequence {-A, A} as the preamble with length N

Raised cosine filter with roll-off factor β = 0.35

Sampling rates = 2, 4, and 8

With / without AWGN

Table 6.3: OAM Simulation Parameters

#### Without AWGN effects

The first set of results is obtained without considering the effect of AWGN. The experiments are simulated for different preamble lengths N and different sampling rates  $\lambda$ . The obtained variances are referred as algorithm precision variances. Figures 6.6 and 6.7 show the simulated error variance results of the symbol timing estimation, and ISI (measured at sampling instant), respectively. As the sampling rate  $\lambda$  increases, the error variance decreases correspondingly. The difference between the expected and simulated ones is referred as modeling error. This modeling error variance is in the order  $10^{-6}$  and becomes dominant when the symbol timing error gets smaller.

Figure 6.7 shows the error variances of ISI. As shown in Equation (3.10), the ISI error is a combination of 1) the error due to the imperfection of the interpolation filter, 2) the error due to the imperfection in timing estimation, and 3) the AWGN. Because this simulation does not consider the contribution of AWGN, the ISI error contains only the first two errors.

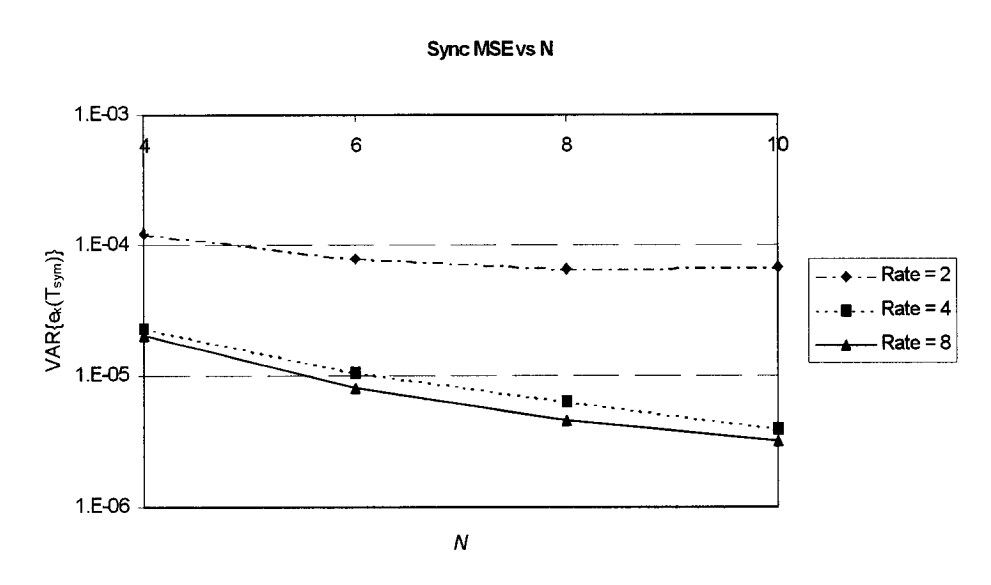


Fig. 6.6: MSE of STR versus preamble length N (without noise)

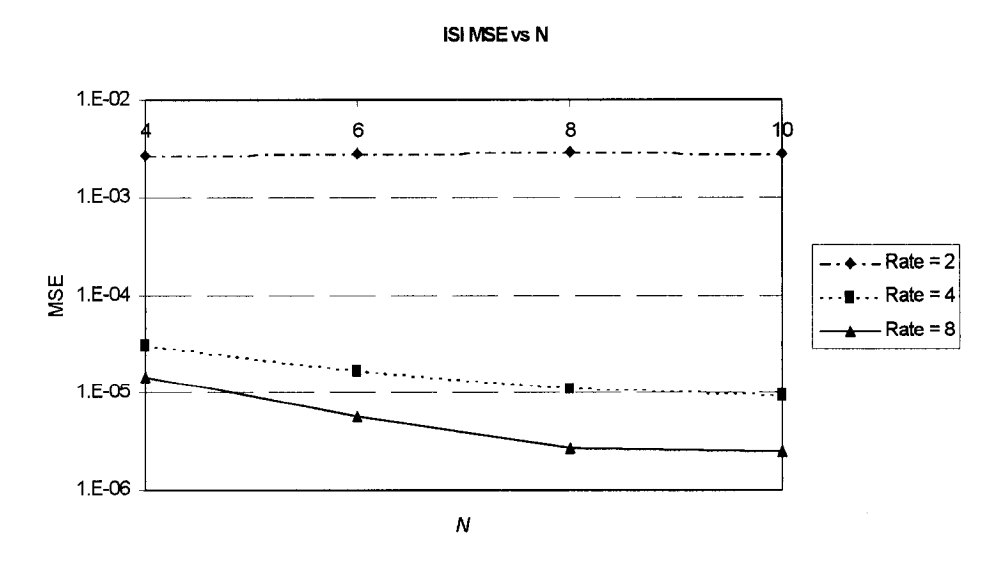


Fig. 6.7: MSE of ISI versus preamble length N (without noise)

#### With AWGN effects

The second set of simulations considers the effect of AWGN on the system. Figures 6.8 to 6.11 show all simulation results on the error variance of the symbol timing estimation. Comparing these figures with Figure 6.6 shows that all simulation curves tend to approach the ones obtained in Figure 6.6 at high signal to noise ratio  $(E_b/N_o)$ . In fact, the curves for  $E_b/N_o$ =20dB in Figure 6.11 is almost identical to the ones obtained in Figure 6.6. Furthermore, the obtained results of symbol timing error statistics for 4-QAM systems (Figures 6.8 to 6.10) are very similar the ones for 2-PAM systems (Figures 6.3 to 6.5). As the two systems are predicted to have similar performance (Sections 6.2.2 and 6.2.3), these results agree to the theoretical expectation.

Figures 6.12 to 6.14 show simulation results on the error variance of the ISI (measured at sampling instant) for several values of average bit energy  $(E_b/N_o)$ . The thick, solid lines are the variance of the injected AWGN, which is denoted as  $e_{\eta}$ . If exact timing estimation and perfect signal recovery can be achieved, this variance is identical to that of the ISI error. It is thus referred to as an ideal reference. As shown in these figures, increasing the preamble length N makes the curves closer to the ideal curve.

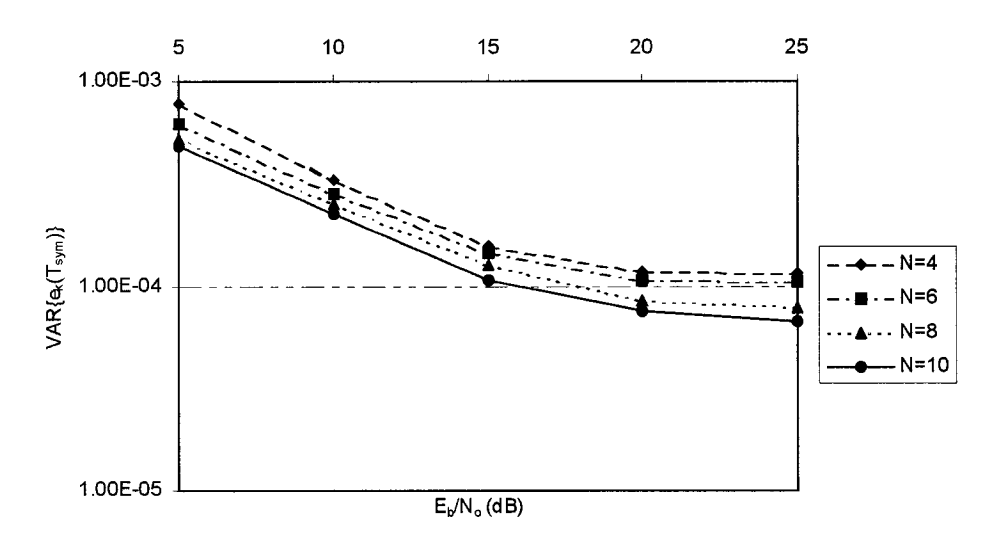


Fig. 6.8: MSE of Estimated Timing versus  $E_b/N_o$  for sampling rate  $\lambda = 2$ 

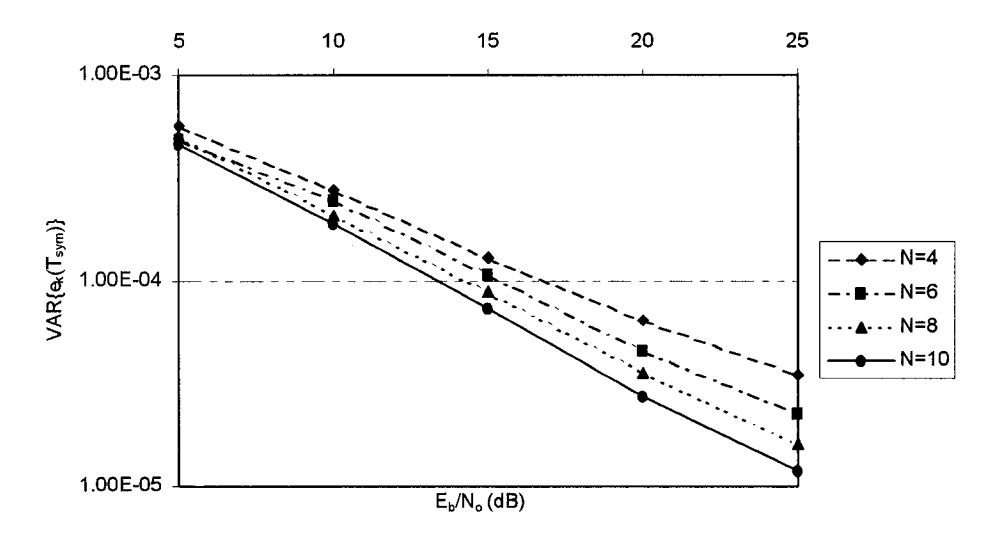


Fig. 6.9: MSE of Estimated Symbol Timing versus  $E_b/N_o$  for sampling rate  $\lambda=4$ 

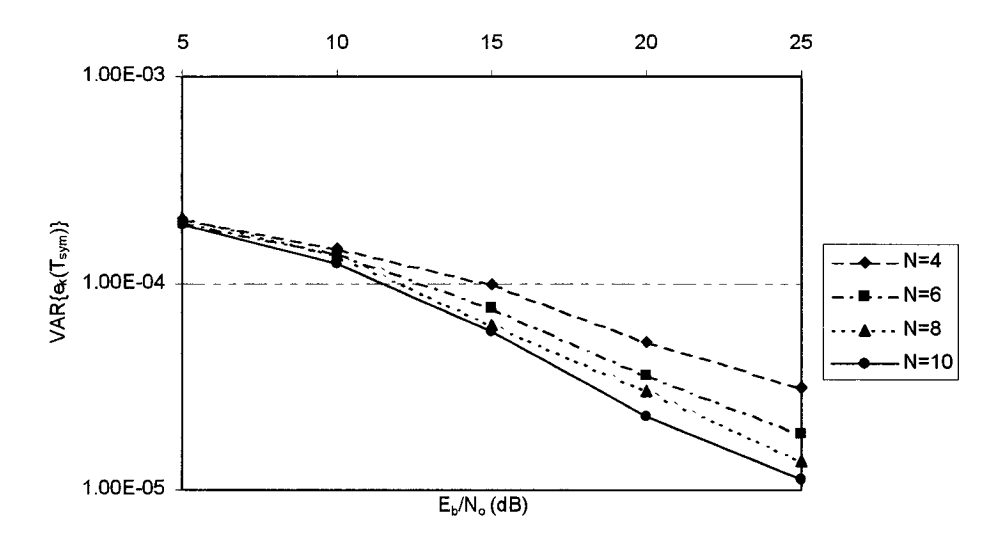


Fig. 6.10: MSE of Estimated Symbol Timing versus  $E_b/N_o$  for sampling rate  $\lambda$  = 8

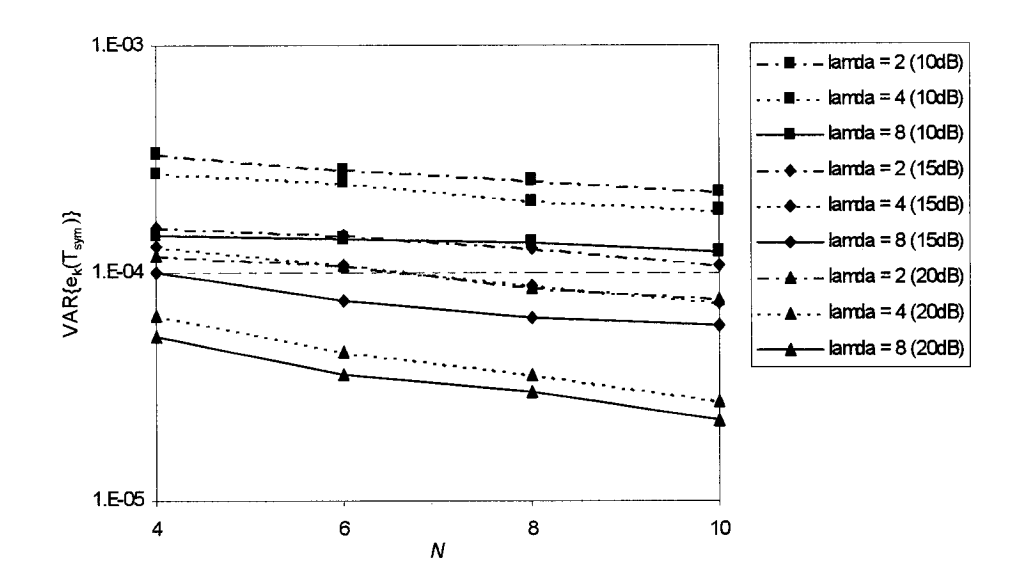


Fig. 6.11: MSE of Estimated Symbol Timing versus preamble length N

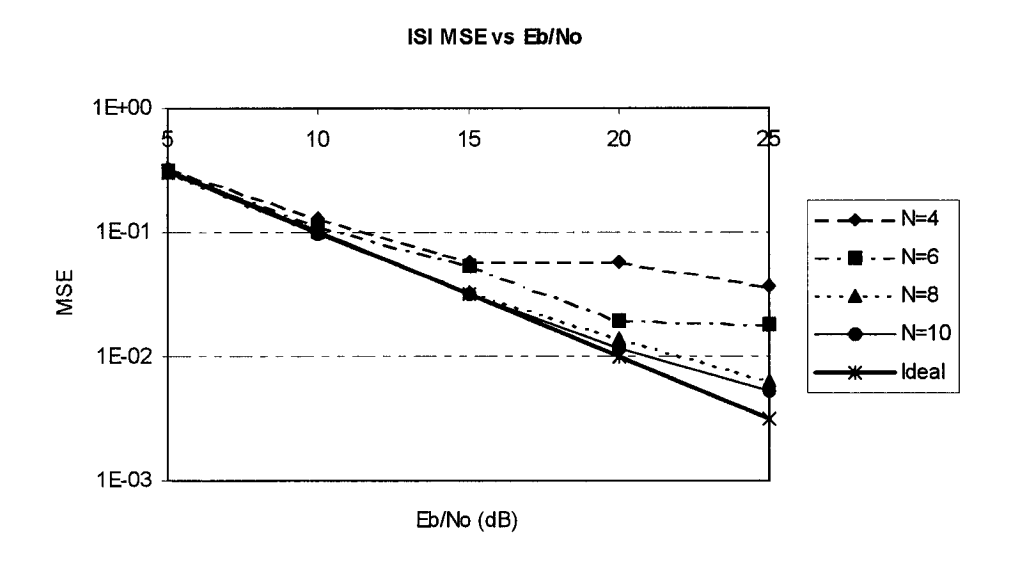


Fig. 6.12: MSE of ISI vs. Eb/No for sampling rate  $\lambda = 2$ 

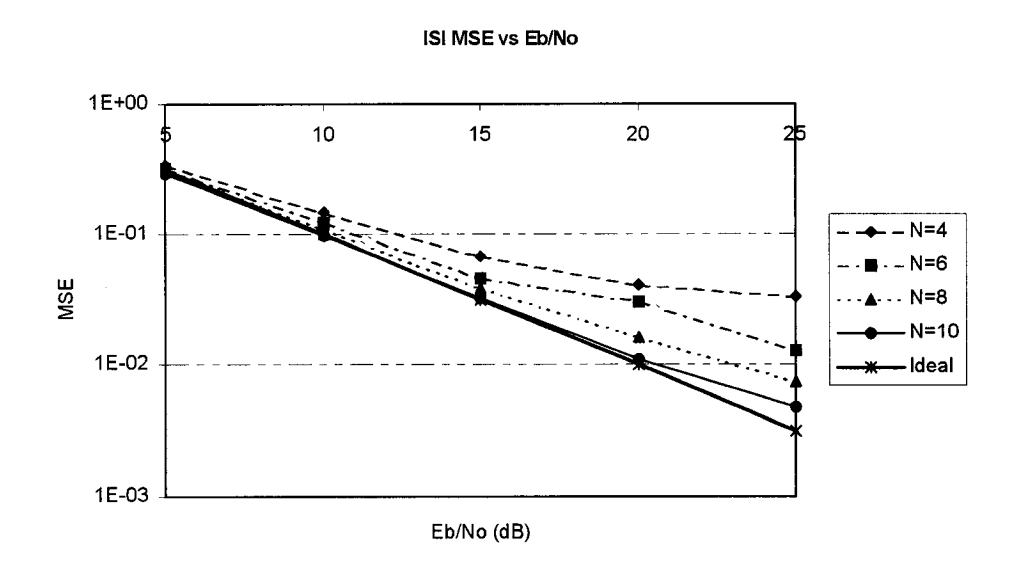


Fig. 6.13: MSE of ISI error vs. Eb/No for sampling rate  $\lambda = 4$ 

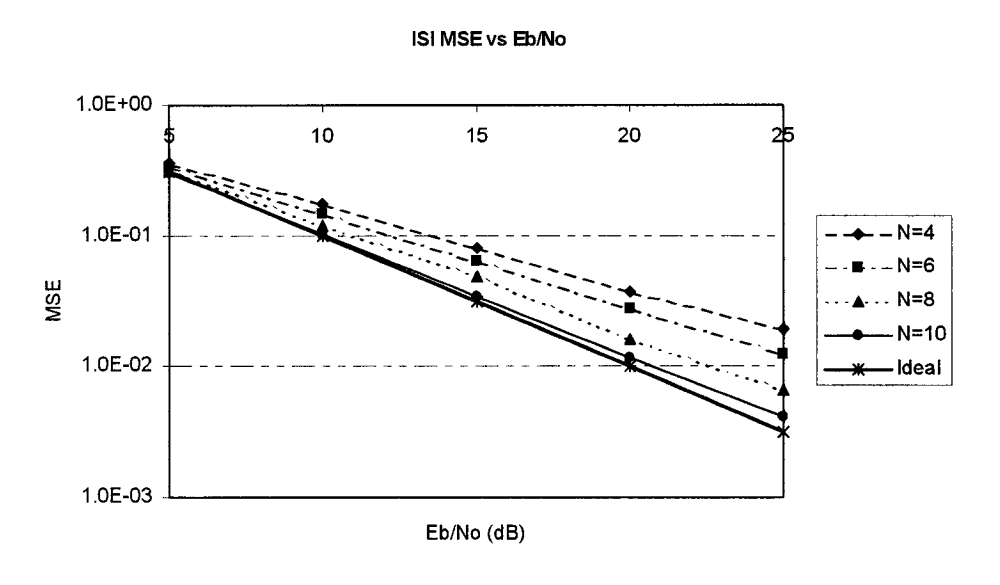


Fig. 6.14: MSE of ISI error vs. Eb/No for sample rate  $\lambda = 8$ 

### 6.3 Conclusion

This chapter presented the applications of the proposed STR techniques to two M-

PAM and  $M^2$ -QAM systems. The techniques are generalized in these systems so that they can operate at any sampling rates. It is shown that sampling at high rates provides more samples per symbol interval for better performance improvement. In addition, the joint ML estimator of I and Q channels in  $M^2$ -QAM systems is proved to perform 3dB better than the one in M-PAM systems. Many analytical and experimental results can be used for trade-off between performance and complexity/speed.

A case-study of optimal Lagrange parabolic interpolators that minimize timing estimation errors has been investigated. Simulations have shown that the system performs very well in the AWGN. It is also interesting to notice that our optimal interpolators are very similar to the ones obtained in [39]. Since the case-study is only one of our many possible considerations, it implies that the approach in [39] is only a sub-solution of our algorithm.

### Chapter 7. Conclusion

This thesis proposes the efficient all-digital feedforward STR techniques for linear modulation schemes M-PAM and  $M^2$ -QAM, and the design of optimal interpolation filters. This chapter highlights the key findings and recommends new avenues for future research which time did not permit in this work.

#### 7.1 Summary of Results

Chapter 2 explains the concept and the structure of the interpolation filters for all-digital receivers. A low-complexity hardware implementation can be obtained using the modified Farrow structure for the second-degree, symmetric interpolator. It is proven that only M/2 coefficients is actually required, compared with 3M coefficients in the original structure.

Chapter 3 develops the theoretical backgrounds on all-digital symbol timing recovery techniques that employ interpolation filters. The symbol-timing estimation process, which is, in most of the cases, based on the maximum-likelihood (ML) concept, is proposed. Joint optimization of signal detection and timing estimation are discussed.

Chapter 4 discusses the interpolation filters for symbol timing recovery (STR). The need for an interpolation filter is explained. It is shown that recent conventional interpolation filters are either not optimal, or suboptimal but not able to be implemented in on-line computation manners. A new interpolation filter methodology for minimum mean-square error (MMSE) is introduced to overcome the problems of these filters. Simulation results are included to show the performance gain, whereas the modified Farrow structure is given to show hardware complexity gain realizable by the proposed

interpolation filter.

Chapter 5 analyses the statistical performance of all-digital symbol timing recovery techniques at the sampling rate  $T_{sym}/T_s$ =2. Tracking performance for the synchronization system employing several interpolation filters are studied. Simulation results are included to show the correctness of the theory and the analysis.

Chapter 6 provides generalizations of the proposed timing estimation techniques for PAM and QAM systems. The proposed feed-forward STR techniques employing interpolation filters can be applied for higher sampling rate to achieve better accuracy, with the tradeoff in more hardware complexity and possible lower operated clock speed. In addition, the joint ML estimator of I and Q channels in  $M^2$ -QAM systems is proved to perform 3dB better than the one in M-PAM systems. Analytical and experimental results can be used for trade-off between performance and complexity/speed.

### 7.2 Topics for Further Research

The following is a partial list of issues for future research.

- 1. Quantization effect on BER performance. Practical implementations add quantization noise to all operations, thus degrade the performance of the STR, and the overall BER performance. The effect of quantization should be investigated.
- 2. Fading effects. In general, the scheme should work with multi-path fading; however, there is performance degradation. Effects of fading should be further studied.
- 3. Study of the interaction between carrier recovery, symbol timing recovery, and equalization. When one of three operations (STR, CR, and equalization) is derived, the other two operations are assumed to be perfect. However, this can never be true in real systems. The interaction between these three operations for all-digital receivers should be analyzed.
- 4. Extensions of the feedforward algorithms to the non data-aided case. Although the algorithms of this thesis are extensively discussed for data-aided operation, it can be modified and extended to suit non data-aided (NDA) conditions. The effect of oversampling rate and interpolation filter on NDA versions would be interesting.

### **Bibliography**

- [1] D. Kim, M. J. Narasimha, and D. C. Cox, "Design of optimal interpolation filter for symbol timing recovery," *IEEE Trans. Commun.*, vol. 45, pp. 877-884, July 1997.
- [2] C. W. Farrow, "A continuously variable digital delay element," in *Proc. IEEE Int. Symp. on Circuits and Systems*, Espoo, Finland, pp. 2641-2645, June 1988.
- [3] F. M. Gardner, "Interpolation in digital modem-Part I: Fundamentals," *IEEE Trans. Commun.*, vol. 41, pp. 501-507, Mar. 1993.
- [4] L. Erup, F. M. Gardner, and R. A. Harris, "Interpolation in digital modem-Part II: Implementation and performance," *IEEE Trans. Commun.*, vol. 41, pp. 998-1008, June 1993.
- [5] V. Välimäki, and T. I. Laakso, "Principles of fractional delay digital filters," in *Proc. EEE Int. Conference on Acoustics, Speech, and Signal Processing*, vol. 6, pp. 3870 -3873, 2000.
- [6] V. Välimäki, M. Karjalainen, and T. I. Laakso, "Fractional delay digital filters," in Proc. IEEE Int. Symp. on Circuits and Systems, Chicago, Illinois, pp. 355-358, May 1993.
- [7] A. Yardim, T. I. Laakso, L. P. Sabel, and G. D. Cain, "Frequency-sampling design of delay-root-Nyquist filters," *Electronics Letters*, vol. 33, pp. 35-37, Jan. 1997.
- [8] V. Valimaki, "A new filter implementation strategy for Lagrange interpolation," Proc. IEEE Int. Sym. on Circuits and Systems, vol. 1, pp. 361-364, 1995.

[9] J. Vesma, and T. Saramaki, "Interpolation filters with arbitrary frequency response for all-digital receivers," *Proc. IEEE Int. Sym. on Circuits and Systems*, vol. 2, pp. 568-571, 1996.

- [10] H. Ridha, J. Vesma, T. Saramak, and M. Renfors, "Derivative approximations for sampled signals based on polynomial interpolation," *Proc. IEEE Int. Conf. on Digital Signal Processing Proceedings*, vol. 2, pp. 939-942, 1997.
- [11] J. Vesma, "A frequency-domain approach to polynomial-based interpolation and the Farrow structure," *IEEE Transactions on Circuits and Systems II: Analog and Digital Signal Processing*, vol. 47, No. 3, pp. 206-209, March 2000.
- [12] J. Vesma, R. Hamila, M. Renfors, and T. Saramaki, "Continuous-time signal processing based on polynomial approximation," *Proc. IEEE Int. Symp. on Circuits and Systems*, vol. 5, pp. 61-65, 1998.
- [13] J. Vesma, and T. Saramaki, "Optimization and efficient implementation of fractional delay FIR filters," *Proc. IEEE Int. Symp. on Circuits and Systems*, vol. 1, pp. 546-549, 1996.
- [14] J. Vesma, and T. Saramaki, "Design and properties of polynomial-based fractional delay filters," *Proc. IEEE Int. Symp. on Circuits and Systems*, vol. 1, pp. 104-107, 2000.
- [15] J. Vesma, M. Renfors, and J. Rinne, "Comparison of efficient interpolation techniques for symbol timing recovery," *GLOBECOM* '96, vol. 2, pp. 953-957, 1996.
- [16] M. Nagahara, and Y. Yamamoto, "A new design for sample-rate converters," Proc. of the 39th IEEE Conference on Decision and Control, 2000, vol. 5, pp. 4296 4301.
- [17] K. Tzu-Chieh, A. Kwentus, and A. N. Willson Jr, "A programmable interpolation filter for digital communications applications," *Proc. IEEE Int. Symp. on Circuits and Systems*, vol. 2, pp. 97-100, 1998.

[18] V. Zinvojnovic, and H. Meyr, "Design Of Optimum Interpolation Filters For Digital Demodulators," Proc. IEEE Int. Symp. on Circuits and Systems, vol. 1, pp. 140-143, 1993.

- [19] G. Watkins, "Optimal Farrow coefficients for symbol timing recovery," *IEEE Communications Letters*, vol. 5, No. 9, pp. 381-383, Sept. 2001.
- [20] P. J. Kootsookos, and R. C. Williamson, "FIR approximation of fractional sample delay systems," *IEEE Transactions on Circuits and Systems II: Analog and Digital Signal Processing*, vol. 43, No. 3, pp. 269 -271, March 1996.
- [21] H. Johansson, and P. Lowenborg, "Reconstruction of nonuniform sampled bandlimited signals using digital fractional filters," *IEEE Int. Symp. on Circuits and Systems*, vol. 2, pp. 593-596, 2001.
- [22] R. M. Aguilar-Ponce, and G. Jovanovic-Dolecek, "A multirate approach to design of fractional delay filters," *Third International Workshop on Design of Mixed-Mode Integrated Circuits and Applications*, pp. 143-146, 1999.
- [23] D. Verdin, and T. C. Tozer, "Simulating asynchronous timing-recovery loops using multirate techniques," *IEE Colloquium on Communications Simulation and Modelling Techniques*, pp. 13/1-8, London 1993.
- [24] S. R. Dooley, and A. K. Nandi, "Notes on the interpolation of discrete periodic signals using sinc function related approaches," *IEEE Transactions on Signal Processing*, vol. 48, No. 4, pp. 1201-1203, April 2000.
- [25] L. Wasserman, and A. N. Willson Jr, "A variable-rate filtering system for digital communications," *Proc. IEEE International Conference on Acoustics, Speech, and Signal Processing 1999*, vol. 3, pp. 1497-1500, 1999.
- [26] X. Xiang-Gen, "Fractional delay filter design when sampling rate higher than Nyquist rate," *Electronics Letters*, vol. 33, No. 3, pp. 199-201, Jan. 1997.

- [27] S. Tassart, and P. Depalle, "Analytical approximations of fractional delays: Lagrange interpolators and allpass filters," *IEEE International Conference on Acoustics, Speech, and Signal Processing 1997*, vol. 1, pp. 455-458, 1997.
- [28] D. Fu, and, A. N. Willson Jr., "Design of an improved interpolation filter using a trigonometric polynomial," *Proceedings of the 1999 IEEE International Symposium on Circuits and Systems*, vol. 4, pp. 363-366, 1999.
- [29] A. Yardim, G. D. Cain, and A. Lavergne, "Performance of fractional-delay filters using optimal offset windows," in *Proc. Int. Conf. on Acoust., Speech, Signal Processing*, Munich, Germany, April 1997, pp. 2233-2236.
- [30] H. Zhang, M. Xenfors, "A study on performance improvement of the interpolation with a half-band filter," 3rd International Conference on Signal Processing, 1996, Vol 2, pp. 1691-1694.
- [31] G. D. Cain, N. P. Murphy, and A. Tarczynski, "Evaluation of several variable FIR fractional-sample delay filters," in *Proc. Int. Conf. on Acoust., Speech, Signal Processing*, Adelaide, Australia, April 1994, pp. 621-624.
- [32] J. Vesma, T. Saramaki, and M. Renfors, "Combined matched filter and polynomial-based interpolator for symbol synchronization in digital receivers," *Proc. IEEE Int. Symp. on Circuits and Systems*, Vol 3, pp. 94-97, 1999.
- [33] A. Gottscheber, P. Fines, and A. H. Aghvami, "Combined interpolator filter for timing recovery in a fully digital demodulator," in *Proc. IEEE Int. Conf. on Communications*, New Orleans, Louisiana, USA, May 1994, pp. 1467-1471.
- [34] D. Liu, and C. Wei, "A digital timing recovery scheme for TDMA digital mobile radio," *IEEE Int. Symp. on Circuits and Systems*, 1996, Vol 1, pp. 152-154.
- [35] D. Liu, and C. Wei, "Asynchronous symbol timing recovery with adaptive interpolation filter for high data-rate digital mobile radio," *Proc. IEEE Int. Symp. on Circuits and Systems*, Geneva 2000, Vol 2, pp. 85-88.

[36] D. Kim, M. J. Narasimha, and D. C. Cox, "Unbiased timing-error estimation in the presence of nonideal interpolation," *IEEE Trans. on Communications*, Vol. 45, No.6, pp. 647-650, June 1997.

- [37] K. Bucket, and M. Moeneclaey, "Periodic timing error components in feedback synchronizers operating on nonsynchronized signal samples," *IEEE Trans. on Communications*, Vol. 46, No. 6, pp. 747 -749, June 1998.
- [38] R. Hamila, J. Vesma, H. Vuolle, and M. Renfors, "Effect of frequency offset on carrier phase and symbol timing recovery in digital receivers," 1998 URSI Int. Symp. on Signals, Systems, and Electronics, 1998, pp. 247-252.
- [39] K. Bucket, and M. Moeneclaey, "Optimisation of second-order interpolator for bandlimited direct-sequence spread-spectrum communication," *Electronics Letters*, Vol. 28, Issue: 11, 21 May 1992, pp. 1029-1031.
- [40] V. Tuukkanen, J. Vesma, and M. Renfors, "Combined interpolation and maximum likelihood symbol timing recovery in digital receivers," *IEEE Int. Conf. on Universal Personal Communications Record*, Vol 2, pp. 698 -702 1997.
- [41] U. Lambrette, and H. Meyr, "Two timing recovery algorithms for MSK," *IEEE Int. Conf. on Communications*, 1994, vol. 2, pp. 1155 -1159.
- [42] D. Efstathiou, and A. H. Aghvami, "Preamble-less nondecision-aided (NDA) feedforward synchronization techniques for 16-QAM TDMA demodulators," IEEE Transactions on Vehicular Technology, Vol 47, No 2, pp. 673 -685, May 1998.
- [43] W. P. Zhu, M. O. Ahmad, and M. N. S. Swamy, "A fully digital timing recovery scheme using two samples per symbol," *IEEE Int. Symp. on Circuits and Systems*, 2001, Vol 2, pp. 421 -424.
- [44] V. Tuukkanen, J. Vesma, and M. Renfors, "Efficient near optimal maximum likelihood symbol timing recovery in digital modems," *IEEE Int. Symp. on Personal, Indoor and Mobile Radio Communications*, Vol 3, pp. 825-829, 1997.

[45] R. Hamila, J. Vesma, and M. Renfors, "Joint estimation of carrier phase and symbol timing using polynomial-based maximum likelihood technique," *IEEE Int. Conf. on Universal Personal Communications*, Vol 1, pp. 369-373,1998.

- [46] L. P. Sabel and W. G. Cowley, "Block processing feedforward symbol timing estimator for digital modems," *Electronics Letters*, vol. 30, pp. 1273-1274, Aug. 1994.
- [47] R. Morawski, Low-Complexity Structures for Digital Symbol Timing Recovery.

  M.Sc. Thesis, Montreal, Quebec, Canada: Concordia University, Department of Electrical Computer Engineering, Feb. 2000.
- [48] L.P. Sabel, and W.G. Cowley, "A recursive algorithm for the estimation of symbol timing in PSK burst modems," *Global Telecommunications Conference*, 1992. pp. 360-364.
- [49] D. Kim, Synchronization for All Digital Receivers, Ph. D. Thesis, Stanford University, October 1996.
- [50] J. Vesma, Timing Adjustment in Digital Receivers Using Interpolation. M.Sc. Thesis, Tampere, Finland: Tampere University of Tech., Department of Information Technology, Nov. 1995.
- [51] J. Vesma, Optimization and Applications of Polynomial-Based Interpolation Filters. Ph. D. Thesis, Tampere, Finland: Tampere University of Tech., Department of Information Technology, Nov. 1999.
- [52] K. H. Cho, J. Putnam, and H. Samueli, "A VLSI architecture for a frequency-agile single-chip 10-MBaud digital QAM modulator," *GLOBECOM* '99, Vol 1a, 1999, pp. 168-172.
- [53] K. H. Park, D. K. Shin, J. S. Lee, and M. H. Sunwoo, "Design of a QPSK/16 QAM LMDS downstream receiver ASIC chip," 2000 IEEE Workshop on Signal Processing Systems, pp. 210-217, 2000.

[54] F. M. Gardner, "A BPSK/QPSK timing-error detector for sampled receivers," *IEEE Trans. Commun.*, vol. COM-34, pp. 423-429, May 1986.

- [55] S. Ries and M. Th. Roeckerath-Ries, "Combined matched filter/interpolator for digital receivers" in *Proc. VIII European Signal Processing Conf.*, Trieste, Italy, Sep. 1996, pp. 627-630.
- [56] F. M. Gardner, "Demodulator reference recovery techniques suited for digital implementation," ESA Final Report, Aug. 1988.
- [57] K. H. Mueller and M. Muller, "Timing Recovery in Digital Synchronous Data Receivers," *IEEE Trans. on Comm.*, pp. 516-531, May 76.
- [58] F. M. Gardner, "Timing adjustment via interpolation in digital demodulators," *ESA Final Report: Part* I, June 1990.
- [59] H. Meyr, M. Moeneclaey, and S. A. Fechtel, *Digital Communication Receivers*. John Wiley & Sons, 1998.
- [60] J. G. Proakis, Digital Communication Systems. McGraw-Hill, 4th ed., 2000.
- [61] K. Feher, Digital Communications: Satellite/Earth station engineering. Prentice-Hall, 1983.
- [62] U. Mengali and A. N. D'Andrea, Synchronization Techniques for Digital Receivers. Plenum Press, 1997
- [63] S. Haykin, Adaptive Filter Theory. Prentice Hall, 3rd ed., 1996
- [64] E. Kreyszig, Advanced Engineering Mathematics. John Wiley, 7th ed., 1993.

# Appendix A. Some Known Interpolation Filters

Some known interpolation filters are presented in this Appendix. Many of them are based on Lagrange polynomials, and shown in Tables A.1, A.2, and A.3. They are widely mentioned in literature for their simple hardware structure. However, they are not optimal.

Table A.1: Farrow Coefficients for Linear Interpolation

	<i>l</i> = 0	<i>l</i> = 1	
k = -1	0	1	
k = 0	1	-1	

Table A.2: Farrow Coefficients for Cubic Interpolation Filter

	<i>l</i> = 0	<i>l</i> = 1	<i>l</i> = 2	<i>l</i> = 3
k = -2	0	-1/6	0	1/6
k = -1	0	1	1/2	-1/2
k = 0	1	-1/2	-1	1/2
k = 1	0	-1/3	1/2	-1/6

The piece-wise parabolic interpolation filter can be given as

Table A.3: Farrow Coefficients for Parabolic Interpolation Filter

	<i>l</i> = 0	<i>l</i> = 1	<i>l</i> = 2
k = -2	0	-γ	γ
k = -1	0	γ+1	-γ
k = 0	1	γ-1	γ
k = 1	0	-γ	γ

Vesma and Saramaki [13] introduce two alternative interpolation filters which were optimized in the frequency domain.

Table A.4: Farrow Coefficients for Vesma Interpolation Filter I

	<i>l</i> = 0	<i>l</i> = 1	<i>l</i> = 2
k = -2	0	-0.6741	0.6741
k = -1	0	1.4542	-0.4542
k = 0	1	-0.5458	-0.4542
k = 1	0	-0.6741	0.6741

Table A.5: Farrow Coefficients for Vesma Interpolation Filter II

	<i>l</i> = 0	<i>l</i> = 1	<i>l</i> = 2
k = -3	0	0.2418	-0.2418
k = -2	0	-0.6449	0.6449
k = -1	0	1.4726	-0.4726
k = 0	1	-0.5274	0.4726
k = 1	0	-0.6449	0.6449
k = 2	0	0.2418	-0.2418

## **Appendix B. Unbiased Timing Error Estimation**

### **B.1 Mean of the Timing Error Estimation**

The mean of the estimated timing error can be formulated as

$$E[\varepsilon] = \int_0^1 \varepsilon(\mu) p df(\mu) d\mu$$
 (B.1)

If  $\mu$  is uniformly distributed in [0, 1], then  $pdf(\mu)=1$ , and Equation (B.1) become

$$E[\varepsilon] = \frac{1}{2} \int_0^1 \left( \mu - \frac{1}{2} + \frac{1}{4\gamma} \tan\left(\frac{\pi}{2} \left(\frac{1}{2} - \mu\right)\right) \right) d\mu$$
 (B.2)

$$E[\varepsilon] = \frac{1}{2} \left( \frac{\mu^2}{2} - \frac{\mu}{2} + \frac{\pi}{8\gamma} \ln \left( \cos \left( \frac{\pi}{2} \left( \frac{1}{2} - \mu \right) \right) \right) \right) \Big|_{0}^{1} = 0$$
 (B.3)

### **B.2** Variance of the Timing Error Estimation

Since the timing error estimation has a zero mean, its variance can be derived as

$$VAR[\varepsilon] = \int_0^1 \varepsilon^2(\mu) p df(\mu) d\mu$$
 (B.4)

$$VAR[\varepsilon] = \frac{1}{4} \int_0^1 \left( \mu - \frac{1}{2} + \frac{1}{4\gamma} \tan \left( \frac{\pi}{2} \left( \frac{1}{2} - \mu \right) \right) \right)^2 d\mu$$
 (B.5)

Solving the integral results,

$$VAR[\varepsilon] = \frac{1}{32\gamma^2} \left(\frac{4}{\pi} - 1\right) - \frac{1.4863}{4\gamma\pi^2} + \frac{1}{24}$$
 (B.6)

The minimum occurs at,

$$\frac{1}{\gamma_{min}} = -\frac{b}{2a} = \frac{\frac{1.4863}{4\pi^2}}{\frac{1}{16}(\frac{4}{\pi} - 1)}$$
 (B.7)

$$\gamma_{min} = \frac{\frac{1}{16} \left(\frac{4}{\pi} - 1\right)}{\frac{1.4863}{4\pi^2}} \cong 0.4536$$
 (B.8)

#### **B.3** Bound of the Variance

$$e_{i}[\mu] = \frac{\mu}{2} + \frac{\sum_{n=0}^{N-1} (-1)^{n} f_{1}[2n+i]}{4E \left[\sum_{n=0}^{N-1} (-1)^{n} f_{2}[2n+i]\right]}$$
(B.9)

$$E[e_{i}[\mu]] = \frac{1}{2}E\left[\mu^{2} + \mu \frac{\sum_{n=0}^{N-1} (-1)^{n} f_{1}[2n+i]}{E\left[\sum_{n=0}^{N-1} (-1)^{n} f_{2}[2n+i]\right]} + \frac{\left(\sum_{n=0}^{N-1} (-1)^{n} f_{1}[2n+i]\right)^{2}}{4\left(E\left[\sum_{n=0}^{N-1} (-1)^{n} f_{2}[2n+i]\right]\right)^{2}}\right]$$
(B.10)

$$E[e_{i}[\mu]] = \frac{\mu^{2}}{2} + \frac{\mu}{2} \frac{E\left[\sum_{n=0}^{N-1} (-1)^{n} f_{1}[2n+i]\right]}{E\left[\sum_{n=0}^{N-1} (-1)^{n} f_{2}[2n+i]\right]} + \frac{E\left[\left(\sum_{n=0}^{N-1} (-1)^{n} f_{1}[2n+i]\right)^{2}\right]}{8\left[E\left[\sum_{n=0}^{N-1} (-1)^{n} f_{2}[2n+i]\right]\right)^{2}}$$
(B.11)

where,

$$E\left[\sum_{n=0}^{N-1} (-1)^n f_l[2n+i]\right] = \sum_{n=0}^{N-1} (-1)^n E[f_l[2n+i]]$$
 (B.12)

$$E\left[\sum_{n=0}^{N-1} (-1)^n f_l[2n+i]\right] = \sum_{n=0}^{N-1} \sum_{m=0}^{M-1} c_l(m) (-1)^n \sin(2n+i-m-\mu)$$
 (B.13)

$$E\left[\left(\sum_{n=0}^{N-1} (-1)^n f_l[2n+i]\right)^2\right] = E\left[\sum_{n=0}^{N-1} (-1)^n f_l[2n+i] \sum_{p=0}^{N-1} (-1)^p f_l[2p+i]\right]$$
(B.14)

$$E\left[\left(\sum_{n=0}^{N-1} (-1)^n f_l[2n+i]\right)^2\right] = \sum_{n=0}^{N-1} \sum_{p=0}^{N-1} (-1)^{n+p} E[f_l[2n+i]f_l[2p+i]]$$
(B.15)

$$E[f_{l}[2n+i]f_{l}[2p+i]] = E\left[\sum_{m=0}^{M-1} c_{l}(m)x(2n+i-m)\sum_{k=0}^{M-1} c_{l}(k)x(2p+i-k)\right]$$
(B.16)

$$E[f_{l}[2n+i]f_{l}[2p+i]] = \sum_{m=0}^{M-1} \sum_{k=0}^{M-1} c_{l}(m)c_{l}(k)E[x(2n+i-m)x(2p+i-k)]$$
 (B.17)

$$E[x(n)x(p)] = E\left[\left(r(n) + \frac{\eta(n)}{A}\right)\left(r(p) + \frac{\eta(p)}{A}\right)\right]$$
 (B.18)

$$E[x(n)x(p)] = r(n)r(p) + \frac{E[\eta(n)\eta(p)]}{A^2}$$
 (B.19)

For white Gaussian noise,

$$E[x(n)x(p)] = r(n)r(p) + \frac{\sigma^2}{A^2}\delta(n-p)$$
 (B.20)

## **Appendix C. Impulse Response of the Raised-Cosine Filter and Its Derivatives**

The impulse response of the raised-cosine function is

$$g(t) = \frac{\sin(\pi t/T)}{\pi t/T} \frac{\cos(\pi \beta t/T)}{1 - (2\beta t/T)^2}$$
(C.1)

where T denotes the symbol period  $(T_{sym})$ .

The first derivative is

$$g'(t) = \frac{\cos(\pi t/T)\cos(\pi \beta t/T)}{t(1 - (2\beta t/T)^2)} - \frac{T\sin(\pi t/T)\cos(\pi \beta t/T)}{\pi t^2 (1 - (2\beta t/T)^2)}$$

$$-\frac{\beta \sin(\pi t/T)\sin(\pi \beta t/T)}{t(1 - (2\beta t/T)^2)} + \frac{8\beta^2 \sin(\pi t/T)\cos(\pi \beta t/T)}{\pi T (1 - (2\beta t/T)^2)^2}$$
(C.2)

whereas,

$$g'(0) = 0 \tag{C.3}$$

$$g'(mT) = \frac{\cos(\pi m)\cos(\pi \beta m)}{mT(1-(2\beta m)^2)}, m \neq 0$$
 (C.4)

$$\sum_{m=-\infty}^{\infty} (g'(mT)T)^2 = 2\sum_{m=1}^{\infty} \frac{\cos^2(\pi\beta m)}{m^2(1-(2\beta m)^2)^2} = B(\beta)$$
 (C.5)

Since the term in the series decreases with  $m^8$ , the series can be approximated with a few terms (i.e. m is finite).

The second derivative is

$$g''(t) = \frac{-\pi \sin(\pi t/T)\cos(\pi \beta t/T)}{Tt(1 - (2\beta t/T)^{2})}$$

$$+ 2\frac{T\sin(\pi t/T)\cos(\pi \beta t/T) - \pi t\sin(\pi t/T)\cos(\pi \beta t/T)}{\pi t^{3}(1 - (2\beta t/T)^{2})}$$

$$- 2\frac{\pi \beta \cos(\pi t/T)\sin(\pi \beta t/T)}{Tt(1 - (2\beta t/T)^{2})} + 16\frac{\beta^{2}\cos(\pi t/T)\cos(\pi \beta t/T)}{T^{2}(1 - (2\beta t/T)^{2})}$$

$$+ 2\frac{\beta \sin(\pi t/T)\cos(\pi \beta t/T)}{t^{2}(1 - (2\beta t/T)^{2})} - 8\frac{\beta^{2}\sin(\pi t/T)\cos(\pi \beta t/T)}{\pi Tt(1 - (2\beta t/T)^{2})^{2}}$$

$$- \frac{\pi \beta^{2}\sin(\pi t/T)\cos(\pi \beta t/T)}{Tt(1 - (2\beta t/T)^{2})} - 16\frac{\beta^{3}\sin(\pi t/T)\sin(\pi \beta t/T)}{T^{2}(1 - (2\beta t/T)^{2})^{2}}$$

$$+ 128\frac{\beta^{4}t\sin(\pi t/T)\cos(\pi \beta t/T)}{\pi T^{3}(1 - (2\beta t/T)^{2})^{3}}$$
(C.6)

where,

$$g''(0)T^2 = (8 - \pi^2)\beta^2 - \frac{\pi^2}{3}$$
 (C.7)